University of Tennessee, Knoxville
TRACE: Tennessee Research and Creative Exchange

Doctoral Dissertations | Graduate School

8-2014

# IN-LINE MICROFLUIDIC PARTICLE PRECONCENTRATOR AND DETECTOR FOR CONTINUOUS FLOW MONITORING

Quan Yuan
*University of Tennessee - Knoxville*, qyuan1@vols.utk.edu

Follow this and additional works at: https://trace.tennessee.edu/utk_graddiss

 Part of the Biomedical Commons, Electrical and Electronics Commons, and the Electronic Devices and Semiconductor Manufacturing Commons

## Recommended Citation

Yuan, Quan, "IN-LINE MICROFLUIDIC PARTICLE PRECONCENTRATOR AND DETECTOR FOR CONTINUOUS FLOW MONITORING. " PhD diss., University of Tennessee, 2014.
https://trace.tennessee.edu/utk_graddiss/2878

This Dissertation is brought to you for free and open access by the Graduate School at TRACE: Tennessee Research and Creative Exchange. It has been accepted for inclusion in Doctoral Dissertations by an authorized administrator of TRACE: Tennessee Research and Creative Exchange. For more information, please contact trace@utk.edu.

To the Graduate Council:

I am submitting herewith a dissertation written by Quan Yuan entitled "IN-LINE MICROFLUIDIC PARTICLE PRECONCENTRATOR AND DETECTOR FOR CONTINUOUS FLOW MONITORING." I have examined the final electronic copy of this dissertation for form and content and recommend that it be accepted in partial fulfillment of the requirements for the degree of Doctor of Philosophy, with a major in Electrical Engineering.

Jayne Wu, Major Professor

We have read this dissertation and recommend its acceptance:

Syed Islam, Nicole McFarlane, Elias Greenbaum

Accepted for the Council:

Carolyn R. Hodges

Vice Provost and Dean of the Graduate School

(Original signatures are on file with official student records.)

# IN-LINE MICROFLUIDIC PARTICLE PRECONCENTRATOR AND DETECTOR FOR CONTINUOUS FLOW MONITORING

A Dissertation Presented for the
Doctor of Philosophy
Degree
The University of Tennessee, Knoxville

Quan Yuan

August 2014

Copy right @ 2014 QuanYuan
All rights reserved

# ACKNOWLEDGEMENT

First of all, I express my deepest gratitude to my major advisor, Dr. Jie Wu, for her guidance and encouragement through my research in the field of microfluidics and bio-particle detection. Thanks to her mentoring, my graduate study at University of Tennessee was far more rewarding than I could ever have expected. Her mentorship was paramount in providing a well rounded experience consistent my long-term career goals. I feel most fortunate being exposed to her work ethic, commitment to excellence, charisma and acumen, in addition to professional training.

I would also like to thank Dr. Greenbaum for providing the foundation and guidance on the development of the advanced chlorophyll fluorometers project. His insightful ideas and extensive knowledge provides me a great help on designing the in-line resettable lab-on-a-chip devices. I would like to thank Dr.Islam and Dr. McFarlane for serving on my PhD committee. Their honest and meaningful comments make my research more complete.

I sincerely thank Dr. Barbara R. Evans and Dr. Shigetoshi Eda, for providing and preparing all the bio-samples and reagents for my projects. I would give thanks to the staff and my student colleagues in Micro Analysis System Laboratory, my family and friends, for their help and support during my research work.

Last but not the least, I must thank the sponsors: US National Science Foundation and the University of Tennessee Research Foundation. Special thanks to Center for Nanophase Materials Sciences division, for providing cleanroom facility to fabricate the electrodes and sensor in my research.

# ABSTRACT

This dissertation presents the design and prototyping of three in-line microfluidic devices for continuous monitoring of particulate flows. The three devices are AC electrokinetic (ACEK) and acoustic sample preconcentration techniques for resettable particle enrichment, and an in-line somatic cell counter for mastitis monitoring.

For the ACEK preconcentrator, ACEK is a new and promising technique to manipulate micro/bio-fluid and particles. There are many advantages over other techniques, such as low applied voltage, low cost, portability and notable biocompatibility of lab-on-a-chip (LOC) device. We successfully developed a 3D multi-level electrode platform to extract bioparticles via AC electroosmosis (ACEO) and negative Dielectrophoresis (DEP). Based on ACEO and N-DEP, the device can exert a drag force on particles through fluid motion and collect and concentrate particles. Optimization with respect to AC frequency, external pumping rate and opening size of mesh electrode have been performed.

This research also studies the concentration effect by acoustic wave on diatom cells in seawater environment, since ACEK has limitation in high conductivity medium. Acoustic trapping uses mechanical resonance to focus the target particles into the designated trapping area. It has the advantages of high trapping efficiency, contactless trapping and compatibility with various fluids. Furthermore, since the trapping effect and the vertical trapping location are dependent on the particle properties, binary particle separation and sorting are also highly possible.

Another contribution of this dissertation is the ACEK based capacitive somatic cell counter for use in dairy industry. Using our design, capacitive sensing is capable of

detecting and quantifying target concentration in many types of biological solutions. The capacitance changing rate of device can be correlated with different concentrations of somatic cells. In this work, we successfully detected the concentration level of somatic cells in raw milk. The results were verified by flow cytometry.

# TABLE OF CONTENT

# LIST OF FIGURES

# CHAPTER ONE: INTRODUCTION

## 1.1 Overview of microfluidic and lab on a chip

Micro-total-analysis system (μTAS), also referred to as laboratory-on-a-chip (LOC) is a miniaturized device that perform all or part of a biochemical analysis. LOC devices may incorporate microfluidic components, microsensors, microactuators, and customized surfaces created by chemical modification or coatings with inorganic and organic materials.

The goal of μTAS and LOC devices is to achieve increased efficiency and reliability through integration of channels, mixers, separators, reactions chambers, electrodes, and detectors into single devices and reduced reagent consumption. Microfluidics is the study of transport processes in microchannels. Microfluidic devices make up the primary components of many μTAS and LOC devices. The specific microfluidic devices with different functions, such as channels, valves, mixers, pumps, filters, and heat exchangers have been reported in many literatures. These components allow metering, dilution, flow switching, particle separation, mixing, pumping, incubation of reaction materials and reagents, and sample dispensing or injection. By utilizing the microfluidic technology, device will improve throughput of samples, increase accuracy, and lower analysis cost.

The focus of microfluidic device development in this thesis is mainly related with detection schemes. Current detection and diagnostic devices are highly labor-intensive and lack of automation, and have to be tested in the central clinical laboratories with trained technician. Further, the traditional detection methods often cannot meet the limit

of detection requirement for practical samples. Therefore, system integration and the improvement of sensitivity become the two main challenges in the development of portable detection device. The advent of LOC technology provides new methods to overcome these two challenges.

## 1.2 Challenge of detection and particle concentration

Many techniques have been developed or adopted for detection of chemical, medical and biological processes using LOC devices. No matter which method we choose, the limit of detection is always a concern. For example, direct detection and measurement of pathogenic particles are very difficult in biological threat and environmental security area, since the density of the target particles can extremely low [1]. Also, bioterrorism is becoming more and more serious for homeland security [2]. In all these situations, the target particles are extremely diluted in air, water, soil and other solutions, and its concentration level is very low, but still harmful to people.

Many types of particles desire real time detection, including protein, E-coil, chlorella, diatom, air-born pathogen and other microorganisms. The size of these particles may be varied, but they share the same difficulty in detection sensitivity. In order to solve this problem, a preconcentration step of the microparticles is often used.

Various enrichment methods have been developed. Each method has its own advantages and disadvantages, and we should choose the suitable method based on the requirements of the target microorganisms and the device. This dissertation focuses on the research on improving the concentration level of microorganism of algae (chlorella) and diatom to allow for effective optic detection in real-time. AC electrokinetic method

(AC electroosmosis and dielectrophoresis) and acoustic standing wave force are chosen to be used with our preconcentrator since the ease with system integration and automation. Both methods are of low cost, small form factor and simple to operate. Also, an in-line portable detection method based on impedimetric sensing technology has been introduced for the measurement of somatic cells in dairy industry. The ultra-high sensitivity and integration ability make the impedimetric sensing method very attractive and competitive for the micro and nano- particle detection.

## 1.3 Outline of this dissertation

The outline of this thesis is as follows. Chapter two presents a detailed literature review on various trapping methods and their applications in microfluidics. The analysis and comparison for each trapping method have been explored and investigated based on the requirements for each different sample and devices. The theory of AC electrokinetic and acoustic method then has been discussed in Chapter three. Chapter four describes the experiment and design of particle trapping device based on ACEK techniques. Numerical simulation using finite element methods (COMSOL multiphysics) are conducted to verify the flow pattern. The acoustic trapping method for the diatom and chlorella concentration will be presented in chapter five. In chapter six, a capacitive changing rate based particle detection microchip has been introduced for diagnosis the mastitis disease on the aspect of counting the somatic cell level in raw milk. Finally, the conclusion and future work are presented in chapter seven.

# CHAPTER TWO: LITERATURE REVIEW ON PARTICLE ENRICHMENT IN LAB ON A CHIP SYSTEM

The ability to confine and manipulate particles in aqueous solution is highly desired for many fundamental and applied biochemical research and engineering. In the past decade, many particle enrichment methods have been developed for the use with LOC devices. These particle enrichment methods are based on diverse mechanisms, such as electrokinetic, magnetic, optical, hydrodynamic and acoustic techniques. In this chapter, we described these particle enrichment methods by classifying them into two major categories, namely non-electrokinetic and electrokinetic mechanisms.

## 2.1 Hydrodynamic trapping

Hydrodynamic trapping is a particle trapping method based on flow mechanic phenomena in the solution, including obstacles in the flow[1], stagnation point flows[2], micro-vortices [3] and micro-eddies [4], to limit and confined the particles.

Generally, hydrodynamic trapping can be categorized into two groups contact-based and non-contact methods. Contact based methods use fluid flow to control and confine particles against the channel wall or pre-set obstacles [5-7]. Contact-based methods are efficient in trapping very large numbers of particles and especially effective in a high flow rate device. However, hydrodynamic trapping has not shown a very performance on smaller particles. An example of contact-based flow device is produced by Di Carlo and Lee's group who designed a hydrodynamic trapping array, where trapping post arrays were arranged in slanted rows in a flow-through chamber[8]. Each post was designed

with a recess cavity to capture single cells or a smaller group of cells. The structure and results of this hydrodynamic trapping device are shown in figure 2-1.

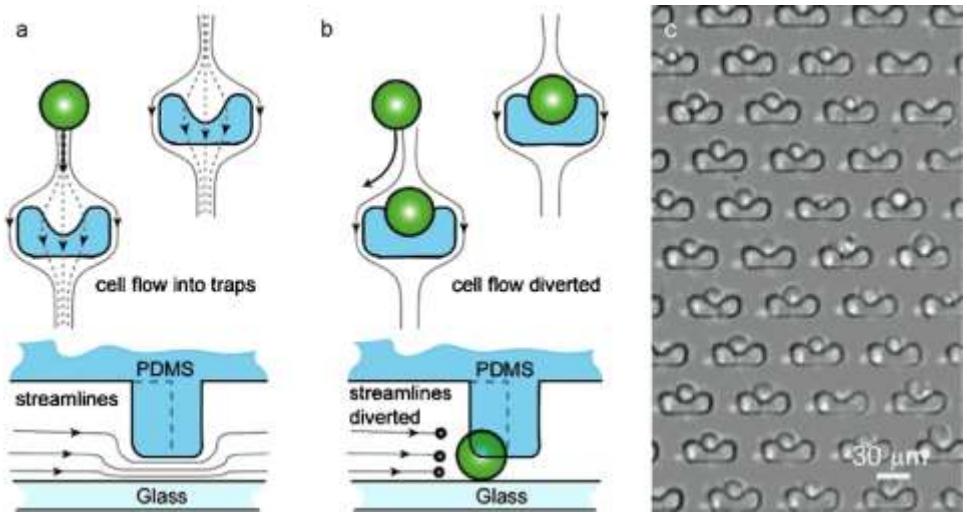


Figure 2-1 Hydrodynamic single cell trapping array as demonstrated by Di Carlo et.

Noncontact particle trapping methods are based on the stagnation point of flows, and can provide high resolution manipulation of single particles. It even has been used to study the dynamics of single DNA molecules. DNA dynamics can be characterized in a stagnation point flow with manual feedback control [9] and in a passive stagnation point flow without any active feedback control [10].

Reference [11] presents a very nice example of non-contact based hydrodynamic trapping. It is a flow-through device embedded with a meandering microchannel. The trapping sites were formed via channel that crossed the meander channel and displayed a smaller flow resistance than the main channel until a particle got trapped. This LOC system also provides a particle releasing function with a laser setup, which locally

generates microbubbles to change the pressure of the trapping site and then release the trapped particles. The mains structure of this device is shown in figure 2-2.

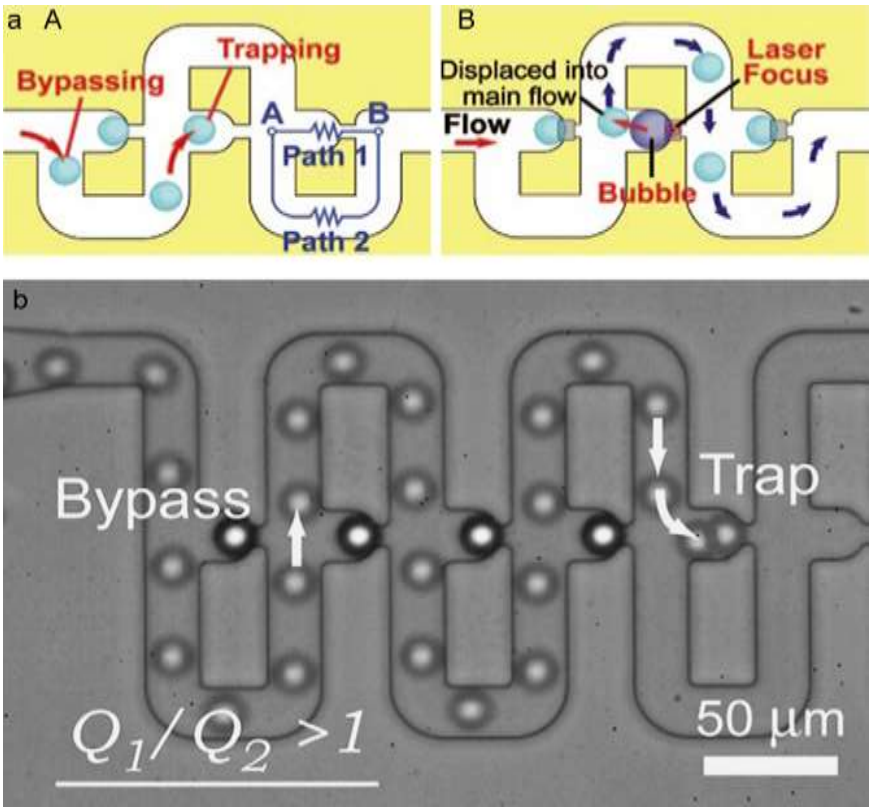


Figure 2-2 (a) Schematic of meander channel cross-flow trapping (b) Meander channel-cross-flow trapping in array format with release mechanism by laser induced bubble generation.

## 2.2 Optical trapping

Laser light sources have been used to trap and control particles (including cells) in aqueous solution. Selection, relocation, and precision control (trapping) of cells are possible through the use of light. Optical tweezer has been widely used in particle tapping research. Optical tweezer works by transferring momentum from tightly focused laser to

the particle. A transparent particle refracts and scatters the light and distorts the profile of the beam. The forces produced by this process cause the particle to be trapped near the beam focus [12]. Once a particle interacts with the light, it is simultaneously pulled to the center of the beam, where the light intensity is maximal. Then the particle will be pushed in the same direction as the beam travelling. Optical "tweezers" and "scissors" have been used to select single cells on a microchip, move them to the select channel, and lyse them using an optical scissors [13].

Another optical device for trapping and actively manipulating cells and microspheres is based on vertical-cavity surface emitting lasers (VCSELs)[14]. Laser output from the VCSEL functions as traditional Gaussian fundamental laser mode to optically trap biological cells, which is desired since the highest density of the light is located at the outer ring of the optical aperture. This allows for stronger optical confinement to be obtained for a lower total power. Also the VCSEL could be manufactured in an array form. Flynn group have demonstrated transport of human red blood cells on a small array, and suggest the possibility of an addressable optical tweezers which is suitable for a much larger array.

Single-cell sorting based on optical trapping and manipulation has also been demonstrated using human blood as a model system [15]. A counter-propagating dual-beam optical trapping was developed for improved manipulation of cells in 3D (figure 2-3). The He-Ne laser beams with wavelength 632.8 nm are directed onto the target sample, with white illumination from the top.

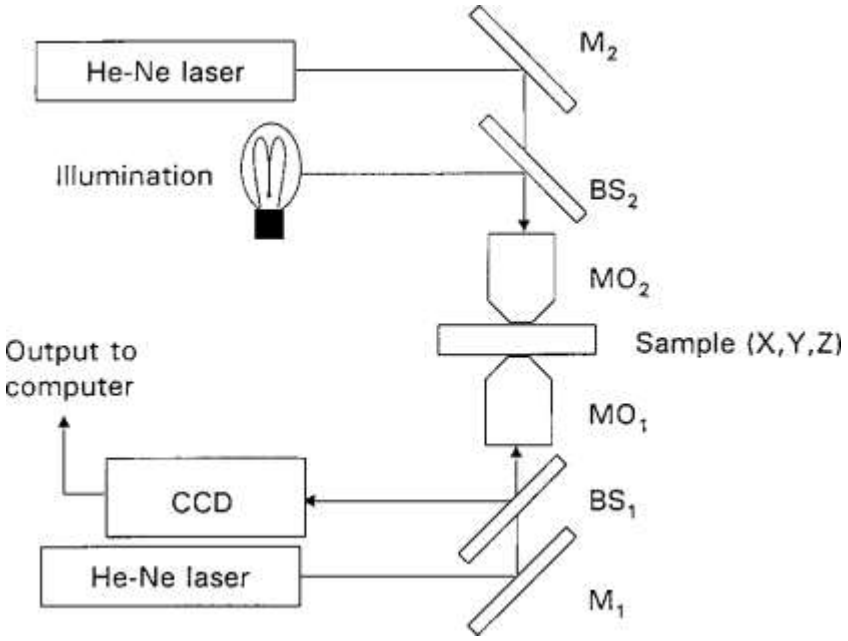


Figure 2-3 A counter-propagation dual-beam optical trapping was developed for improved manipulation of cells in 3D

## 2.3 Magnetic particle enrichment

Magnetic trapping techniques utilize magnetic fields and magnetic particles of different kinds and sizes. Traditional magnetic particles have a magnetic core and a non-magnetic coating that can be modified with receptor molecules to bind to specific target particles. Magnetite is one of the more common materials, as it is hard to oxidize. Magnetic trapping is suitable for both small and large magnetic particle. Bioparticle can be bond with magnetic particle to achieve trapping. The range of the particle size is from 5 nm up to micro-scale. The smaller particle which is less than 42 nm can be consider as non-magnetic particle, once the external magnetic field removed. Larger particle will maintain a center degree of magnetization even after the magnetic field removed.

Therefore, for the larger magnetic trapping, it is more difficult to remove once trapped than the smaller particle [16].

From the aspect of type of magnets used to generate the magnetic field, the magnetic trapping can be divided by utilizing permanent magnets and electromagnet. The microfluidic system using permalloy magnetic elements are designed and fabricated by Simstrup et al [17]. The permanent magnets were embedded and aligned perpendicular into the channel. A homogenous magnetic field has been generated perpendicular to the microfluidic channel. By supplying the magnetic field, fluorescent particles (1 μm) were trapped in fluid flow with flow rate (5 μl/min) and a successful release of trapped particles was shown.

Also, the magnetic trapping has been used to the DNA sequencing and hybridizing. Lund-Olesen group used a magnetic bead with a diameter of 1 μm to bind with DNA. In the hybridization channel embedded with a staggered Herringbone mixer, the magnetic particles confined at each trapping location were leveled out and improved the diffusion of DNA.

A magnetic trapping system using electromagnets has been demonstrated by Lee et al [18]. They deposited two layers of gold conductor with an insulative layer in between to generate magnetic field. The local magnetic field can be generated by driving a current through the conductors. The objects in the magnetic field were able to move, hold and even rotate. Reference [19] developed a flow-through device for trapping magnetic particles by using micro coils and magnetized micro pillars. A trapping ratio of 84% was achieved, which is a decent trapping efficiency.

## 2.4 Acoustic trapping

Acoustic trapping is receiving more attention as an effective and nonintrusive method of manipulating particle in microfluidic systems. The combination of microfluidics and acoustic standing wave technology has led to a very effective strategy for non-intrusive manipulation of micro-particles in integrated systems. The ultrasonic standing wave generates a harmonic potential cavity where particle trapping takes place. The absorption of high frequency acoustic energy by the cell and fluid generates pressure forces that cause aggregation of cells at pressure node or antinode.

The acoustic trapping technique is able to move and spatially localize particles and cells in an acoustic resonator. Acoustic force has been widely used to induce retention against flow and aggregation of particles in the specific trapping location. Acoustic trapping device generates trapping effect by inducing movements in solids and fluids by means of piezoelectric materials, through which an electric signal is converted in to mechanical vibration.

The key advantages of acoustic trapping are shown as follows:

- By using programmable signal generators, vibration waves of complex shape and frequency content can be generated easily and repeatedly.
- By appropriate tailoring of the transducer set-up, different modes of waves and vibrations can be produced and measured selectively.

According to above-mentioned advantages, acoustic trapping can be used for various benefits, such as reducing the time needed to create 3D cell cluster, enhancing particle- based bioassays and facilitating interaction studies of both cells and particles.

The area of enrichment of low concentration samples and washing or fractioning of cell population prior to selectively detection method becomes more and more popular in microfluidic system. Several configurations and methods of the acoustic trapping device have been introduced.

Standing waves are the most commonly mechanism used to build up acoustic potentials with high intensity in acoustic trapping system. Standing waves can be generated by several methods and configurations, such as two opposing identical transducers, single focused reflector transducer, layered resonators, transversal resonators and SAW device. These different types of resonator configuration can be divided into two different groups, one is multiple nodes resonator and the other is half-wave length resonator. Each design has its own requirements on excitation conditions and fitting particle. The configuration and application for each design are presented next.

### 2.4.1 Multiple resonator

For the two opposing transducers method, Wu et al. firstly presented an early example of an acoustic tweezers based on this principle in 1991[20]. Two focused transducers opposing each other were operated under frequency 3.5 MHz. A well-defined potential were created in order to trap the latex bead and frog eggs. The particle trapped in Wu's device is rather large, however later on Hertz presents a similar device for the trapping of 2.1 μm glass particle with a frequency 11 MHz [21]. Figure 2-4 shows the main configuration of Hertz device. The design generated lateral forces of the same magnitude as the axial forces to promote 3D-trapping. Since the focal point is located

several wavelengths away from the transducer, the size of device is rather large and greatly limit the application in microfluidic system.

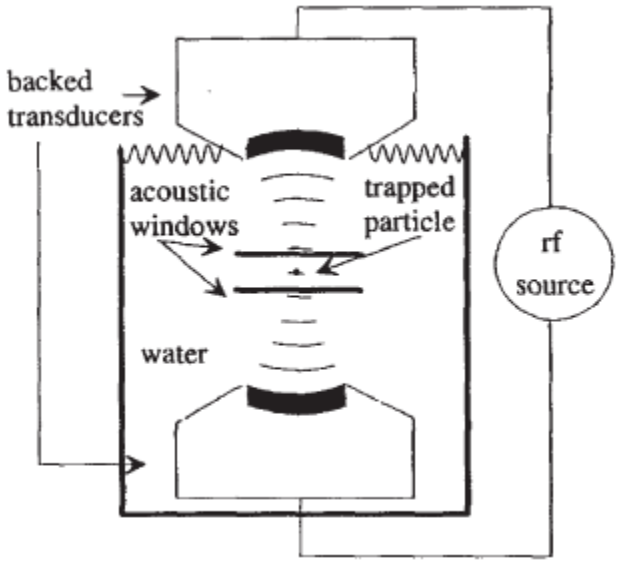


Figure 2-4 Two opposing focused transducers in a confocal arrangement generating a standing wave field where the particles can be trapped. The trapping force is strongest in the focal spot.

A single focused transducer and a reflector can also produce the standing wave field. Combined the principle with microfluidic set-up for trapping in quartz capillaries, Wiklund et al. designed and fabricated the counter reflect acoustic trapping device[22]. The main structure is shown in the figure 2-5. There are several nodes created along the capillary where particles were trapped. The entire device assembled the capillary, transducer and reflector together and totally is immersed in water bath to ensure that the acoustic waves from the focused transducer entered the capillary. Compared with two

counter transducer device, it is greatly improved by reducing the device dimension and also being able to trap small particles in micro-scale.

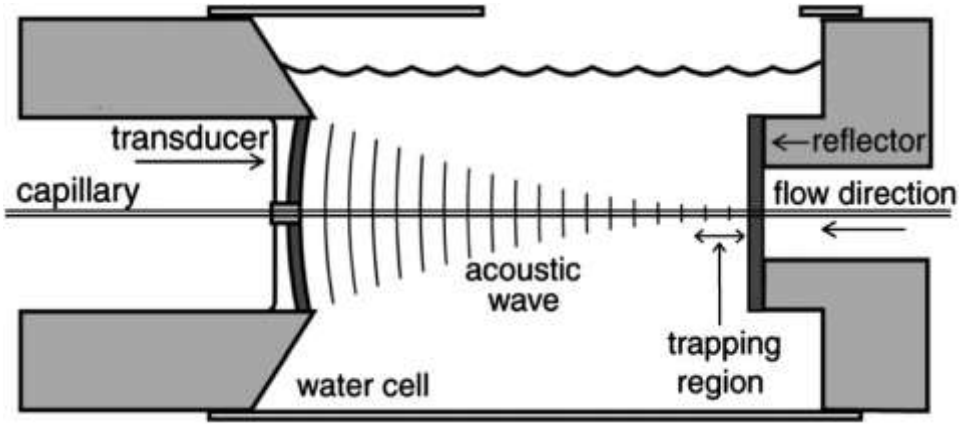


Figure 2-5 Particles are trapped in a standing wave in a capillary using a focused transducer and a reflector.

### 2.4.2 Half wavelength resonators

The two resonator configuration contains multiple nodes with server wavelength of the standing waves, which actually is not very suitable for the microfluidics system. Although multiple node resonators can sometime be beneficial, the most common device uses half wavelength resonator.

Layered resonator is one kind of half-wave length resonators. A layered resonator consists of multiple layers which all have a very specific role in the resonator system as the sound wave passes through them, building up the resonance. The different layers can be seen in figure 2-6. The transducer generates sound or vibration and pass through the coupling layer, which is fabricated in order to get good acoustic transmission. The

matching layer, also called transmission layer, were deposited as the bottom of resonator chamber and also acts as a reflector layer of the surface standing wave. The particles and cells are pumped into or trapped in the fluid layer. At the top of chamber is the reflector layer that is responsible for reflecting the incoming wave back into the fluid layer.

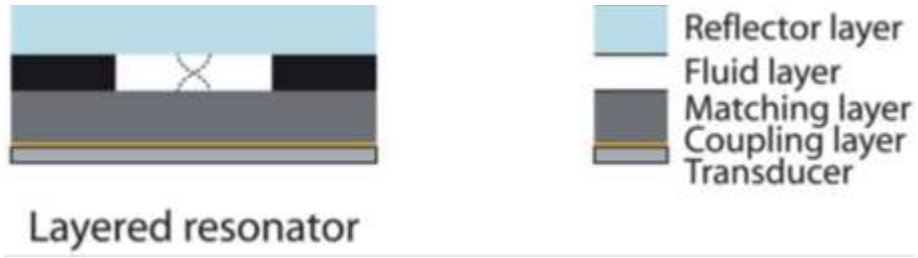


Figure 2-6 The structure of a layered resonator

The half wavelength resonator reduces the size of total trapping device significantly, which makes the integration of acoustic trapping in microfluidic systems possible. Base on this principle, Spengler and Coakley introduced a system to study the properties of several different cells [23]. The system was designed as a layered resonator to achieve high Q-values. A matched reflector and a spacer were used together with a 3 MHz resonator to create a chamber with a half-wave length resonance. The lateral component of the acoustic radiation force was holding the particle in the channel against the flow. Later on, an alternative design was fabricated incorporating a circular transducer, shown in figure 2-7 [24].

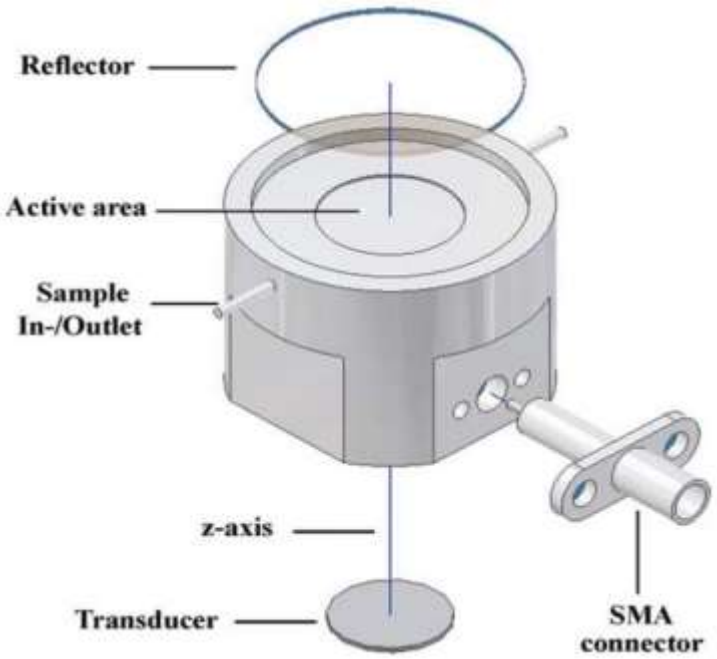


Figure 2-7 Schematic of a layered resonator, based on a circular transducer, matching layer and a glass reflector. The lateral component of the radiation force will hold the particles in chamber, once the sample flow is injected in the chamber.

There is one point need to mention that, for the half wavelength resonator, the particles usually are trapped in the center of channel (pressure node). The quarter wavelength fluid cavity can be used to push particles towards the surface which is needed for capturing specific particles [25].

Rather than layered resonator, a transversal resonator is designed and operated a standing wave perpendicular to the incident direction of actuation. The main structure is shown in figure 2-8. The transversal mode of the acoustic trapping can be achieved by exciting the resonator at a frequency that matches half wavelength with respect to the channel width. The resonator of this device should be made of materials with low

acoustic losses with a high-Q value, such as glass, silicon or metal, because the entire device is actuated in the transversal mode [26]. An obvious advantage of the transversal resonator configuration is that acoustic trapping is performed in plane with resonator chip, and it is very convinced to observe the whole trapping procedure. Also the integration with other microfluidic component is very easy to be accomplished.

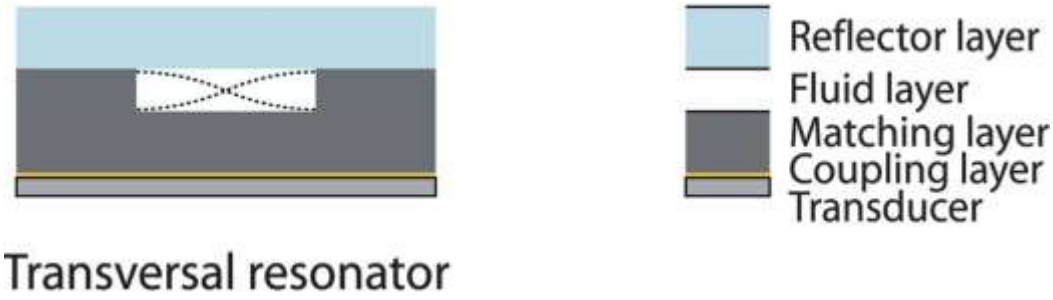


Figure 2-8 the structure of a transversal resonator

### 2.4.3 SAW array resonator

The Surface Acoustic Wave device consists of interdigitated electrode transducer positioned outside the channel to generate surface waves to confine and manipulate particle in the channel. Typical SAW devices are fabricated in PDMS using soft lithography. With the metal evaporation and lift-off technique, the metal straps have been fabricated on a piezo-electric substrate ($LiNbO_3$) to create the interdigitated electrodes. The channel is fabricated by modeling PDMS on a SU-8 photoresist. The PDMS channel then can be bond on the transducer wafer by plasma evaporation. An improved SAW device are designed and fabricated by Shi et al., called standing surface acoustic wave (SSAW) [27]. The two SAW transducers are deposit oppositely beside the channel and

generate the pressure field. The waves of the two opposing field will enter the channel to determine the position of the SSAW and trap the particle. This device avoided the water/sample fluid directly contact with the transducer and greatly improved the stability of the trapping device. The main principle and schematic of one example device are shown in figure 2-9.

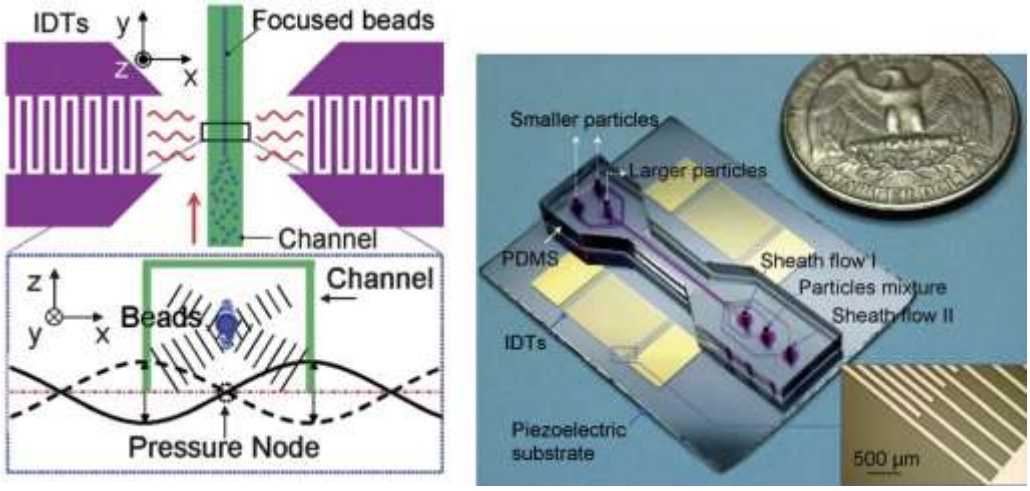


(b)

Figure 2-9(a) Basic principle of SSAW device for the beads trapping. (b) Real SSAW device with a PDMS channel.

## 2.5 Electrokinetic trapping methods

Electrokinetic is one kind of electric force interacts on the particles and fluid motion in microfluidic system. Electrokinetic effect in microfluidics includes electro-osmosis, electrophoresis, electro-thermal, streaming potential, and dielectrophoresis. Electrokinetic phenomena in microfluidic devices for moving fluid and

particles (including proteins, cells, bacteria and viruses) is essential for μTAS and other LOC applications. According to the electric source type, the electrokinetic can be defined with DC electrokinetic and AC electrokinetic. From the main mechanism aspect, trapping particles by using electrokinetic methods can be achieved with fluid motion and particle motion. In fluid motion method, particles are manipulated by the fluid due to the fluid viscosity and typically trapped at a stagnation point in the fluid field. For the particle motion method, electric force directly acts on the particle and concentration the specific area. Both of the two methods have their own benefit, suitable condition and exciting requirement. In next section, the basic principle and applications for each method will be introduced.

### 2.5.1 Fluid motion trapping

Particle enrichment can be accomplished by fluid motion generated by AC electro-osmosis, and AC electro-thermal effect. It has no dependence on particle size and owns larger effective area as it takes advantage of the hydrodynamic flow. Generally, particles suspendly stay at the stagnation point in the flow. Electrofluidic forces include AC electroosmosis and AC electrothermal effects that require only a low voltage (a few volts) to generate fluid motion. Electrokinetic trapping by the fluid motion can provide a very efficient delivery of target molecules to the trapping sits and enable a high degree of integration and automation for the whole system.

#### 2.5.1.1 Electro-osmosis trapping

Electro-osmosis refers to the microfluidic motions generated at the electrode surface. It is caused by the Coulomb force induced by an electric field on net mobile electric charge in a solution. Both DC and AC electrical signal can be used to generate fluid motion. Due to the limitation of exciting requirement and experiment condition, DC electroosmosis (DCEO) is typically used for the fluid pumping, but not the particle concentration. Therefore, in this section we mainly introduce the AC electoosmosis trapping device and applications.

ACEO refers to the microfluidic motions generated at electrode surfaces when ac signals are applied. ACEO flow occurs when the moving ions drag the surrounding fluid with them due to the viscous effect, creating “bulk flow”. Typically it happened at low frequencies when the interfacial impedance dominates. Concentrators of particles using ACEO flow are reported by several groups. There are mainly two major configurations of ACEO flow so far. One uses “side-by-side” electrode pairs [28] and the other uses “face-to-face” electrode plats [29]. Both designs produce non-uniform electric field distribution and creating tangential electric fields along electrode surface, leading to ACEO flows.

An example of using side-by-side electrode configuration is show in figure 2-10 which is used a dot-ring shape to generate ACEO flow [30]. ACEO electrofluidic force generates microflows that convey particles from the bulk of the fluid onto the electrode surface.

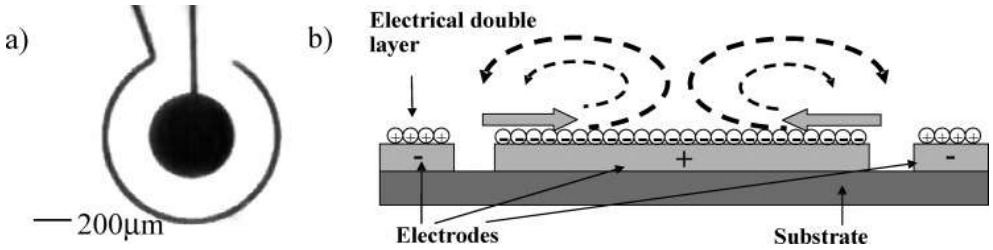


Figure 2-10 (a) Electrode design of the ac electroosmotic processor (top view). (b) Schematic (side view) illustrating electrode polarization and formation of a electroosmotic flow. Solid arrows represent the AC electroosmotic force and dotted lines indicate the flow pattern. Particles are trapped at the flow stagnation point which generated by the counter-rotating.

Another example of side by side ACEO trapping is to use planar electrodes for on-chip bioparticles trapping [31]. The device configuration is shown in figure 2-11. Two large vortices and two small vortices are generated by the ACEO flow and the particles are trapped at the stagnation location created by the counter-rotating vortices.

The utilizing of a DC offset AC signal for the ACEO flow greatly improve the trapping effect, which is known as “Biased ACEO”. Electrochemical reactions at the electrodes also can generate ACEO flow due to Faradaic charging. Since most bioparticles are negatively charge, the particle with biased ACEO will move toward positively biased electrodes [32]. As shown in figure 2-12, experiments have demonstrated superior capability of biased ACEO in concentrating particles.

Figure 2-11 (a) Electric field distribution above a pair of planar electrodes. The tangential component changes sign at the predicted stagnation lines (axes: relative dimensions). (b) With capacitive charging, four counter-rotating vortices are formed above the electrodes due to changes in tangential electric fields. (c) Experiment result of assembled E.coli lines on an array of electrodes at 1 Vrms. An an appropriate strength of electrode polarization, particles aggregate at the stagnation point.

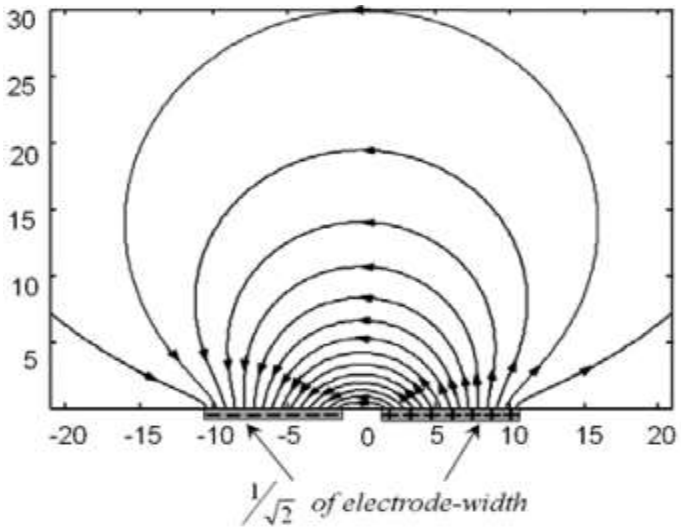


(a)

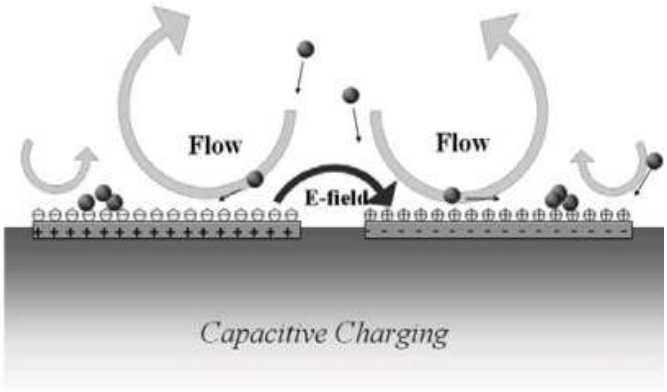


(b)

Figure 2- 11 (a) and (b) continued

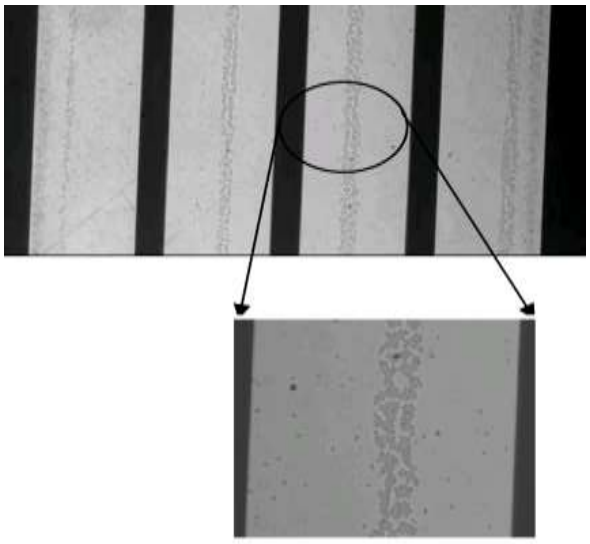

(c)

Figure 2- 11 (c) continued

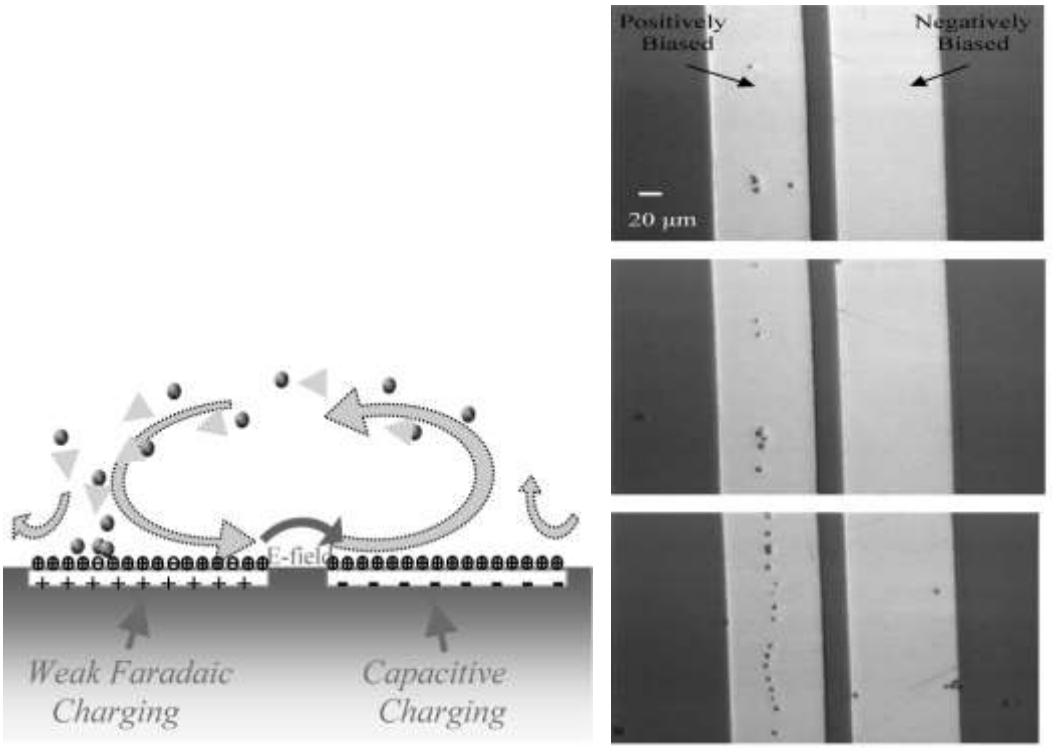


(a) (b)

Figure 2-12 (a) At an appropriately biased AC potential, asymmetric vortices are formed above two electrodes, streamlines from capacitive charging and faradaic charging become connected, forming a large vortex over the electrode pair. Particles can be moved from the right to the left electrode. (b) Three frames of Chlorella forming a line by biased ACEO at an interval of 40s.

An example of "face-to-face" electrode design is shown in figure 2-13. Two electrodes are facing each other in parallel and of different size. The ITO (indium tin oxide) glass slide was used as the top electrode and Au with Si substrate are the other electrodes. Tangential electric fields are generated at the edge of the smaller electrode.

ACEO flow are driven along the electrode towards its center, conveying particles from the bulk of fluid onto the electrode surface.

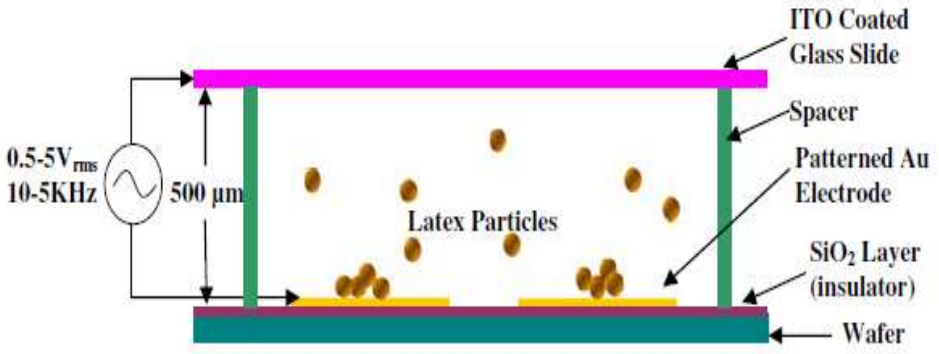


(a)

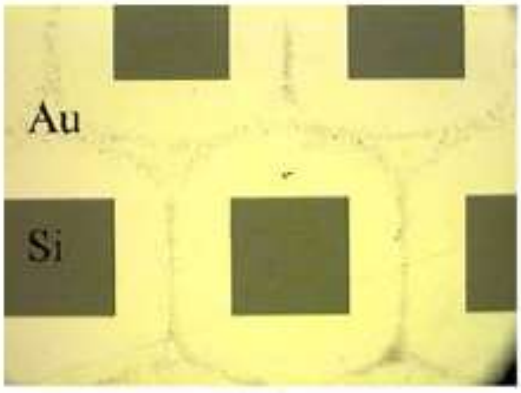


(b)

Figure 2-13 Micrographs of trapped particles by parallel plate electrode. Bright areas are conductive (Au) electrodes and dark areas are the insulative base (Si) (a) Schematic of the experimental setup of parallel plate particle trap. (b) 200 nm particles forming hexagonal patterns. Particles are trapped along the center lines of the Au stripes [33].

#### 2.5.1.2 AC electrothermal trapping

ACEO trapping is limited by the sample conductivity, and only suitable for the low applied frequency. Peak ACEO velocity decrease with increasing conductivity, and can be neglected for the fluid with a conductivity more than 100 mS/m. Therefore, AC electrothermal trapping is used to trap the particles in most of bio-fluidic solution.

AC electrothermal effect results from the interactions of AC electric fields and temperature gradients in the fluid. Electrothermal fluid flow is produced in the bulk fluid in the region near the electrodes and has noticeable conductivity and voltage dependence. Similar as ACEO flow, ACET flow still have two major configurations for the trapping device, “side by side” and “face to face”. Reference[34] demonstrates a “face to face” ACET trapping device, as shown in Fig 2-14. 500 nm fluorescent particles (Molecular Probes) have been trapped in the working fluid with a high conductivity 0.22S S/m.

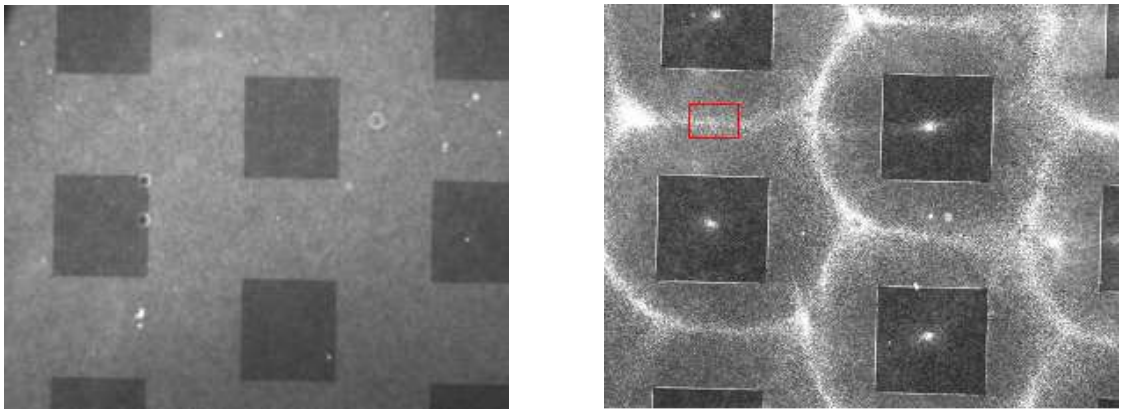

(a)Before applying AC voltage (b) 5 minutes after applying AC Voltage

Figure 2-14 Wafer surface before and after AC signals being applied to generate convection and to trap particles. Particles were directed towards null points of electric fields, and became trapped. (Bright areas indicate high density of particles)

### 2.5.2 Particle motion trapping

In particle motion trapping, electrokinetic forces are directly exhibits on the particle to concentrate or even separate particles. There are two main electrokinetic forces for the particle trapping. One is electrophoresis (EP) and the other one is dielectrophoresis (DEP), which uses DC electric signal and AC electric signal respectively.

#### 2.5.2.1 Electrophoresis trapping

Electrophoresis is the effect by which charged species in a fluid are moved by an electric field relative to the fluid molecules. The charged species accelerates until the electric force is equal to the frictional force. In electrophoresis the liquid is stationary, while the particles move under the influence of the electrical charge. DC electrophoresis is used for charged bioparticles, and combined with techniques of nanoporous ion-permeable membranes for the operation. Reference[35] designed a microfabricated porous membrane structure that enables electrokinetic concentration of DNA and protein samples. The concentration of the trapped DNA increased 100-fold. Another type of online trapping device is called free flow electrophoresis, which includes electric field gradient focusing (EFGF), field-amplified sample stacking (FASS), and isotachophoresis (ITP). These three methods capitalize on spatial gradients of electrophoretic velocity of sample analytes as affected by gradients in ion density, mobility, or solvent viscosity. EFGF uses an opposing hydrodynamic flow and an electric field gradient to concentrate and separate proteins. Proteins can be concentrated up to 10000-fold [36]. FASS uses a gradient in electrolyte conductivity and resulting non-uniform electric fields to produce inhomogeneous electromigration fluxes. FASS can reach a concentration factor of 1100

using a capillary [37] and a factor of 100 using microchip [38]. For the ITP device, the sample is set between a terminating electrolyte with low mobility ions and a leading electrolyte with relatively high mobility ions. Reference [39] presents milionfold signal enhancement of 100 pM analytes using on-chip transient ITP method and its integration with CE.

#### 2.5.2.2 Dielectrophoresis trapping

Dielectrophoresis (DEP) is the physical phenomenon whereby dielectric particles, in response to a spatially non-uniform electric field, experience a net force directed toward locations with increasing or decreasing field intensity according to the electrical properties of particles and medium. Generally, there are two types of DEP, one is called positive dielectrophoresis (pDEP) and the other is called negative dielectrophoresis (nDEP)[40]. pDEP is one kind of force attracting the particles to the area of the maximum electric field gradient, while nDEP is repulsing the particles to the area of the minimum electric field gradient. Both of these two forces can be used to trap the particles by using different device configuration. Figure 2-15 shows two examples of pDEP and nDEP traps, respectively. The low-field region is at the center of the polynomial electrodes and the high-field regions are along the electrode edges. At frequency above the interfacial relaxation frequency (the crossover frequency), the particles are less polarizable and experience negative DEP. At low frequencies, the particle becomes more polarizable and experience positive DEP which trapped at the edges of electrodes.

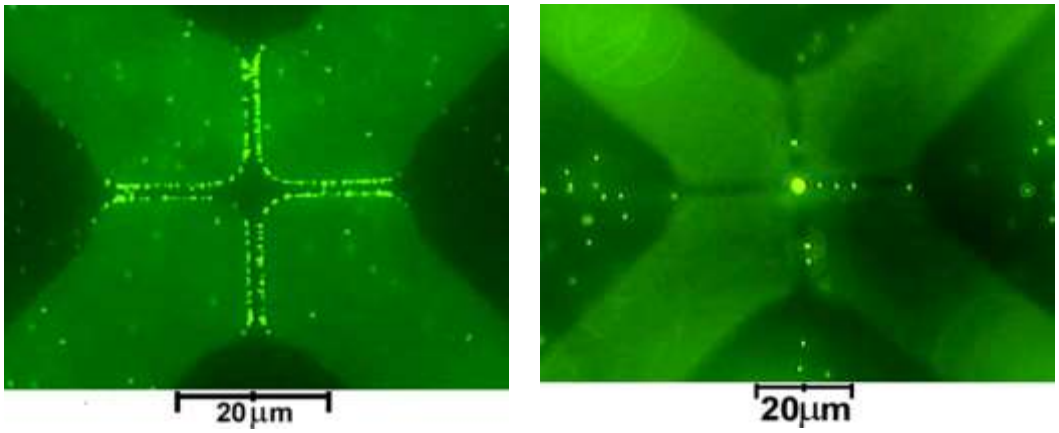


(a) (b)

Figure 2-15 (a) Positive DEP with an applied signal of 5 V peak to peak at 500 kHz. The particles collect along the edges of the electrodes at the high-field regions.(b) Negative DEP for an applied signal of 5 V peak to peak at 5 MHz. The particles are repelled from the edges, collecting in the low-field region [41].

DEP is proposed for cell and particle sorting, trapping, cell-ac-impedance analysis, cell lysis, and even the manipulation of molecules and reagents droplets. Since the 1960s, this technique has been successfully used for the manipulation of microbioparticles. By using the difference of dielectric properties between live and dead cells, Li and Bashir (2002)[42] concentrate and separated live and heat-treated, fluorescent stained Listeria innocua cells with great efficiency on micro-fabricated devices with interdigitated electrodes. Medoro et al [43] have shown LOC electronic manipulation and detection of microorganisms based on the use of closed dielectrophoretic cages combined with impedance sensing. A printed circuit board (PCB) prototype was used to trap, concentrate, and quantify polystyrene micro-beads. Their result showed the effectiveness of the

approach for particle manipulation and detection without the need for external optical observation or chemical labeling. Trapping and isolating particles from complex sample solutions using a bead-based assay for virus detection, and DEP deflector has been demonstrated. Individual antibody-coated beads with hepatitis A virus bound to their surface were trapped by nDEP in a field cage and analyzed by fluorescence microscopy [44]. In addition to simple electrode layouts, a series of bar-shaped electrodes can generate a travelling-wave dielectrophoretic force (twDEP), useful for controlling the motion of the bioparticles. Lee and Fu (2003) review the use of dielectric forces for trapping and manipulation cells, proteins and DNA.

## 2.6 Comparison of the different trapping techniques

According to trapping method described above, a comparison result of the advantage and disadvantage for each method have been list in TABLE 2-1.

Due to the damage of particles, especially on the bio-particle, the optical trapping technique should not be considered in this project. Also magnetic trapping require the magnetization of particle, or binding with magnetic particles, and the experiment is very complex and un-reliable. Therefore, magnetic trapping are not our choice either. Actually, both of these two methods are suitable for very smaller particles and single particle trapping. Algae and diatom trapping are kind of cluster trapping and cannot be trapped by these two method very well. The trapping force of hydrodynamic is not as strong as other techniques which make the trapping result less stable and reliable. The trapping effect of hydrodynamic is easy to be influenced by other noise force.

Acoustic trapping method is suitable for bio-particle (size: several μm) in a pump-through system. It shows a very good performance on cell cluster trapping with a rather high trapping efficiency. Since it is not electric conductivity dependent method, it is best to use acoustic trapping for the enrichment of diatom trapping.

AC electrokinetic trapping is also a decent method for the bio-particle trapping. The system is not very complex and easy fabricated. The trapping effect is quite stable and repeatable. In case the algae live in a freshwater environment with a low electric conductivity, the ACEO and DEP combined trapping method is the first choice for this project.

Table 2-1 Comparison of different trapping techniques

| | Advantage | Disadvantage |
|---|---|---|
| **Optical** | Good performance on single cell trapping<br>Trapping force (100-2000pN) | Damage particle,<br>Not suitable for bio-particles,<br>Particle transparent required<br>High system complexity<br>Off-line application |
| **Magnetic** | Bio-particle compatible<br>Cluster trapping<br>Trapping force (2-1000pN) | Magnetic particle required,<br>High system complexity<br>Off-line application |
| **AC Electrokinetic** | Bio-particle compatible<br>Performance good on both single and cluster trapping.<br>Trapping force (200-400pN)<br>Low system complexity | ph, ion, clean surface required |
| **Acoustic** | Bio-particle compatible,<br>Performance good on cluster trapping,<br>Trapping force (100-400pN)<br>Low system complexity | Less reliable on single particle trapping |
| **Hydrodynamic** | Bio-particle compatible,<br>Suitable for both single and cluster particle trapping<br>Low system complexity | Trapping effect is not very good, easy to be influenced by other force (Noise) |

# CHAPTER THREE: BASIC THEORY OF PARTICLE ENRICHMENT

Particle trapping in micro-fluidic system can be achieved in several different ways, such as acoustic trapping, optical trapping, magnetic trapping, hydrodynamic trapping, protein rolling trapping and electrokinetic trapping. As described in the last chapter, each method has its own advantages and disadvantages. In this chapter, the basic principles of acoustic and AC electrokinetic particle trapping methods used in this dissertation have been introduced.

## 3.1 Acoustic enrichment by standing wave

. Acoustic trapping has been widely used for non-contact trapping of cells or microparticles. Particle manipulation based on acoustic standing wave has been developed and investigated in a macro scale system for the last five decades. More recently it has entered microfluidic area, and demonstrated the integration of particle trapping and manipulation in lab-on-a-chip system.

A standing acoustic wave is able to produce stationary pressure gradients [1] [2]. The pressure gradient will exert forces on the particle in a liquid medium. The distribution and amplitude of the forces are directly related with the density and compressibility of the particles and medium. Generally, acoustic forces for particle trapping are divided into primary radiation forces (PRF), lateral radiation forces (LAT) and secondary inter-particle forces [3]. Figure 3-1 schematically illustrates the basic principle of acoustic enrichment.

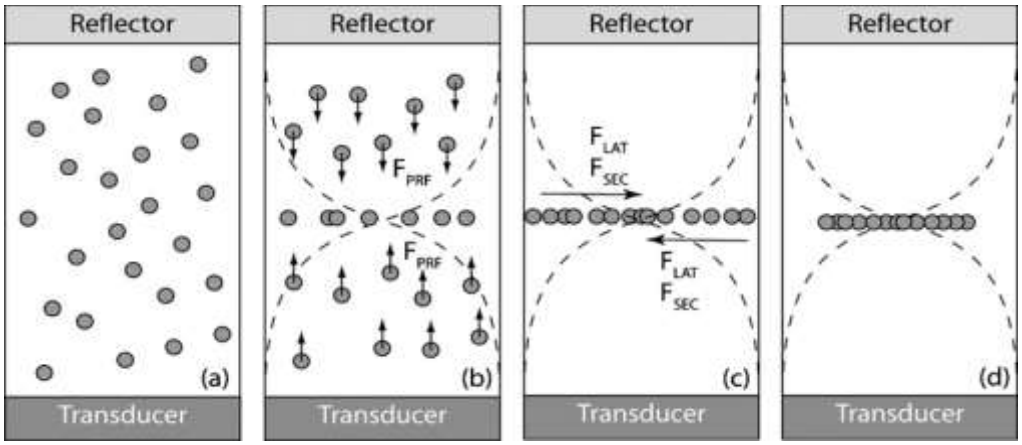


Figure 3-1 (a) Particle freely suspended in a medium.(b) Single node standing wave forces the particles towards the node by primary radiation force. (c) Particles towards the central axis of the standing wave by the lateral force. (d) Particle trapping complete[4].

The primary radiation force is the largest force on particles subject to a harmonic standing acoustic wave. The direction of PRF is vertical and perpendicular to the flow direction, shown in figure 3-2.The lateral radiation force is generated by spatial variations in the acoustic pressure field. The direction of LAT is horizontal which is same as the flow direction. It will keep the particles positioned at sable point in the fluid. The inter-particle force is created by pressure wave being reflected on particles. It is one kind of force between particles. It helps the particles form cluster, and stabilize trapped particles, which is good for the particle enrichment.

### 3.1.1 Primary radiation forces

Particles in an acoustic standing wave field will encounter acoustic primary radiation force. Whether they would be forced onto pressure node or pressure antinode depends on the material properties of density and compressibility. A node is a point along

a standing wave where the wave has minimum amplitude (zero displacement). The opposite of a node is an anti-node, a point where the amplitude of the standing wave is a maximum. Figure 3-2 shows a clear demonstration of the primary radiation force in microfluidic channel. When there is a standing wave in the solution, the acoustic pressure at x, the distance from a pressure node in the solution, is described by [5]

$$\Delta p(x) = p_0 \sin(kx)\cos(\omega t) \tag{3-1}$$

where k is $2\pi/\lambda$, the wave number of ultrasonic radiation, $p_0$ is the acoustic pressure amplitude , $\omega$ is the angular frequency, and t is time.

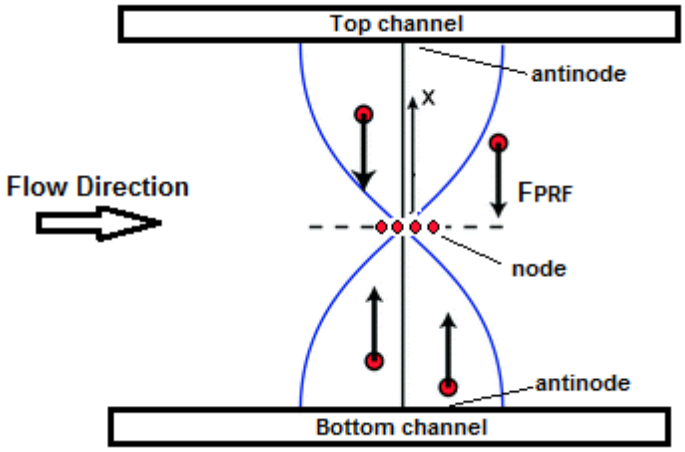


Figure 3- 2 Geometry associated with primary radiation force

L.V.King [6] introduced the theory of acoustic trapping force on the compressible circular discs, while Gorkov, Yoshioka and Kawashima presented the acoustic trapping theory on the compressible spherical particles later on [7]. In this dissertation, we consider the forces of a standing-wave acoustic field act on the compressible particles

with a sphere structure. According to the latter theory, the primary radiation force acting on a compressible sphere, such as chlorella and diatom used in this work, can be described as

$$F_{PRF} = \frac{-\pi P_0^2 V \beta_0}{2\lambda} A\sin(2kx) \tag{3-2}$$

where V is the volume of particle, and A is a constant given by

$$A = \frac{5\rho_P - 2\rho_0}{2\rho_P + \rho_0} - \frac{\beta_P}{\beta_0} \tag{3-3}$$

where $\rho_P$ and $\rho_0$ is the density of the particle and solution, $\beta_p$ and $\beta_0$ is the compressibility of particle and solution. Most particles will be affected by the acoustic force as long as the particles property differs from the surrounding medium. With the same surrounding medium, different particles will have different constant A, which makes particle separation possible. When A is positive, the particle moves to the node position and aggregate there. If A is negative, the particle moves to the antinode position. Also, according to equation 3-1, it can be seen that microparticles with a larger volume will experience stronger force when placed in an acoustic standing wave. The particle's density and compressibility directly influence the magnitude and direction of the acoustic force.

### 3.1.2 Lateral radiation force

In a real trapping system, the goal is to use the acoustic forces to hold particles against the flow in the channel. Although the primary radiation force (PRF) is commonly used to confine and manipulate the particle in the acoustic standing wave field, the

direction of PRF is perpendicular to the flow through direction and just pushes the particles to the pressure node. Apart from the axial component of PRF, the trapping device actually relies on the lateral radiation force to retain the particle in place, as show in figure 3-3. According to the report of M. Groschl et al [8], the amplitude of lateral radiation force can be expressed as:

$$F_{LAT} = \pi \rho_0 \omega^2 R^2 u_0 u_m \tag{3-4}$$

where, R is the radius of the particle, $u_0$ is the displacement amplitude at the center of the particle and $u_m$ is the difference in displacement amplitude at the edge of the particle compared to the center. From equation 3-4, it can be seen that the lateral radiation force is still size dependent as the primary radiation force. The larger particle encounters a larger lateral radiation force. The greater the difference in amplitude between the center and the edge of the particle, the larger the trapping force will be.

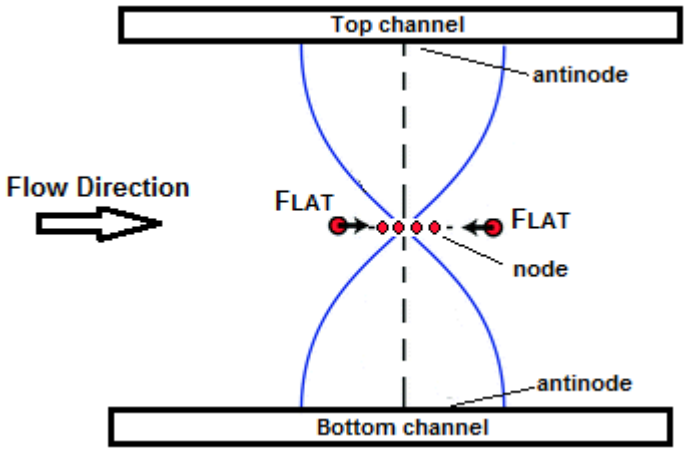


Figure 3- 3 Geometry associated with lateral radiation force

### 3.1.3 Inter-particle force

The third force in the acoustic trapping device is the force generated between particles, so called inter particle force. It is created from the main acoustic field scattering on the particles that are being trapped. The geometry associated with inter-particle force has been demonstration in figure 3-4. The magnitude of the inter-particle force can be described as [9-10],

$$F_{INT} = 4\pi R^6 [\frac{(\rho_P - \rho_0)^2 (3\cos^2\theta - 1)}{6\rho_0 d^4} - \frac{\omega^2 \rho_0 (1/\rho_p c^2{}_0 - 1/\rho_0 c^2)^2}{9d^2}] \quad (3\text{-}5)$$

Where $\theta$ is the angle between the centerline of the two particles and the direction of acoustic wave propagation, $d$ is the distance between two particles. $c_0$ is the speed of sound in the particle and c is the light speed. As shown in equation 3-5, the first term in brackets is called dipole contribution and vanishes at the pressure antinode. The second term in brackets is the monopole contribution and vanishes at the pressure node. Since our device use the half wave length method, the particles will be trapped at the pressure node. Therefore, equation 3-5 can be simplified as [9-10]:

$$F_{INT} = 2\pi R^6 \frac{(\rho_P - \rho_0)^2 (3\cos^2\theta - 1)}{3\rho_0 d^4} \quad (3\text{-}6)$$

Obviously the inter-particle force at the pressure node is strongly dependent on the distance between the particles ($1/d^4$) and brought the particles into close contact (10-100 μm). It helps attracts particles to each other and stabilize the trapped cluster.

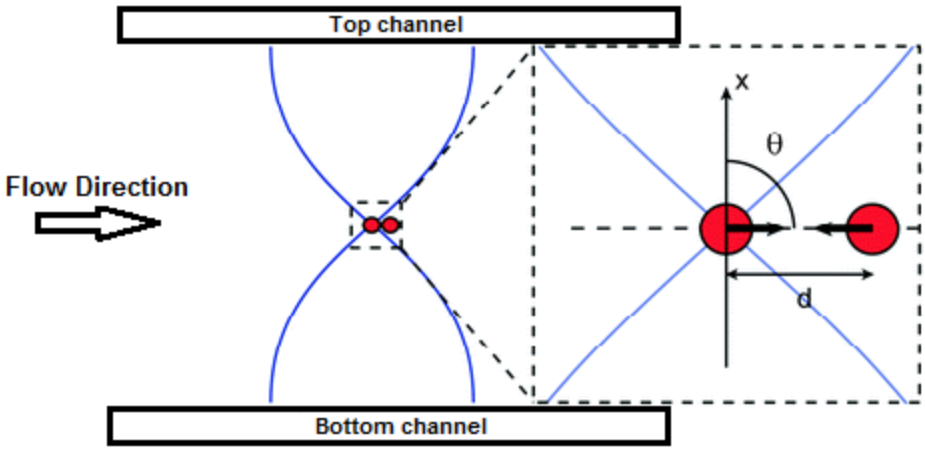


Figure 3- 4 Geometry associated with inter-particle force

### 3.1.4 Particle aggregation position in the field of standing wave, external flow and gravity

In the experiment, the particle undergoes the fluid drag force (external flow), the gravity force as well as the acoustic force in an ultrasound standing wave field. The gravity force to the particle is given by

$$F_g = \left(\rho_p - \rho_0\right) gV \tag{3-7}$$

where g is the gravity acceleration constant. In the vertical direction, the particles experience the gravity and primary radiation force only. The position for the particle aggregation depends on the balance between these two forces. The trapping location in the vertical direction is calculated from equation 3-2 and equation 3-7 (F=Fg)

$$z = \frac{1}{2k}\sin^{-1}\left\{\frac{\left(\rho_0 - \rho_p\right) g}{kAP_0^{\,2}\beta_0}\right\} \tag{3-8}$$

where z is the distance from the node position. The general schematic of this equilibrium is shown in figure 3-5. The solid bolt line in the plot demonstrates the trapping position

without gravity, and the dot line represents the trapping position of the primary radiation force and gravity combined. It is very obviously that the equilibrium position is independent of the size of particle and only determined by the particle property.

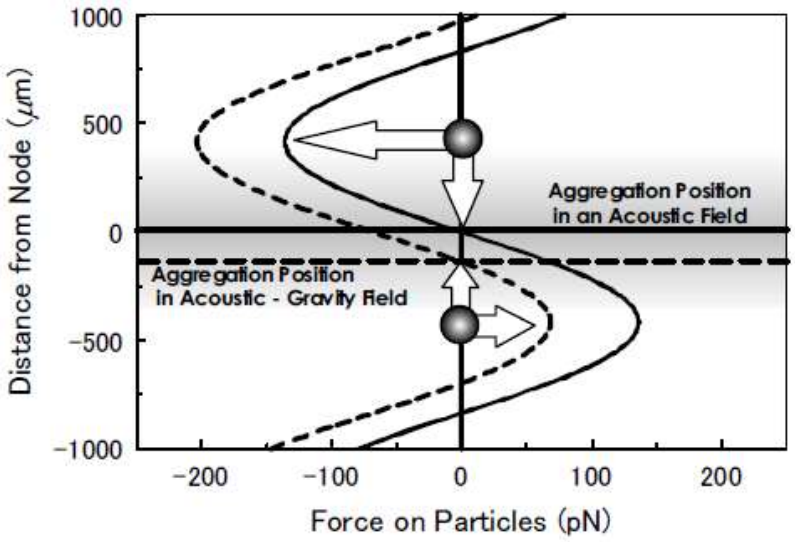


Figure 3- 5 Schematic representation of the principle of particle trapping in PRF-gravity field [5].

In the horizontal direction, the particle encounters the fluidic drag force and lateral radiation force. Later forces is due to spatial variations in the pressure field and acoustic streaming. Same as the force analyze on the vertical direction, the particle will move to the equilibrium position when the drag force is equal to the lateral force. The drag force for a stable particle in a fluid is given by:

$$F_D = \frac{1}{2}\rho_0 u^2 C_d S \tag{3-9}$$

where u is the velocity of the object relative to the fluid, *Cd* is the drag coefficient and *S* is the reference area. Usually for a sphere particle, the drag coefficient is 0.47. In case the lateral force is frequency dependent, the final aggregation position on the horizontal direction is varied by frequency.

## 3.2 AC electrokinetic theory

AC electrokinetics (ACEK) technology has been widely used in microfluidic applications recently. There are mainly three types of ACEK phenomenon, dielectrophroesis (DEP), AC electro-osmosis (ACEO) and AC electro-thermal (ACET) effect. DEP is the motion of particle under a non-uniform electrical field and can be used for particle trapping, detection and separation. ACEO is fluid motion generated by the induced free charges in double lay under electrical field. ACEO is mostly applied to low conductivity fluid pumping. ACET refers to the fluid motion caused by the interaction between electrical field and thermal field through the Joule heating effect. ACET works on the high conductivity fluid pumping. However, the AC electrokinetic trapping methods used in this proposal are only related with ACEO and DEP, therefore, ACET theory will not introduced.

### 3.2.1 Dielectrophroesis

Dielectrophoresis (DEP) is a force exerted on a dielectrical particle when it is in a non-uniform electric field. Particles do not need to be charged but rather charges will be induced at particle surface by electrical field. If the field is uniform, the distribution of induced charges on the particles is uniform and there is no movement. If the field is

non-uniform, the electrical forces on different sides of the particle are not balanced and the particles move. The first DEP research dates back to 1950 by Herbert Pohl [11-12]. Recently, DEP has been used to characterize and selectively isolate particles, such as cells, virus and even DNA. DEP can be readily applied in medical diagnostics, drug discovery, cell therapy, and bio-threat defence.etc.

The strength of the DEP force depends on three factors: the size of particle, the electrical properties (permittivity and conductivity) of the medium, and electrical properties of the particle. Several characteristics of DEP have been shown as below:

a. Dielectrophoresis effect can only happen in an non-uniform electrical field
b. DEP effect can be observed in both AC and DC excitation field, because the DEP force does not rely on the polarity of electrical field.
c. DEP usually can be observed for particles with diameters ranging from approximately 1μm to 1000μm, gravity overwhelms DEP; below 1μm, Brownian motion overwhelms the DEP forces.

DEP effect can be classified in two main types according to the direction of DEP force. One is called positive DEP (PDEP), which means that particles are attracted to high electrical field regions, such as electrode edges. The other is called negative DEP (NDEP), which means that particles are pushed away from high electrical field region. PDEP has been widely used in particle detection, because it can help accumulate and trap particles. NDEP is mostly used for separation in a flow through system.

In order to help understanding the DEP theory, the DEP force equation is given below:

$$F_{DEP} = \pi \varepsilon a^3 \,\mathrm{Re}[\frac{\tilde{\varepsilon}_p - \tilde{\varepsilon}_m}{\tilde{\varepsilon}_p + 2\tilde{\varepsilon}_m}]\nabla \left|E\right|^2 \qquad (3\text{-}10)$$

where $\tilde{\varepsilon}_p$ , $\tilde{\varepsilon}_m$ are the complex permittivity of particles and medium, and $\tilde{\varepsilon}_{p,m} = \varepsilon_{p,m} - i\left(\frac{\sigma_{p,m}}{\omega}\right)$; $\sigma_{p,m}$ is the conductivity of the particle and medium respectively, $a$ is the particle diameter, $\eta$ is the fluid viscosity. The parameter $\frac{\tilde{\varepsilon}_p - \tilde{\varepsilon}_m}{\tilde{\varepsilon}_p + 2\tilde{\varepsilon}_m}$ is known as Clausius–Mossotti factor, and is determined by the conductivity and permittivity of the particle and suspending medium. The value of Clausius-Mossotti factor is between -0.5 and 1. It can be seen from equation 3-10 that the DEP direction depends on the Clausius-Mossotti factor only, indicating whether the particle exhibits positive or negative DEP. The diameter of particle dominate the DEP strength, especially at the same voltage (electrical field), This makes the particle separation by using DEP technology possible.

DEP provides a useful method to manipulate particles. The DEP effect can only influence the motion of particle. DEP has not shown effect on continuous flow. Therefore, in this thesis we will neglect the DEP effect on the ACET pumping.

### 3.2.2 AC electro-osmosis

AC electro-osmosis (ACEO) refers to the motion of polar liquid at the surface of electrodes under the influence of an AC electrical field. Electro-osmosis (EO) phenomenon is the essence of the ACEO effect. In the late 1990, Ramos et al [13] observed steady flows over a pair of micro-electrodes when an AC voltage was applied and dubbed the effect “AC electro-osmosis”. Ajdari predicted ACEO flow in a periodic electrode array and showed how the effect could be used for long-range pumping [14].

In order to explain the ACEO theory, the concept of electrical double layer should be introduced here. When brought into contact with an aqueous solution, most material (solid particles, gas bubble and liquid droplet) will acquire surface electric charges. The surface charges will attract counter ions from the liquid to screen the surface charges. So there are two layers of charges at the interface, hence the name "electrical double layer."

The main mechanism of ACEO pumping is that the free ions in the double layer move under the tangential electrical field. Due to the viscosity between the free ions and fluid, the suspend fluid will be dragged by the motion of free ions and form flows. The general ACEO fluid velocity equation is given as:

$$u_{ACEO} = -\left(\frac{\varepsilon_m}{\eta}\right) \cdot \Delta\xi \cdot E \qquad (3\text{-}11)$$

where $\eta$ and $\varepsilon_m$ are the viscosity and permittivity of the medium, E is the tangential electric field and $\Delta\xi$ is the voltage drop over the charged double layer. In this equation, the permittivity and viscosity of the medium can be considered as constant. ACEO velocity has a linear dependence on the applied electrical field. Typically, a higher fluid conductivity makes the double layer thinner. Therefore, the ACEO pumping effect will drop dramatically in a high conductivity fluid ($10^{-2}$ and $10^{-1}$ S/m) and drop to zero eventually [15].

The double layer is just like a capacitor and will be charged by AC electric current through the resistive fluid bulk. However, if the applied frequency is very high, then there will not be enough time to charge the double layer completely. The time averaged

expression for ACEO velocity as a function of frequency has been shown as below [16],

$$u_{ACEO} \propto \frac{\varepsilon_m V^2}{\eta(1+\delta)L\left[\frac{\omega}{\omega_c}+\frac{\omega_c}{\omega}\right]} \tag{3-12}$$

where V is the applied voltage, L is the electrode spacing (roughly center to center); $\delta$ is the ratio of the diffuse layer to surface layer capacitances (can be considered as constant); $\omega_c$ is the peak frequency for ACEO velocity. It can be seen that around $\omega = \omega_c$, the ACEO velocity reaches its maximum value.

Usually ACEO pumping is suitable for dilute fluids with very low conductivities ($<10^{-3}$ S/m) at low frequency range (<100 kHz). However, for most of biomedical applications, the conductivity of sample solution is pretty high ($>10^{-2}$ S/m), ACEO cannot be used anymore. Instead, acoustic method should be used.

# CHAPTER FOUR: DEVELOPMENT OF AC ELECTROKINETIC FOR THE CHLORELLA CONCENTRATION OF ADVANCED CHLOROPHYLL FLUOROMETERS

A minute amount of toxin present in water is sufficient to affect the health of algae, which can be found by its induced fluorescence curve. Therefore, monitoring the health condition of microalgae lived in water is an effective method for identifying the toxicity in source of drinking water [1][2]. However, conventional method to monitor algae health uses a chlorophyll fluorometer which is a high-cost instrument. Also the limit of detection can only reach 0.1 ng/mL and is not practical for real-time algae monitoring. To realize distributed algae monitoring in the source fresh water, a low-cost and portable device is needed. To answer this need, an ACEK (ACEO and DEP) based algae trapping microfluidic chip was designed and fabricated, which was shown to enrich algae, hence improving the limit detection, and finally enables the development of a portable, integrated and automatic system.

## 4.1 Advanced chlorophyll fluorometer introduction

In a nutshell , the LOC chlorophyll fluorometer developed in this work consists of two main parts. One is the particle concentration by utilizing the ACEK technology and the other is microalgae fluorescent measurement by a pulse amplitude modulated (PAM) fluorometer[3][4].

Light absorbed by chlorophyll within algae can be either used for photosynthesis, emitted as fluorescence, or dissipated as heat. Lots of studies demonstrate that

fluorescence is an effective indicator of damage to the photosynthetic apparatus, induced from environment factor, such as toxins in the source water.

After chlorophyll a/b protein complex in the algae received the active light, the excitation is transferred to the reaction centers of two photosystems (PSI and PS II), where the photosynthetic reaction occurs [5]. Chlorophyll fluorescence is generated within these systems and affected by the energy transfer processes. The fluorescence response is varied due to the difference of health condition for algae. Healthy algae typically show a rather weak fluorescent effect, while the un-healthy algae have a stronger fluorescent light. It is probably because the light energy absorbed by the algae is transferred to chemical energy and stored inside, but the un-healthy algae cannot store the energy and only release fluorescent light instead.

Fluorescence quenching curve is a typical method to monitor the photosynthetic reaction of green algae and cyanobacterica [6]. It is a curve with a rapid rise of fluorescence effect at first, and then followed by a decline to reach a steady level. Algae with different concentration levels shows varied fluorescence quenching curve. Figure 4-1 shows the induced fluorescence curve of a group of different concentration of algae. Obviously, we can see that the quenching effect is getting weaker with lower concentration, therefore in order to monitor the quenching effect of algae, especially in a very diluted environment, the concentration of algae becomes very necessary.

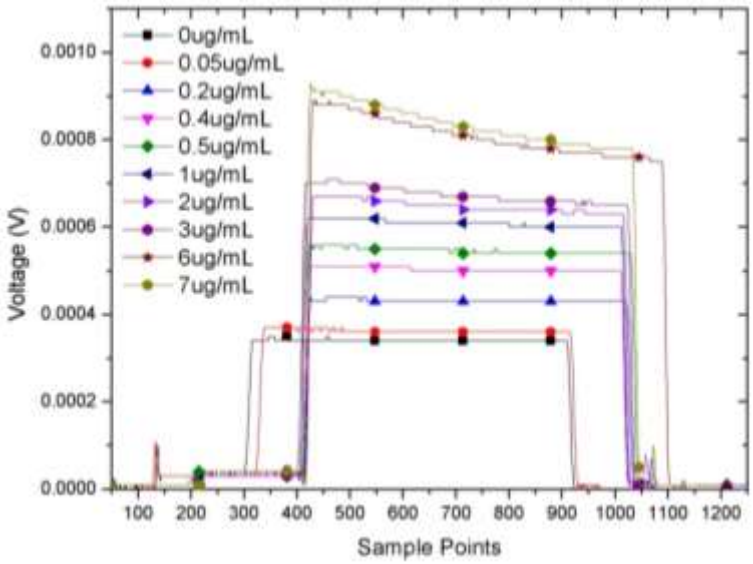


Figure 4- 1 Fluorescence quenching curve of algae with different concentration

We plan to use a light-emitting diode (LED) both as the fluorescence exciting light source and photosynthesis induction (actinic light) light source. Then the fluorescent light quenching curve generated by algae will be measured by the PAM fluorometer.

However, with a low concentration, the optical part of PAM fluorometer could not detect the algae very well and the detection result is not reliable. Also another challenge to PAM chlorophyll fluorometer is the small size for analysis. For a given chlorophyll concentration, the strength of the fluorescence signal is proportional to the sample size. Therefore, smaller volume implies fewer algae and a proportionally lower fluorescence signal. In order to solve this problem, the ACEK technology has been introduced and greatly increased the sensitivity and LOD for algae detection.

As we discussed before in Chapter two, there are numerous methods for the particle trapping. However, the traditional trapping methods have the disadvantage that once the particle trapped, it will be permanently stuck on the device and very difficult to

remove. The trapped algae eventually will block the pumping channel, making it impossible for continuous monitoring. In order to achieve continuous use, a contactless, resettable particle trapping method is needed, which determines the types of ACEK effects (i.e. ACEO and NDEP) to be used in this work.

## 4.2 Device design and fabrication

### 4.2.1 Device structure

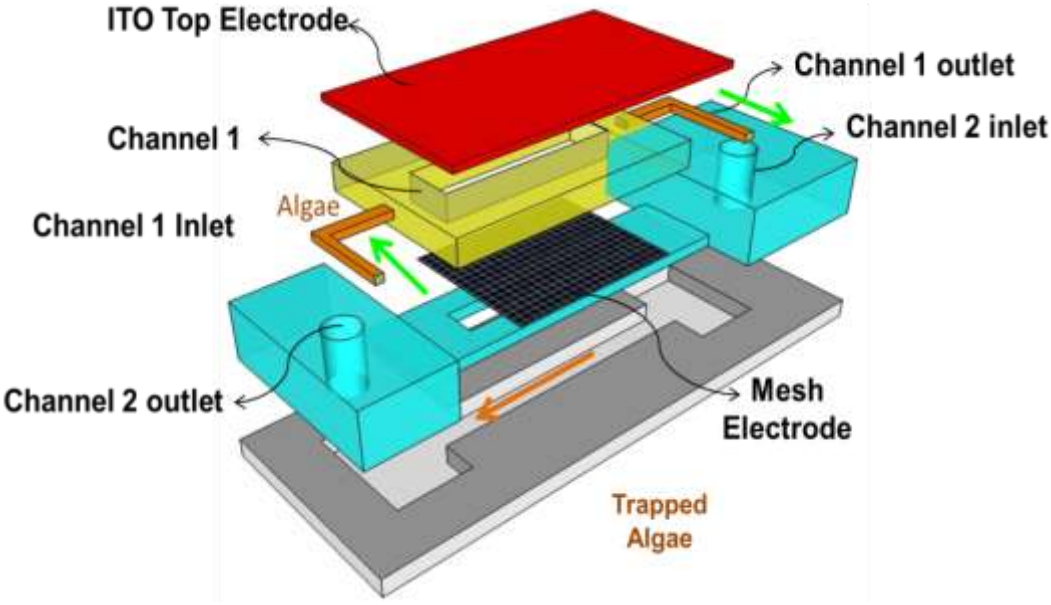


Figure 4-2 Schematic of the setup for ACEO and NDEP trapping in a microfluidic device.

A schematic of the device is illustrated in Figure 4-2. The device consists of five components

- Channel 1, used to flow the sample particles through the electric trapping site, which consists of an ITO electrode and a metallic mesh electrode on the opposite sides of Channel 1.

- Indium tin oxide (ITO) electrode above the trapping site.
- Metallic mesh electrode between Channel 1 and Channel 2.
- The spacer that separates Channel 1 and Channel 2.
- Channel 2, into which the particles are accumulated and later on washed away by wash flow.

Two electrodes with different sizes are face-to-face embedded into Channel 1, a double side PSA micro-channel, so tangential electric field is generated at the edge of the smaller electrode. The larger electrode, constructed by Indium tin oxide (ITO) glass slide, also serves as the channel top which allows visual observation of particle movement. The smaller electrode is made of metal mesh from SPECTRUMLABS. The mesh electrode consists of openings with 50μm×50μm size.

Our device has two operation periods, one is trapping particles and the other is washing the trapped particles away for next cycle of test. Figure 4-3 demonstrates a clearly trapping and washing process. The main concept of the trapping device is that particles are flowed through Channel 1 and collected through the electrode mesh. AC electroosmotic (ACEO) force and/or dielectrophoretic (DEP) force are induced between the ITO and mesh electrodes, which can exert transverse forces on particles and direct them towards the mesh. Because the mesh contains open grids, the particles can pass through the mesh and into Channel 2. Once into Channel 2, the electro-kinetic forces (ACEO and DEP) will disappear because there is no electrical field in Channel 2 and the particles will stay in Channel 2. When Channel 1 is pumping, Channel 2 will be turned off. Therefore, the velocity in the Channel 2 is very low and can be neglected.

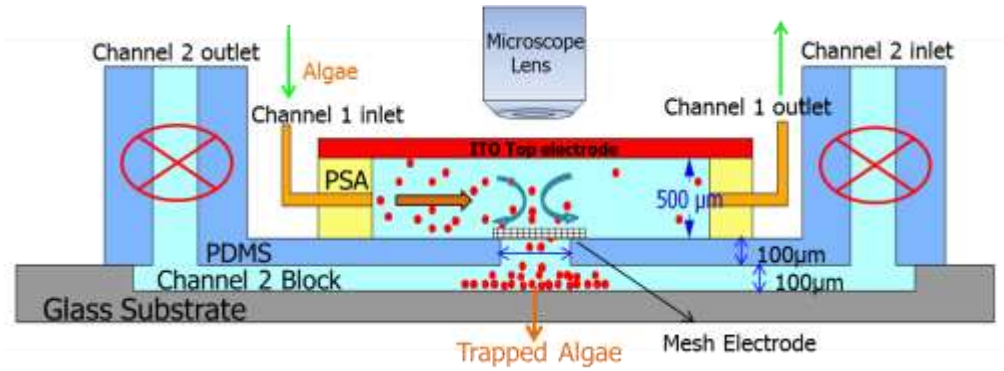


(a)

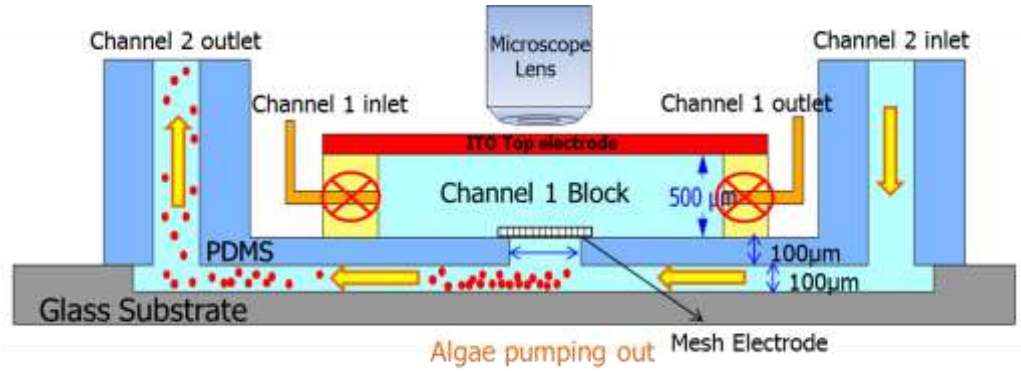


(b)

Figure 4- 3 Particle trapping and releasing procedure (a) Particle trapping in channel 1 and (b) Particle releasing for cycle use in channel 2

In the particle release mode, Channel 1 will be off and Channel 2 open. Clear water will be injected into the Channel 2 to wash the particles away. After the trap (Channel 2) is clear of the target particles, the next cycle of operation can start.

Once reach the trapping zone, the algae will be forced in the center for each micro-grid due to the ACEO flow, and after that algae will go through the micro-grid and deposit in channel 2. Because there is no electrical field and flow field, the algae will stay

in channel 2 and only a small amount of algae can overcome the NDEP force to back to the Channel1.

### 4.2.2 Device fabrication

The device photography has been shown in figure 4-4.This device has two mainly functions, one is particle trapping and the other is particle releasing and trapping site cleaning for the device reuse. There are two channels with four inlet and outlet, 2 or 3 electrode and one glass slide as the substrate base. The fabrication procedure is rather complicated and shows as below:

1. Clean the glass slide with ACETONE and DI water and dry with air gun
2. Attach the 2 layers of PSA double side tape on the cleaned glass slide uniformly (get rid of all air bubble)
3. Use digital craft cutter (Quickutz Silhouette SD) to produce the channel 2
4. Embedded 1 micro-tube into channel 2 as the outlet of the sample for washing step
5. Put metallic mesh electrode on the top surface of channel 2
6. Attach 1 layer PSA tape as spacer with a pre-cutted opening for sample passing between channel 1 and 2.
7. Put 5 layers of PSA tape together and cut by the craft cutter to fabricate channel1
8. Attach channel 1 on the spacer and embedded with two micro-tube as the inlet and outlet for the sample injection
9. Put the ITO as electrode on the top of the channel 1
10. Use Epoxy glue for sealing the whole device to avoid the leaking

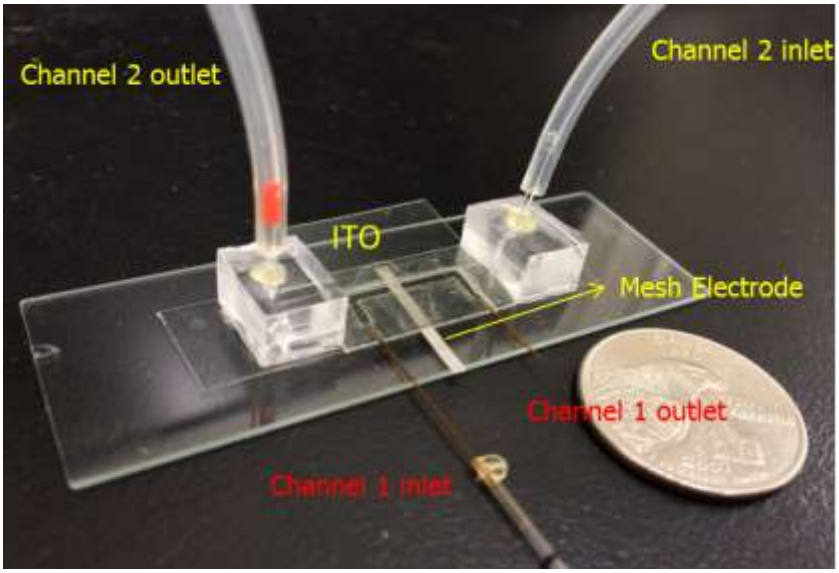


Figure 4- 4 Photography showing the resettable in-line ACEK particle concentrator

### 4.2.3 Problem with the fabrication

Followed by the steps above, the device should be fabricated successfully. However, there will be several major problems encountered in the fabrication. First, the sample leaking problem is the one which greatly influence the trapping effect. The solution leaking will completely change the fluid field and due to the trapping is depend on the ACEO flow, the trapping effect is getting weak or totally disappeared. Although the Epoxy glue is a good material to sealing the channel, it sometimes seeps into channel and blocks the fluid path and made the leaking problem worse. The quantity of the utilized glue and the dry out time should be set to a proper value to make sure the sealing in the good condition. According to the fabrication results, 3 gram of glue is enough for sealing the whole device and 3 minutes dry out time should be workable to avoid the channel blocking.

Second, since the PSA tape is used as the main material for the channel, the air bubble between each layer should be removed by the tweezer or other similar stuff, otherwise the sample fluid will be penetrated into the bubble and finally weak the trapping effect.

Third, the electric chemical reaction property should be considered when supplying the signal. Although the chlorella medium conductivity is not very high, in the freshwater level, with a high applied voltage the chemical reaction will still happen and generate bubbles to block the channel. By using a higher voltage, the concentration effect performance better, but once the reaction happened the device is totally broken and non-reversible. In the DEP property test, we found in the NDEP condition, frequency 10 KHz, if the voltage is lower than 4 Vpp, then the reaction of electrode is limited in a very small value which can be neglected. Therefore, the applied voltage 4Vpp should be considered as a safe level.

## 4.3 DEP characterization of chlorella

As it is desired to achieve non-contact trapping of algae, AC frequency needs to carefully selected, so that the algae will experience negative DEP and will not adhere to the electrodes. Hence, it is necessary to conduct DEP characterization of the target algae in test solution.

Chlorella is a genus of single-cell green algae, and mainly lived in the freshwater environment. It is spherical in shape, about 3 μm to 5 μm in diameter. Since the chlorella

has a very good fluoresce effect, it can be observed under microscope and then the behavior of the whole trapping process will be recorded by the CCD camera.

The living environment of chlorella is in the river and lake, therefore the medium conductivity used in our experiment is 0.02 S/m, which is almost same as the freshwater condition. Two types of electrodes were used for DEP characterization of Chlorella in fresh water, interdigitated microelectrode and mesh electrode. The silicon wafer with interdigitaed electrode is fabricated in Oakridge National lab.

In the wafer experiment, the sample particles are injected in a commercial reservoir (SecureSeal™ Hybridization Chambers, Grace Bio-lab inc) to get a rather stable fluidic environment. That means without any external force (ACEK), there will not be any reason for exciting the particle trapping process. In order to avoid chemical reaction, the applied voltage is limited at 8 Vpp. The chlorella is suspended in the solution freely. For the need of visualizing, the concentration of chlorella in the property detection experiment is diluted to 0.5 μg/mL. The frequency is varied from low frequency of 1kHz to high frequency 20MHz and back in roughly logarithmic increments. The frequency regions of positive and negative dielectrophoresis exhibited by the chlorella are recorded with media conductivity, ranging from 0.019 S/m up to 0.0256 S/m. The experiments are repeated at least 5 times for each frequency conditions with same wafer chip and fresh medium.

According to our experiment result, the positive DEP of chlorella is observed with the applied frequency 5 MHz, at which ACEO flow is virtually non-existent. After supplying the signal, only the particles are suddenly trapped at the edge of the electrode and the bulk fluid motion has not observed. The trapping only happened in a small area

which is very closed to the edge of electrodes. The negative DEP of chlorella are observed at the frequency 10 kHz and coexist with ACEO effect. The particles are repelled away from the electrodes and the fluid motion is very strong at the surface of electrodes. Followed with the fluid, the particle can reach the area which is very far away from the electrode.

The results of our experiments agreed with other group's research. Table 4-1 shows the polarity of DEP force (positive or negative) induced on chlorella. Three different conductivities were used in their experiments, $1.31 \times 10^{-4}$ S/m, 0.0137 S/m (freshwater range), and 0.733 S/m. In Table 4-1, the symbol O and X denote the frequency domains where the repulsive force and attractive force appeared, respectively. It is obviously see that the pDEP was observed at higher frequencies for all the solutions. The crossover frequency is found at 100-200 Hz, 100 kHz, and 1- 2 MHz, indicating a tendency that the crossover frequency shifts to higher frequency with increasing solution conductivity.

## 4.4 Experimental procedures

Proof of concept of chlorella enrichment by ACEK was conducted.

### 4.4.1 Device and equipment

To test the trapping and washing effects, several experiments have been performed. Chlorella with diameters in the range 3 – 5 μm were used for the experiments. The fluid conductivity is 0.02 S/m. The magnitude and frequency of the applied AC signal are 4 Vpp and 10 kHz respectively.

Table 4-1 The direction of dielectrophoretic force induced to chlorella [7]

| | Frequency (Hz) | | | | | | | | | | | | | | |
|---|---|---|---|---|---|---|---|---|---|---|---|---|---|---|---|
| | 1 | 5 | 10 | 20 | 50 | 1k | 10k | 50k | 100k | 200k | 500k | 1M | 2M | 5M | 15M |
| (a) | ○ | ○ | ○ | ╳ | ╳ | ╳ | ╳ | ╳ | ╳ | ╳ | ╳ | ╳ | ╳ | | |
| (b) | ○ | ○ | ○ | ○ | ○ | ○ | ○ | ○ | △ | ╳ | ╳ | ╳ | ╳ | | |
| (c) | ○ | ○ | ○ | ○ | ○ | ○ | ○ | ○ | ○ | ○ | ○ | ○ | ╳ | ╳ | ╳ |

○: Repulsive force, ╳: Attractive force, △ : Direction cannot be clearly judged. (a) 5.37 mM glucose: 1.31 μS/cm ,(b) 4.37 mM glucose/1.0 mM $KNO_3$: 137.5μS/cm, (c) 5.37 mM MBM culture medium: 733.0μS/cm

The dimensions of Channel 1 are 15mm×2mm×600 μm (l × w × h). The dimensions of Channel 2 are 50mm×2mm×100 μm (l × w × h). The sample injection flow rate in Channel 1 is with an average pumping velocity of 284 μm/s. The initial particle concentration density at the Channel 1 inlet is around 4100 cells/μl. The output particle concentration density at the Channel 1 outlet is around 2368 cells/μl. The wash flow rate is 0.35 ml/min with a linear velocity 4828 μm/s. Nearly all the particles are gone. The wash step prepares the device for the next cycle of measurement.

50MHz function/pulse signal generator 8551 (Tabor Electrodnics,USA) has been used as the power supplier. Oscilloscope MSO6012A (Agilent technology, USA) measured the signal for the whole device in real-time. a microscope Nikon eclipse LV100 with CoolSnap photometrics CCD was used to measure the light intensity in the Gray

scale format. Also an image processing software “Image-Pro 3D suite” was utilized for the subsequent data analysis.

### 4.4.2 Trapping and release procedure

As we discussed in last section, the ACEO and NDEP is a decent way to concentrate the particles. ACEO is quite effective for low ionic solution. The good news is that chlorella lives in freshwater which have a low electric conductivity less than 0.02 S/m. In this current project, ACEO effect is used to safely generate the fluidic vortices and concentrate the sample in the solution, as shown in figure 4-5 (video is available at the presentation). The metallic electrode mesh was used in the trapping experiment with the opening 50 μmx50μm. Followed by the flow trend, the chlorella particles are moving at the surface area of the electrode and finally flow through the mesh and trapped in channel 2.

Figure 4- 5 ACEO and DEP flow motion with freshwater conductivity (measured at 0.02S/m). 500 Hz, 4 Vpp ac signal applies to the mesh electrodes.

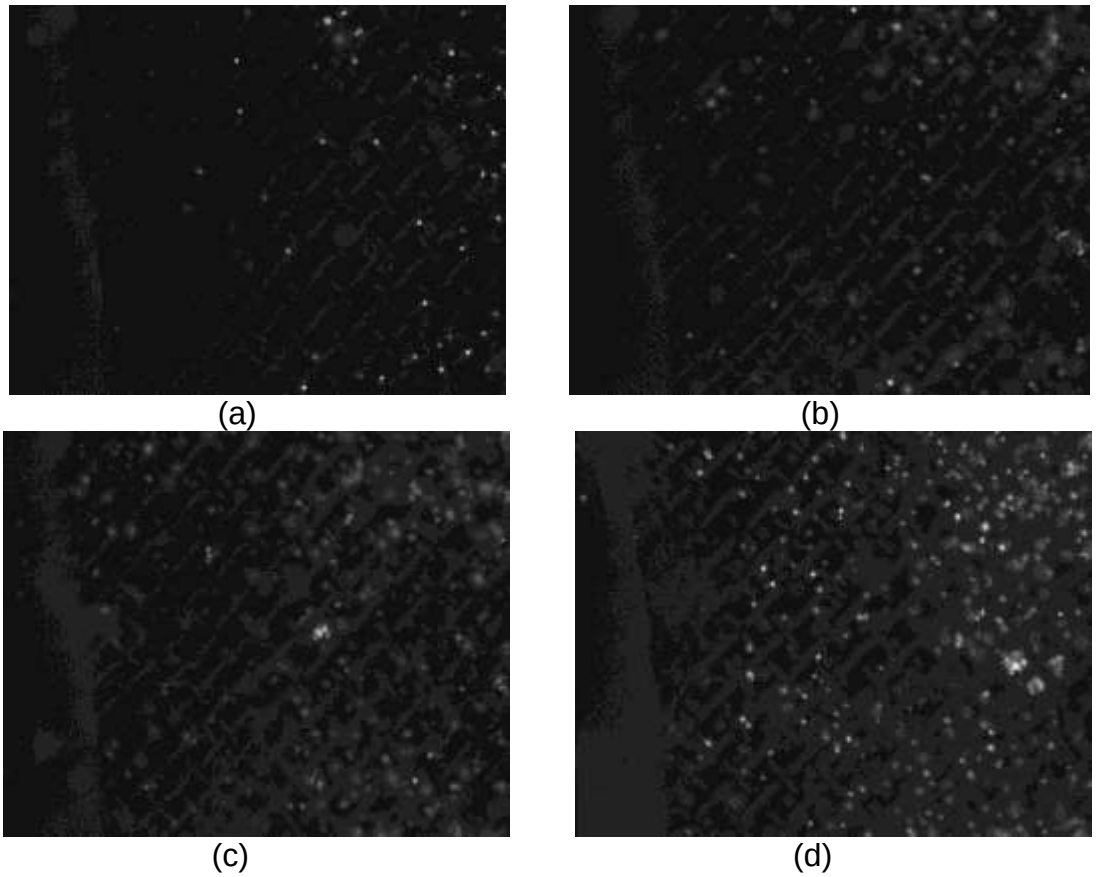


Figure 4- 6 Still images demonstrating the whole procedure of the chlorella trapping within 180 seconds.(a) Start time (b) Trapping lasts 60 seconds (c) Trapping lasts 120 seconds (d) Trapping lasts 180 seconds

The whole trapping procedure of 1st electrode mesh is very quick and simple. Figure 4-6 demonstrate the whole chlorella trapping process. First, there was no accumulation of algae on the device before applying voltage. Only some floating algae suspend around the electrode mesh. When a voltage of 4 Vpp (peak to peak) was applied, the procedure of particle trapping starts. By measuring the grey scale of the microscope picture, we can quantify the trapping effect. The algae will be accumulated to 6-fold than

its original density in 180 seconds. If supplying signal continually, trapped algae retained in the channel to form cluster and the clusters became larger and brighter as new particles brought by the flow continuously. Finally, when the voltage was removed, the trapped algae can be released rapidly and washed away by an external pumping in channel 2.

### 4.4.3 Comparison trapping effect with and without electrical signal

In order to prove the particle concentration is indeed caused by the ACEO flow and NDEP, the comparison results with and without the electrical signal will be employed in the experiment.

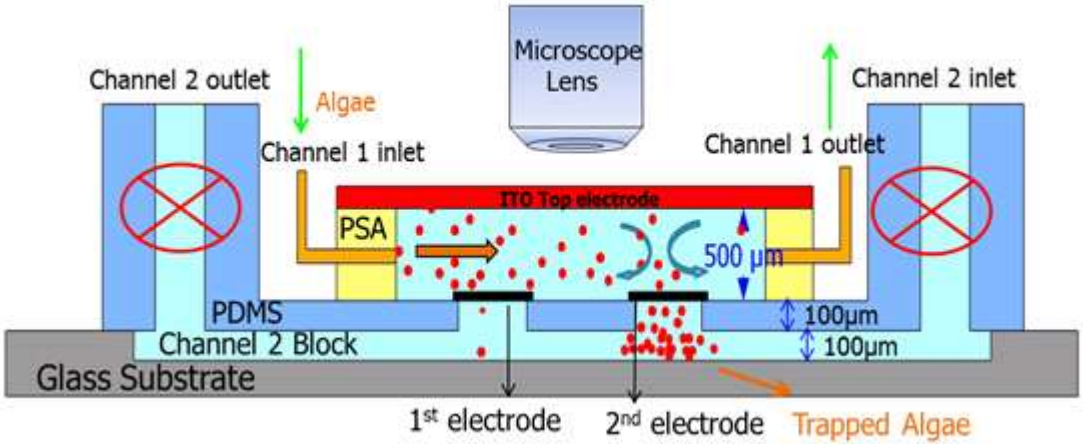


Figure 4- 7 Device schematic for comparing the trapping result of the mesh electrodes with and without ac signal.

Figure 4-7 shows a side view of the trapping device of two electrode mesh with and without ac signal. In order to make sure the experiment condition exactly same, two electrodes mesh were embedded into the channel, 1st electrode mesh and 2nd electrode mesh. When sample injected into the channel from left side (inlet) to right side (outlet),

the ac signal will be applied on the 2nd electrode mesh. There will be no signal on the 1st electrode mesh. Since the flow direction in channel 1 is from left to right, the possibility of trapping particles for the 1st electrode is higher than 2nd electrode.

Figure 4-8 shows the comparison result of 1st electrode and 2nd electrode trapping. It is very clearly shown that there is almost no trapping on the electrode without AC signal (1st electrode), but for the mesh electrode with applied AC signal (2nd electrode), the trapping effect is very obvious. This experiment proved the effectiveness and availability of the ACEO and DEP trapping.

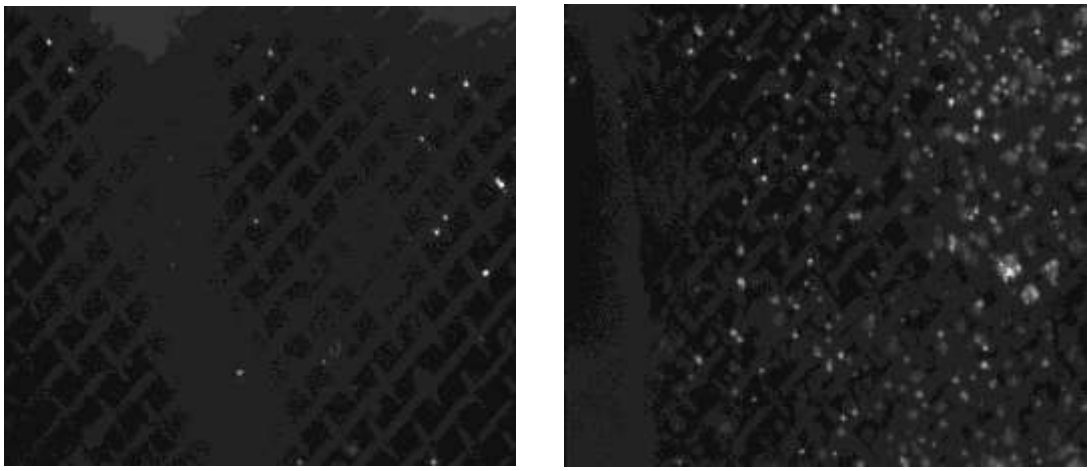

(a) (b)

Figure 4- 8 Comparing results of the electrodes mesh with and without signal. Trapping time lasts 180 seconds. (a) 1st electrodes without ac signal (b) 2nd electrodes with ac signal.

## 4.5 Simulation

Numerical simulation of our algae concentration based on ACEO device has been performed using COMSOL multiphysics (Comsol Inc, Sweden). The dimension of the

device in the simulation is proportional to those of real device. According to the cross section shape of mesh electrode, the rectangle and round electrode have been simulated for the comparison. Figure 4-9 gives the electric field distribution with rectangle and round shape of electrodes in our trapping device. For the rectangle electrode, both normal and tangential electrical field components reach maximum at the edge of electrodes (corner area in the plot). The color plot represents the amplitude of the electric field strength. Almost no tangential field was found at the top electrode surface. The white lines in the plot are the contour of the electrical field strength. Obviously the corner area has the maximum electrical field level. For the electrode with round cross section, the maximum electrode fields are observed at the top surface of the mesh electrode, which still both have the tangential and normal components.

The calculated electrical fields were used to obtain boundary condition in the Navier-Stokes module where fluid dynamics equations apply to solve the velocity field of ACEO. Same as the real experiment condition, an external velocity 200 μm/s has been pumped through the device at the right side of Channel One. All the simulation parameters are exactly same with real experiments. The applied voltage is 4 Vpp, and the frequency used in the simulation is ranged from 500 Hz to 20 kHz for the optimization of frequency response. The conductivity of the fluid is around 0.02 S/m which is equal to the fresh water environment condition.

Since the negative DEP have been observed during experiment, DEP force is added in the simulation. The average size of chlorella are 3- 5 μm and the viscosity of fresh water is around 1.08 Pa.S. Another factor influenced the motion of algae is the gravity

sedimentation. According to reference, the settling velocity of algae ranges from 0.1 cm/h to 2.6 cm/h, whereas we take 1.3 cm/h as the settling velocity in the simulation.

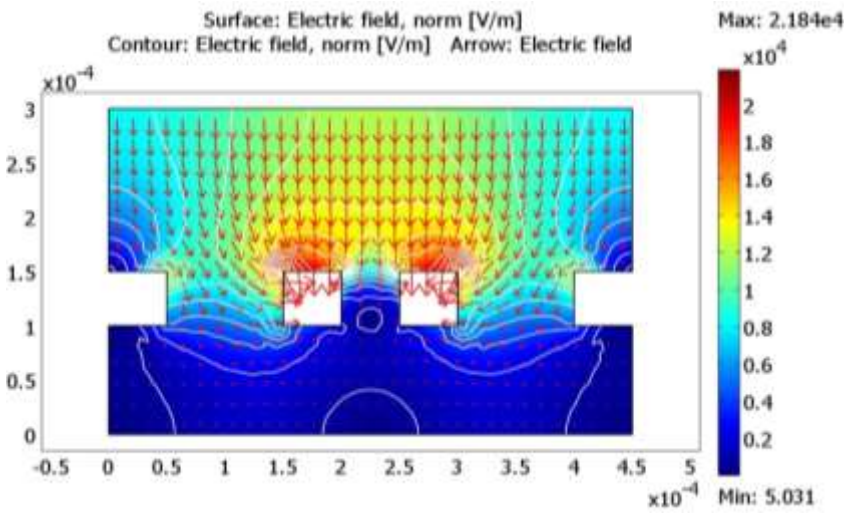


(a)

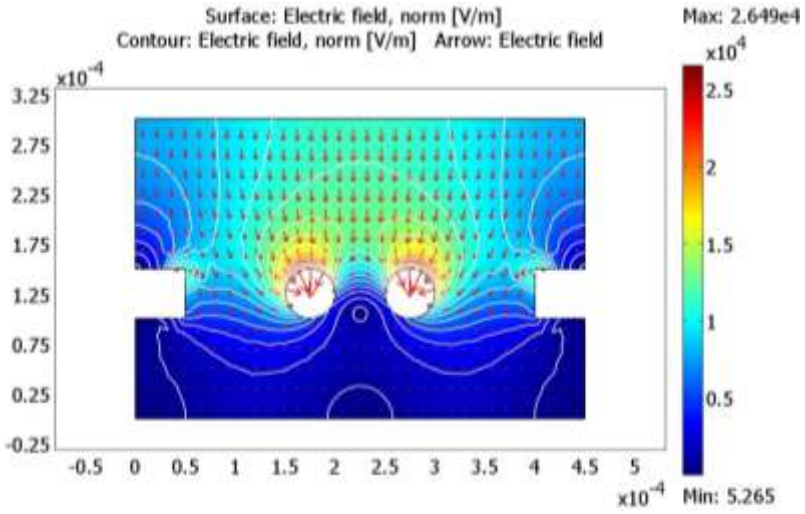


(b)

Figure 4- 9 (a) Electrical Field Distribution of rectangle cross section mesh electrode (b) Electrical Field Distribution of round cross section mesh electrode

Combined all these three factors together, the final simulated result of fluid velocity field for rectangle and round electrode are shown in figure 4-10 (a) and (b), respectively. The arrows in the plot demonstrate both flow direction and velocity magnitude. The simulation result is agreed with experiment and indicates the existence of ACEO rotating vortices which brought the particles from the channel 1 down to the channel 2. Then particles, driven by the fluid motion would eventually be deposited in the Channel two. Compared with ACEO flow velocity, although the sedimentation of algae is weak, it still helps the particle deposition once the algae enter the channel 2.

DEP force is strong and would prevent the algae in channel 2 back to channel 1. The effect area of DEP is rather small only in the corner area or the area which get higher electric field gradient, so to some extend it only prevent the particle back to channel 1but cannot influence the whole fluid motion. In most case, ACEO flow dominates the fluidic field in this trapping device.

## 4.6 Optimization of particle concentration

### 4.6.1 Optimization of frequency response

Since the main mechanism of this trapping device is based on the ACEO flow which is frequency dependent. The trapping effect can be influenced by the frequency as well. The flow velocity varied with different applied frequency. Figure 4-11 shows the result of the verification experiment. The peak of algae velocity is measured at the edge of the electrodes, which get the highest electric field. Data in Fig.4-11 are obtained by measuring algae velocities along the electrode edges. Same as the trapping experiment condition, solution with conductivity 0.02 S/m, applied 4 Vpp have been used in the experiment.

Figure 4- 10 (a) Simulated fluid velocity profile within the device chamber for the rectangle cross section mesh electrode (b) Simulated fluid velocity profile within the device chamber for the round cross section mesh electrode

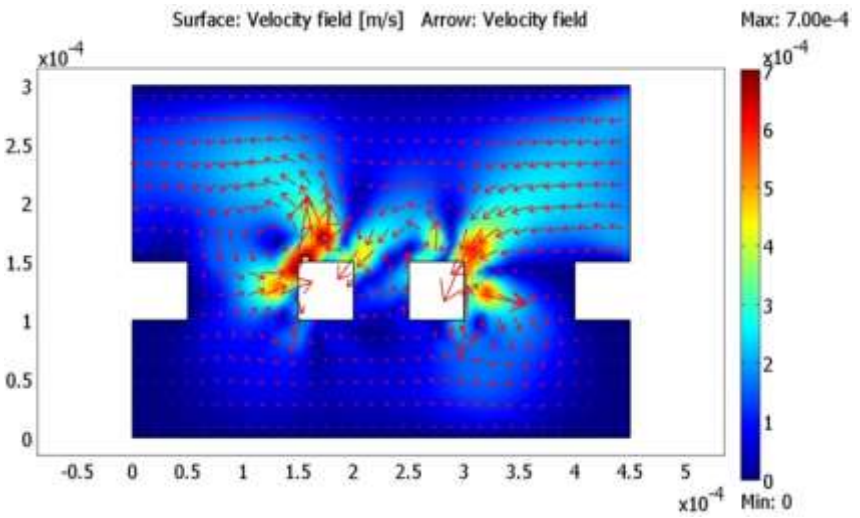


(a)

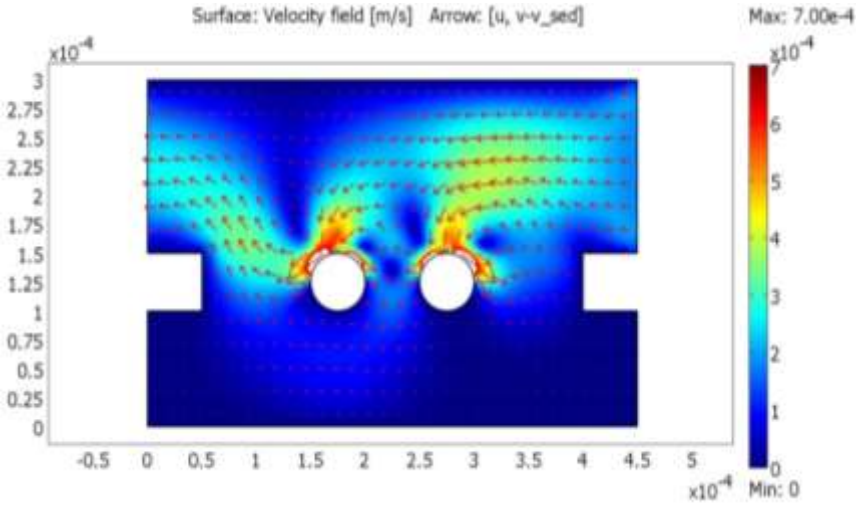


(b)

Figure 4-10 (a) and (b) continued

The needle electrode with almost same diameter as the mesh electrode was facilitated as the test electrode, and the other electrode is ITO. The results shows flow velocity reach maximum at around 500 Hz. The reason for the frequency dependence of ACEO is that, at higher frequencies, the ions in the double layer have less time to redistribute themselves as the AC electrical field switches direction, and finally reduce the velocity at high frequency. At very low frequency, there is sufficient time for the ions to redistribute and completely screen the electric fields at the electrode, which drastically lower the flow velocity.

Since the photosynthesis effect, the concentration of sample can be represented by the light intensity through the CCD camera. Figure 4-12 shows the light intensity as a function of time with varied frequency. It clearly demonstrates that the concentration effect is also frequency dependency which is agreed with ACEO velocity frequency dependency profile, the optimized frequency both for trapping and ACEO flow is around 500 Hz. This implies the main concentration mechanism is indeed ACEO flow.

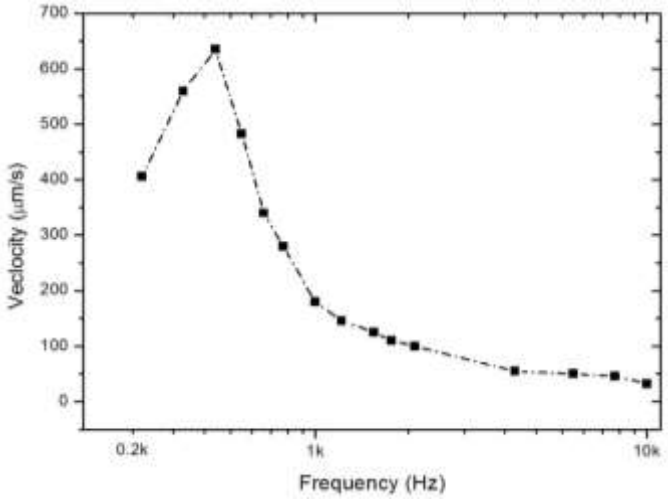


Figure 4- 11 Experiment result of ACEO velocity as a function of applied frequency

### 4.6.2 Optimization of flow rate response

In order to enhance and trapping effect per unit time, the external flow rate has been considered and optimized. Faster external flow makes the cell concentration more difficult, because the drag force of flow is getting larger and the time for the cell pass through the sensor is getting shorter. The dragging force of the flow increased with a higher volume external flow, and even the trapped cell can be removed. However, the high external flow will bring more cell sample into the channel and this greatly increases the particle detection sensitivity via time response. Therefore, there will be an optimized flow rate of concentrating the algae for detection.

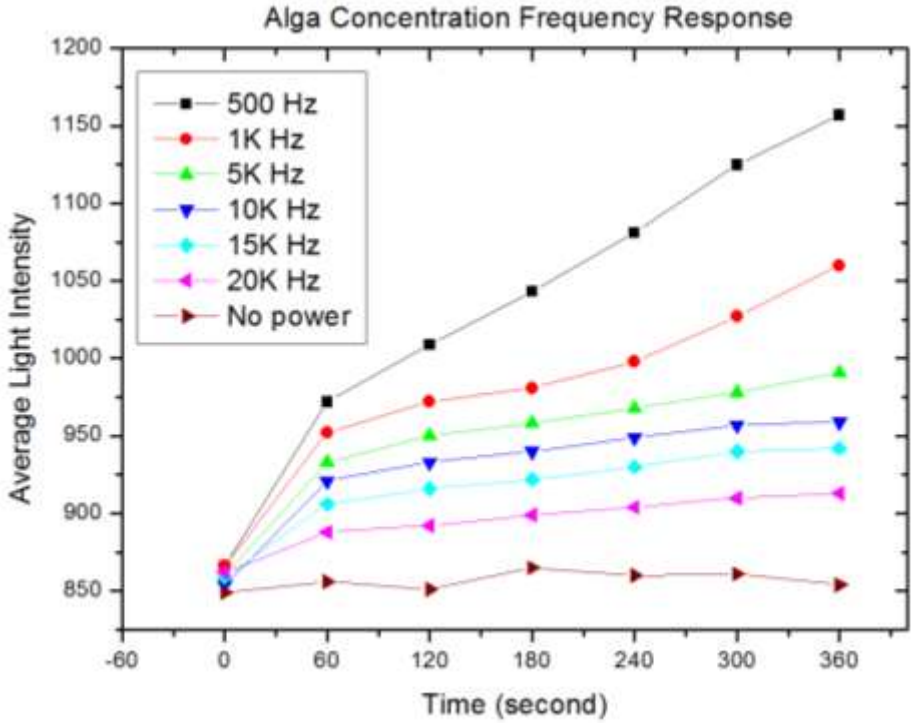


Figure 4- 12 Optimization results of frequency response as the measurement of average light intensity.

This time we used a grid counting mesh to quantify the trapping effect, and we characterize the ability to trap algae against fluid flow for varying flow rates. The algae density at inlet channel 1 and outlet channel 2 have been counted and the difference of cell density should be the algae trapped in the channel. Moreover, sedimentation of gravity will also trap the particle in the channel while the sample is pumping through. In order to eliminate the sediment effect, the difference of cell density at inlet and outlet of channel without power has been measured and recorded. Therefore, the actual sample trapped on the sensor due to ACEO is the total algae trapped in the channel subtract the algae trapped by the sedimentation.

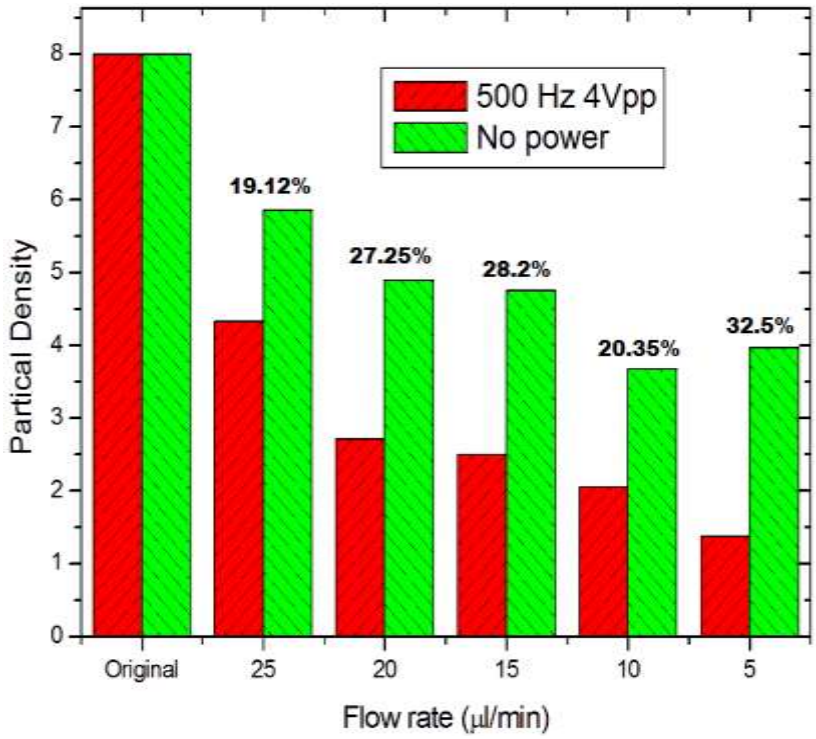


Figure 4- 13 Optimization of the flow rate response as the measurement of the particle density

Figure 4-13 shows the particle concentration as function with varied flow rates. The result for both no power and powered device has been compared to prove that the trapping effect of ACEO is much stronger than the sedimentation and dominate the trapping process. Both of the ACEO and sedimentation trapping effect are better with a lower flow rate, because the time for the sample through the channel lasts longer and more particles will be trapped. However, in the low flow rate range (5 μl/min), the trapping effect of ACEO shows far more good performance than the sedimentation. This is probably due to the ACEO flow dominated the flow field if the external flow rates is low, and the algae sedimentation velocity (3.78 μm/s) is much smaller than ACEO velocity. In the high flow rate, the difference of the trapping effect between the ACEO and gravity is getting less, since the external flow dominate the flow field.

### 4.6.3 Optimization of electrode mesh dimension

In our trapping device, the ACEO velocity is not only influenced by the applied frequency but not also can be affected by the electrode mesh dimension. As we described in chapter 3, the tangential electrical field is the main essence for ACEO flow motion. The larger tangential electrical field will generate larger ACEO flow, and bring more particles into the channel 2 and trapped. Since mesh electrode is used as one electrode in the trapping device, the opening and the width of the electrodes are very important to influence the ACEO flow field and eventually varying the trapping effect.

Three types of electrode mesh with different dimension have been used to verifying the trapping effect as the aspect of light intensity versus time. The size of

opening for these three electrode mesh are 45 μm, 85μm and 120μm, respectively. The width of electrodes are 20μm, 35μm and 45μm, respectively.

With same experiment condition, the device condition before and after trapping are shown in figure 4-14 (a)-(c). Also the result are quantified by measuring the gray scale of the microscope picture and shown in figure 4-15.

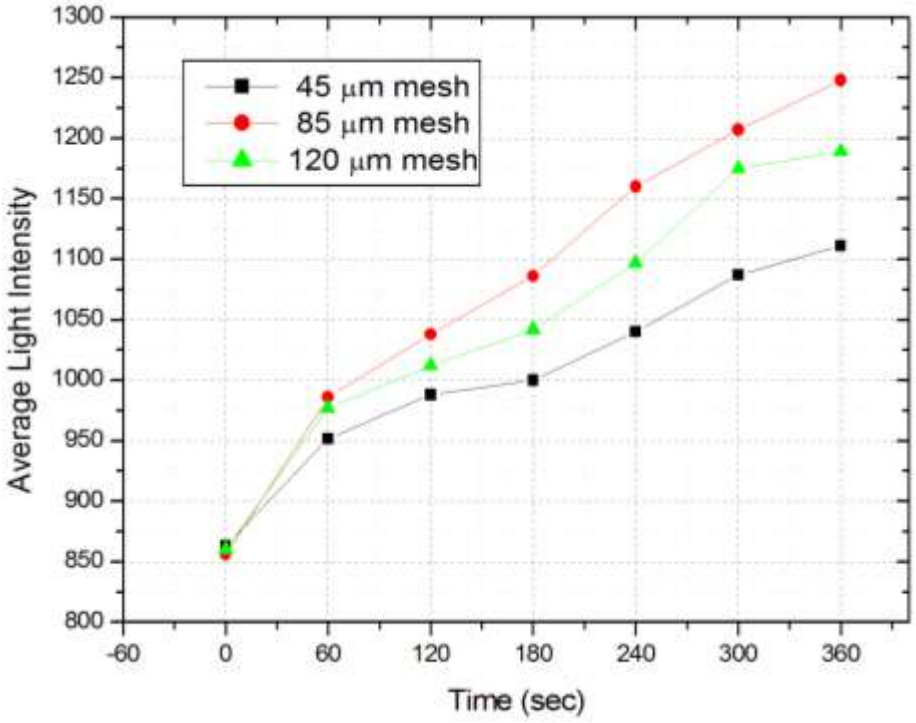


Figure 4- 14 Comparison results of ACEO and DEP trapping with three different mesh electrode.

From figure 4-15, we can see that the electrode mesh with open 85μm shows the best trapping effect. It can be explained that the larger opening electrode has a stronger tangential electric field, which should generate larger ACEO flow.

Figure 4- 15 (a) Trapping effect on the electrode mesh with opening 45μm and width electrode width 20μm,(b) Trapping effect on the electrode mesh with opening 85μm and width electrode width 35μm, (c) Trapping effect on the electrode mesh with opening 120μm and width electrode width 45μm.

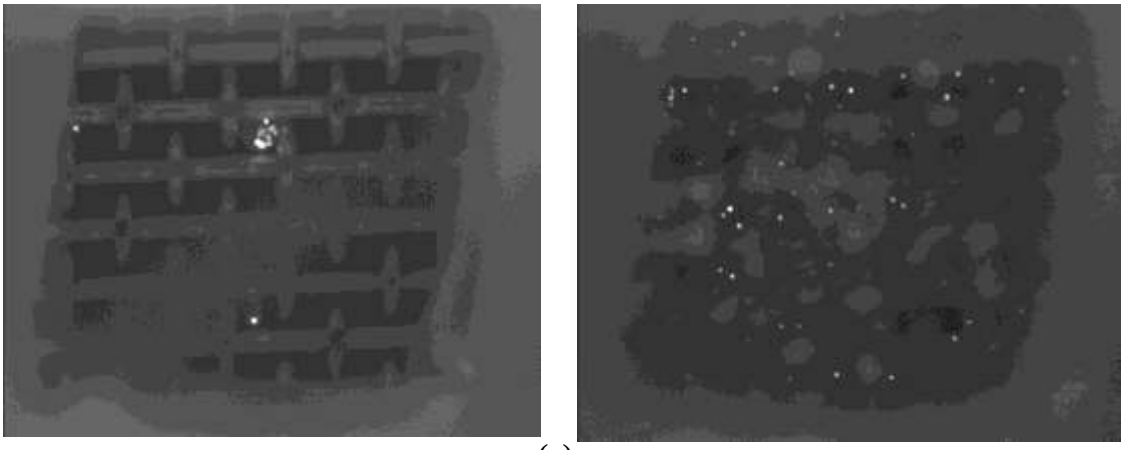

(a)

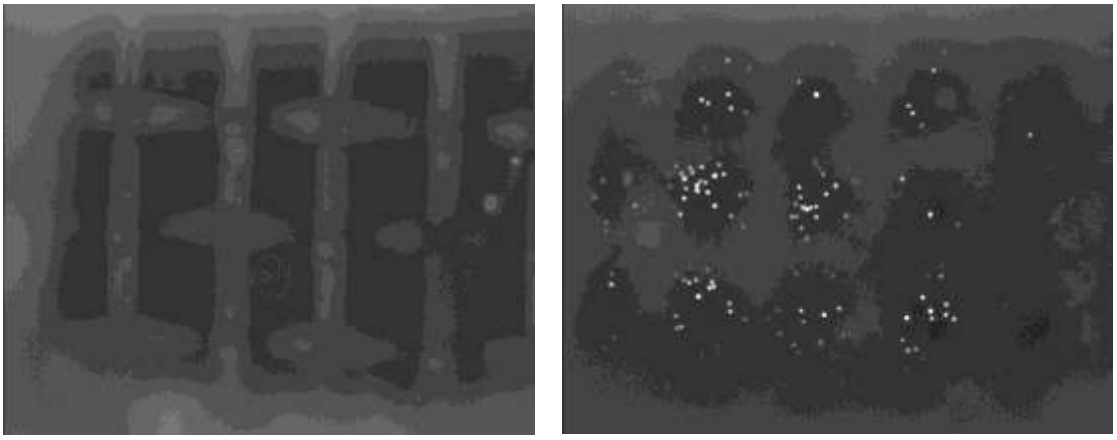

(b)

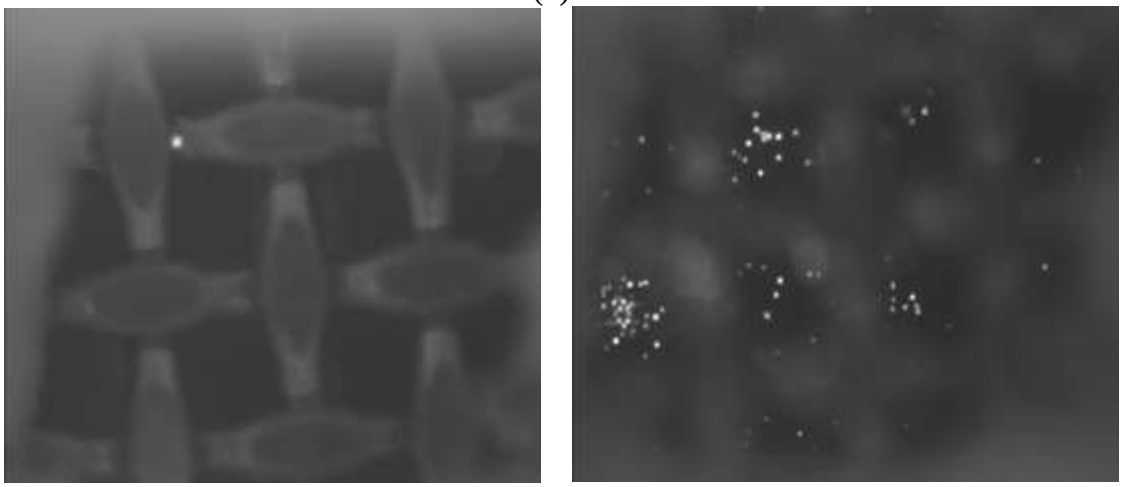

(c)

Figure 4-15 (a), (b) and (c) continued

However, the number of the opening per unit area is less and the ACEO vortex is getting weak. The increasing of the tangential electric field for enhancing ACEO flow cannot compensate the loss of the ACEO vortex. More important, the amplitude of nDEP force decreased by using a large opening mesh electrode and is not enough to prevent most of the particles back into the channel 1. Therefore, the dimension of mesh electrode with a proper value should be investigated to optimize the trapping effect. In these three electrode mesh, the middle one with opening 85μm presents the best trapping condition.

## 4.7 Conclusion

This chapter described the development and experiment of an advanced chlorophyll fluorometers with function of particle concentration based on ACEK technology. We have demonstrated proofs of concept for all the critical technologies involved. We have successfully concentrated chlorella and released the sample. The improvements of our device compared with conventional device are rather low limit detection, low cost, portable and reusable. Also, the optimizations on the aspect of applied frequency, external flow velocity and mesh opening size have been executed to maximum our trapping effect.

# CHAPTER FIVE: RAPID PROTOTYPING OF ROBUST AND VERSATILE ACOUSTIC TRAPPING DEVICE WITH CHLORELLA AND DIATOM IN MICROFLUIDIC

In last chapter, the trapping device based on ACEK mechanism for the chlorella lived in the freshwater has been introduced. Similar to fluorescence quenching of chlorophyll, the health of diatom can also be used to indicate the seawater quality and condition. Particle concentration is also very critical for the detection of diatom. However, due to the requirement of the low fluid conductivity, particles in the fluid with a high conductivity are not suitable for the ACEK trapping. In this case, the acoustic trapping mechanism has been used to concentrate the particles lived in the environment with ultra-high electric conductivity, like diatom in sea water.

## 5.1 Device design and fabrication

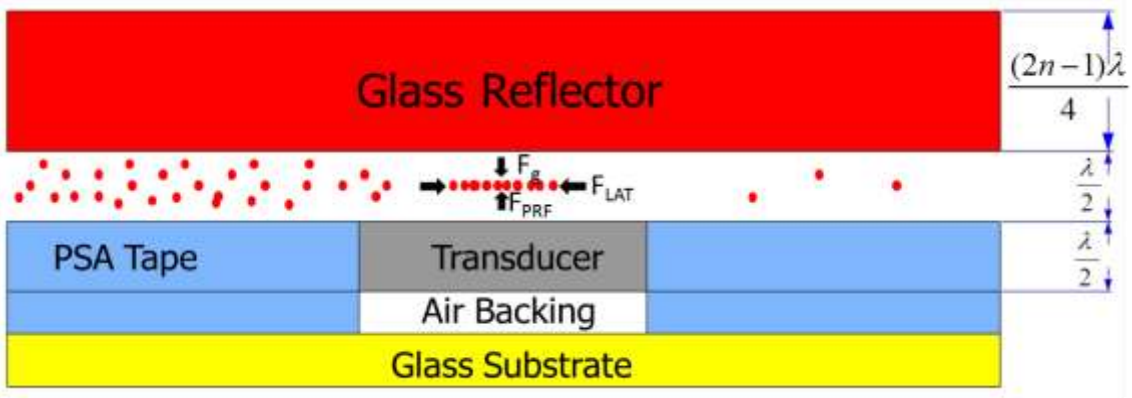


Figure 5- 1 Side view schematic of the acoustic trapping device

As shown in figure 5-1, the particle will be injected in the channel by an external pump. Once particles reach the resonator area, they will be trapped by the acoustic force. This microfluidic device is composed of a base plate of a glass slide, which is dark area

in plot. Then the double side PSA tape (light blue area) were attached on the glass substrate. The PZT single crystal piezoelectric active element were used in the experiment as the transducer, and embedded within the PSA tape. On the top o channel is the glass lip to supply the wave reflection. Since the device is one kind of microfluidic trapping device, the wavelength used in the experiment is in the micro-scale level. Therefore, the applied frequency drops in the ultrasonic range which is more than 2 MHz.

### 5.1.1 Device fabrication

Double-side pressure sensitive adhesive (PSA) tape (Scotch, 3M, USA) were chosen as the primary adhesive material for the device fabrication. The tape got a good chemical resistance and temperature stability. This transparent tape coated with permanent adhesive on both side which makes the observation under microscope possible. Also the advantage of pulling off, rolling smooth and cutting easily allows the device fabrication have a quick and easy modifying [1]. The property of water resistance makes the tape become a decent material as the microfluidic channel wall. A digital craft cutter (Quickutz Silhouette SD) was employed for the through cutting of all channels. Channels could be designed in a CAD software or L-editor software. This cutting method was chosen in order to achieve greater control over the precision and accuracy of the designed channels. The double side tape will be loaded on a back material and put in the cutting machine. The main channel layer and air backing layer are all fabricated by the cutting machine

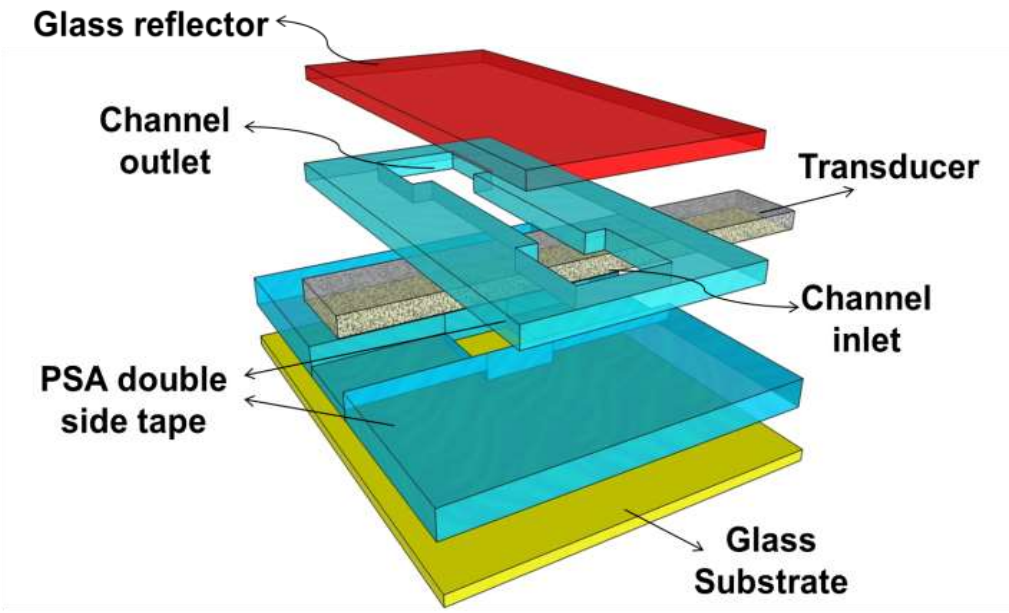


(a)

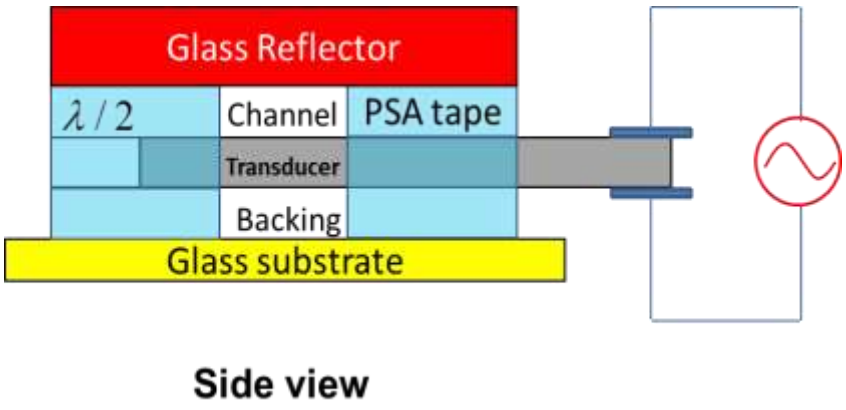


(b)

Figure 5- 2 (a) Schematic of the fabrication of whole trapping device (b) Side view of the device setup

After cutting, the through-cut layers of the microfluidic channel were removed from the backing. A glass slide was utilized as the base substrate for the trapping device. As shown in figure 5-2, the air backing opening with a dimension of 800 μm x 800 μm

will be directly laid on the glass as the first layer. To ensure the flatness of the channel layer, a tweezers will be used to remove the babble in between the two adjacent layers. The through-cut PSA tape were arranged and aligned on the air backing layer as the main channel structure. Then the piezoelectric active element (PMN-PT) mounted with the fabricated through-cut channel will be put on the air backing layer to build the main microfluidic channel. Finally, a glass lid with a very good visibility will cover the whole channel act as the acoustic reflector.

The channel dimension and PMN-PT size are well designed to get the maximum acoustic trapping force. According to the Lund research group [2][3], the channel has been fabricated with length x width x thickness (1000 μm x 800 μm x 50 μm) and the piezo electric element with size (800 μm x 800μm) just fit the whole trapping site. The thickness of glass lid is 150 μm which equals (2λ+1)/4.

### 5.1.2 Sample preparation

All the sample particles used in the trapping experiment are chlorella kessleri and diatom, provided by ORNL, and the concentration were determined as 6.82 μg/mL using the method of Porra. The density of chlorella and diatom are 1.49 g/cm$^3$ and 1.69 g/cm$^3$ respectively. Chlorella used in the experiment has a smaller size 3 μm-5μm than the diatom 10-15 μm. The difference property between the chlorella and diatom makes the two cells separation (trapping in different vertical height) possible.

### 5.1.3 Experimental setup

In order to verify the trapping effect, a microscope Nikon eclipse LV100 with CoolSnap photometrics CCD was used to measure the light intensity in the Gray scale format. Also an image processing software “Image-Pro 3D suite” was utilized for the subsequent data analysis. The signal was supplied by a signal generator (Tabor Electronic, US), from which the input power was monitored using a digital oscilloscope (Agilent 6320).

## 5.2 Particle trapping efficiency

When performing the acoustic trapping experiments, typically the particles size is the first factor which should be considered. According to equation (3-2) and (3-4), it is very obviously to see that larger particles experience a larger trapping force, making them easier to be trapped. The lowest size about the particle size is 1 μm. For the particle size below 1 μm, the primary radiation force is rather weak, and at that level the fluid drag force will dominate the particles motion. With the particle size above 20 μm, gravity will affect the motion of particles even more than the acoustic trapping force, although the rate is highly influenced by the density of particle and the surrounding medium.

The size of algae and diatom are 3-5 μm and 10 μm, respectively, which implies that both of these particles can be accumulated by using the acousticphoresis as the primary radiation force. And they indeed show a great trapping performance, as expected. The trapping efficiency can be easily calculated by the ratio between the number of injected particles and the number of the acoustic trapped particles.

Also the particle trapping efficiency can be affected by the external pumping velocity. In a rather high pumping flow rate, more particles will be escaped due to the high velocity of particle and high fluid drag force. Once the drag force is larger than the lateral force, the particle cannot stay on the nodal position in the horizontal direction and be pumped out. In our experiment, the flow rate range for chlorella and diatom varied from 0.5 μl/min to 2.7 μl/ min and 0.5 μl/min to 4 μl/min, which the particle trapping efficiency for chlorella varies from 82% to 74% and for diatom is between 79% to 85%.

At this experiment, we used an external voltage 15.6 Volts with frequency around 8.56 MHz for chlorella and 8.58 MHz for diatom on the piezo-transducer. In addition, the Nikon microscope is used to measure the light intensity in gray scale format within the measure area 200 μm x 150 μm for chlorella and 205 μm x 179 μm for diatom.

Different external flow rate were tested in order to distinguish the behavior and role of the flow velocity in the trapping process. As shown in figure 5-3 (a), the light intensity of chlorella is increasing linearly with time at first 25 seconds nearly for all the flow rates. Then the light intensity are continually increasing linearly for the sample with low flow rates (0.5 – 1 μl/min). With increasing the flow rate (2-2.7 μl/min), the changing rate of light intensity of the sample decay and finally drop into the saturation region. It is worth mentioning that with higher flow rate, more sample particles will be injected in the channel, which will greatly increase the acceleration rate of light intensity and make the sample detectable in a shorter time.

Figure 5- 3 (a) Normalized light intensity versus time as function of external flow rate (0.5- 2.7μl/min) of Chlorella sample. (b) Normalized light intensity versus time as function of external flow rate (0.5 – 4 μl/min) of diatom sample

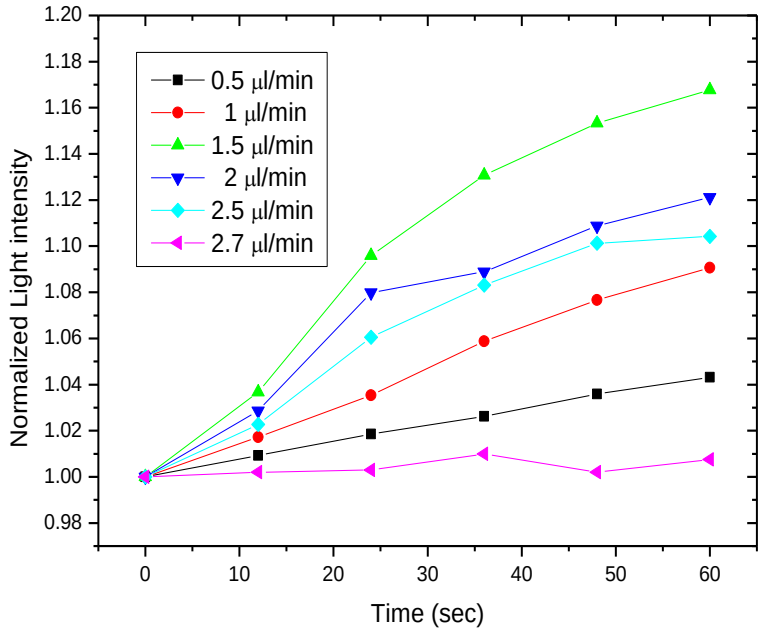


(a)

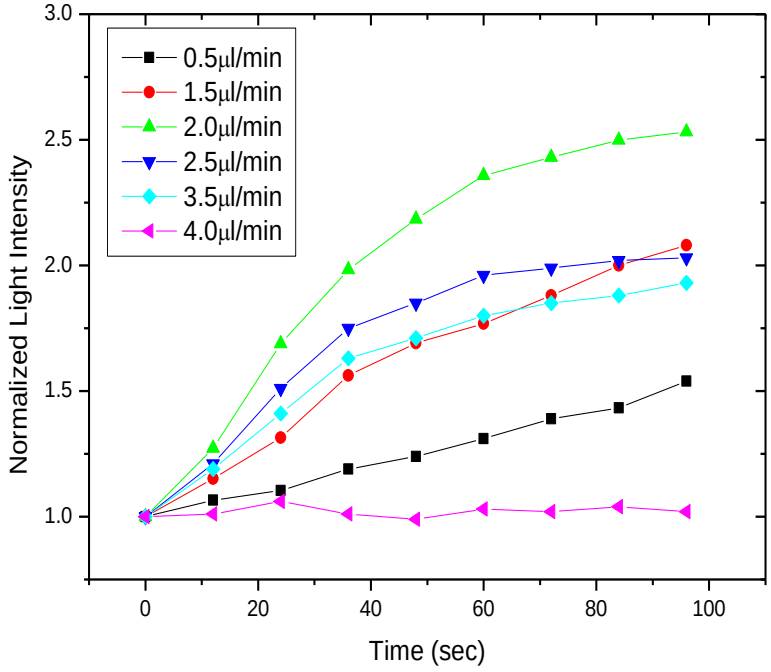


(b)

Figure 5- 3 (a) and (b) continued

However, from equation (3-7), it is easy to draw the conclusion that the fluid drag force is squarely increased with the flow velocity, which means under same lateral acoustic force, the particle will be escaped from the transducer area, once the fluid drag force is larger than the lateral acoustic force. The lateral force shows the largest magnitude at the central area of the piezo-transducer, and decays with the further location from the channel center to the side wall. It is probably due to the widening flow profile in the side-channel intersection, and the limitation of piezo-transducer from the side wall. Actually, with higher flow rate, the particle trapping efficiency decreases, thus there will be a trade-off between the flow rate and sample detectable response time. For the chlorella, we find the 1.5 μl/min shows the best on both of response time and light intensity saturation level. Also, we were trying to figure out the chlorella escaping flow rate which means at this flow rate, the fluid drag force is larger than the lateral acoustic force and all the particles will flee away. In this case for chlorella, the escape flow rate is 2.7 μl/min.

Compared with chlorella, diatoms have a larger size and the lateral acoustic trapping force is larger, and at the same external flow rate the number of trapped diatom will be more than chlorella. Therefore, a higher light intensity saturation level was observed, as shown in figure 5-3 (b), if the time of external pumping is long enough. Same as the chlorella, the best trapping flow rate for diatom is around 2.0 μl/min which is faster than the optimized flow rate of chlorella. The escaping flow rate of diatom is 4 μl/min, which is higher than chlorella as well.

## 5.3Comparison of chlorella and diatom trapping

Due to the difference in material property of chlorella and diatom, the trapping phenomenon for both of the two particles is varied on response time, size of trapping area and aggregation position. Diatom trapping shows a rather quick response, and a high escaping flow rate. The size of trapping area is large, which can reach 275 μm x 168 μm in 60 second.

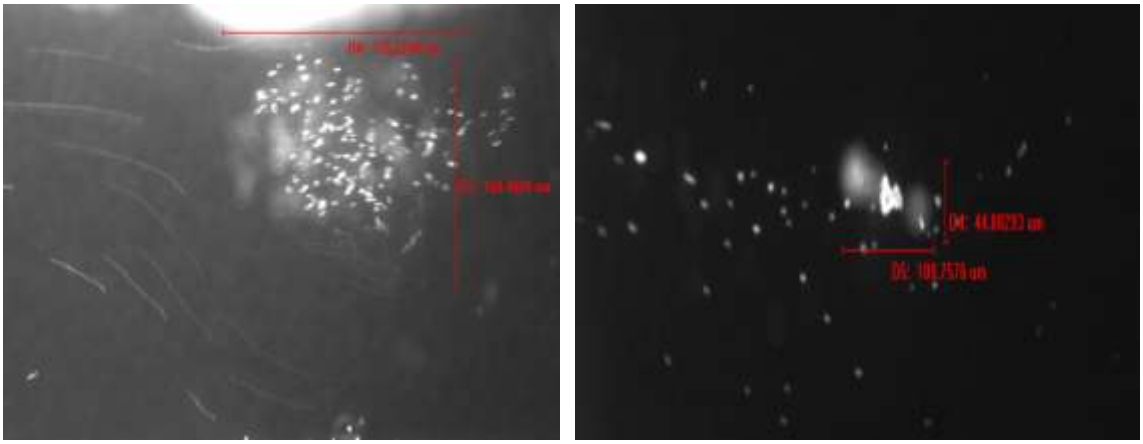

(a) (b)

Figure 5- 4 (a) Diatom aggregation phenomenon in 60 sec (b) Chlorella aggregation phenomenon in 60 second

Figure 5-4 (a) shows the observation of diatom trapping, the two single diatoms seems cannot merge together, in another word, there is a space between each diatom. The fluorescent effect of diatom makes the diatom brighter, but the space area is dark and has low light intensity. This is probably due to the chitin fibrils of diatom. According to the research report from Werner Herth about the chitin fibrils of diatom, the fibrils grow from the valve margins and can be as long as 50 μm and 50-150 nm wide.

When the diatoms are grown without agitation, the long chitin fibrils stay attached to the diatoms. Since the diameter of the chitin is very small and the fluorescent effect is rather weak, the light intensity of fibrils area between each diatom is very small. This explains why the diatoms are not concentrated together but have an isolated trapping, and the trapping area for diatom are much larger than chlorella.

In case the chlorella does not have the chitin fibrils, it can be concentrate closer even be trapped in a point area and makes the light intensity higher for that specific area. From figure 5-4 (b), we can see the trapping area for the chlorella is only in the area 44 μm x 100 μm.

## 5.4 Vertical position of particle aggregation

In the experiment of chlorella and diatom trapping, the particle undergoes the gravity (sedimentation) force as well as the acoustic force in the vertical ultrasound standing wave field. The equilibrium position is determined by the balance between the gravity and ultrasonic radiation force. According to equation (3-8), the vertical trapping position for the particle is independent of the size but is determined by the particle material properties, such as, particle density, acoustic energy. In our design, the nodal position of the acoustic standing wave field is designed in the center of channel which is λ/4 high from bottom. Due to the gravity, different types of particles will stay different position which makes the separation of particle possible.

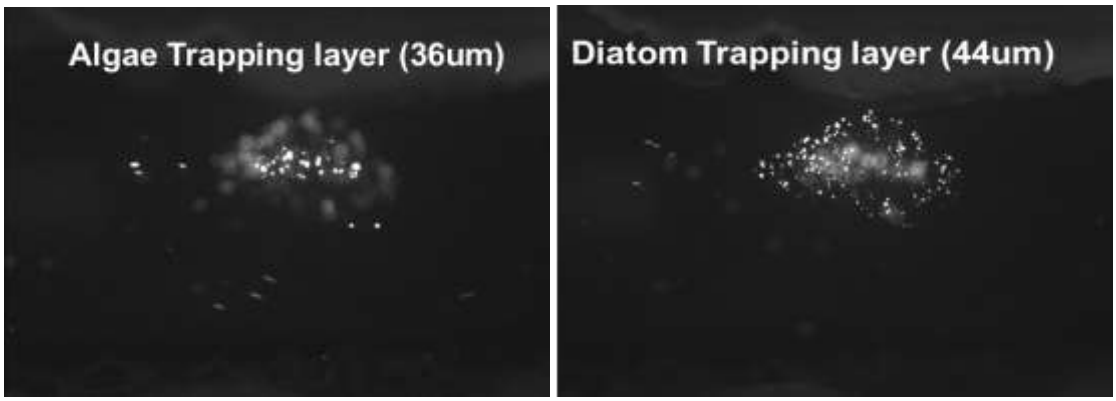


(a) (b)

Figure 5- 5 (a) Vertical trapping location for chlorella (b) Vertical trapping location for diatom

Table 5-1 Density, compressibility and speed of sound for the experiment material

| | Density ρ ($g/cm^3$) | Compressibility β (/Pa) | Speed of sound (m/s) |
|---|---|---|---|
| **Water** | 1.0 | $4.60 \times 10^{-10}$ | 1497 |
| **Sea water** | 1.025 | $4.60 \times 10^{-10}$ | 1497 |
| **Chlorella** | 1.69 | $2.85 \times 10^{-10}$ | |
| **Diatom** | 1.49 | $2.08 \times 10^{-10}$ | |

In order to locate the vertical trapping position, the material properties in our experiment have been list in Table 5-1. According to equation (3-8) and by using the data in the Table 5-1, we can easily calculate the vertical position for both chlorella and diatom. The wavelength in the experiment is around 220 μm and our channel is designed 110 μm height, so the nodal position is in the central of channel which is around 55 μm high above the bottom. The calculated result of vertical trapping position is 34 μm height from bottom for chlorella and 41 μm for diatom. In the experiment, we use the device to

adjust focus length of microscope, then we can exactly locate the vertical trapping position for each particle. From figure 5-5, we can see that the measured vertical position is 36 μm and 44 μm for the chlorella and diatom respectively, which is almost same height as the calculation result. Obviously, the diatom position is higher than the chlorella.

## 5.5 Conclusion

In this chapter, we present a noncontact acoustic trapping method for the diatom in the seawater environment. The in-line trapping device demonstrates notable particle enrichment ability with trapping efficiency more than 80%. Also we have proposed a simple method for the fabrication of our microfluidic device based on PSA tape, which is greatly reduced the fabrication time and failure rate. The PSA fabrication method is straightforward and does not require any sophisticated or costly microfabricaiton protocols. More important, the different trapping horizontal location for different types of microparticles (eg, chlorella, diatom) prove that the separation and sorting of cells can be achieved by this acoustic trapping mechanism.

# CHAPTER SIX: IN-LINE SOMATIC CELL COUNTER FOR MASTITIS DETECTION

In the last two chapters we mainly talked about the particle enrichment for the mechanisms of AC electrokinetics and acoustics. However, no matter which method we used, the final purposes for the enrichment and concentration are to increase the sensitivity and stability of the biosensor for particle detection and quantification. In this chapter, we are going to introduce a detection method based on impedimetric sensing technology for the measurement of somatic cells in dairy industry.

## 6.1 Introduction of mastitis disease diagnosis

Mastitis is a common infectious disease affecting dairy cows, which is caused by bacterial infection of udder tissues[1]. Once the infection happens, the immune system of cows will respond and fight the infection with an increase of the number of immune cells referred to as somatic cells, primarily white blood cells (leukocytes)[2]. The number of somatic cells in milk, i.e. somatic cell count (SCC), is an important measure of milk quality used throughout the world. An elevation of SCC above 200,000 cell/mL is generally considered abnormal and an indication of inflammation in the udder[3-4]. An abnormal increase of SCC in diary milk lowers milk quality and reduces shelf-life of milk and dairy products [5-6].

Mastitis is a very costly disease that constantly plagues dairy industry. Annually, mastitis causes approximately $2 billion in losses to the U.S. dairy industry, and 60%of the losses, or $1.2 billion, comes from subclinical mastitis[7-9]. Cows with mastitis are easy to identify with the swollen teats and thick, curdled discharge in the milk, while subclinical cases are difficult to detect due to lack of visual symptoms. Subclinical

mastitis in cows can still lead to abnormally high SCC in milk. In the USA, the SCC limit specified by the Pasteurized Milk Ordinance is 750,000 cells/ml for Grade "A" raw milk; whereas in the European Union this limit is 400,000 cells/ml[10]. On January 1, 2012, the U.S. dairy industry began transitioning to a producer-level milk sampling program to verify SCC compliance with EU regulations for products exported to the EU.

Therefore, it is very important to have a cow-side and real time somatic cell counter that tests SCC of the milk as it leaves the cow, providing an immediate assessment of milk quality. Such an instrument will also greatly enhance the ability of dairy producers to identify cows with mastitis and make timely and informed decisions of herd management.

Several methods have been developed for somatic cell counting, such as direct microscopic somatic cell counting[11-12], electronic particle counting[13-14] and cytometry. The gold standard to determine SCC is to count the somatic cells with methylene blue staining under a microscope. This is extremely time consuming, requires trained personnel and a laboratory and can be costly[15]. Consequently, many farms measure individual cow SCC values on a monthly basis, which provides limited effectiveness in the detection and control of mastitis. Existing cow-side SCC assessment methods include DeLaval portable somatic cell counter, which is relatively expensive at $2.50 per test and ~ $5,000 for the detection unit. California Mastitis Test, which is inexpensive, needs to be conducted manually with qualitative and subjective results[16]. Both tests are off line. There is an urgent need to develop methods for quantification of milk SCC with minimal labor input and at low cost, so that it can performed daily on each cow.

Most milking units today come equipped with conductivity sensors that flag cows with clinical mastitis but cannot identify cows with subclinical mastitis. AfiLabs, a milk analyzer from Afimilk, can find SCC range in increment of 200, milking system of the milk as it leaves the cow, providing an immediate measure of milk quality. However, this system is quite expensive, adding an additional $150,000 to the cost of a new 16 unit milking system. Effective control of mastitis requires timely detection of mastitis in cows so that appropriate therapeutic and management measurements can be taken.

In this chapter, we present the development of a real-time, inexpensive microfluidic detection system. It uses a capacitive sensing method and a microelectrode flow cell to quantitatively determine SSC of raw milk, based on monitoring the capacitance change of the microelectrodes. In this study, somatic cells in raw milk samples were separated from lipid in a flow channel using differences in specific gravity. Electrochemical approaches are advantageous particularly for rapid and simple on-site measurement, due to the simplicity of the measuring equipment. The change of capacitance is only related with the SCC level, and other background noise (such as the lipid, water percentage, impurity particle) can be avoided. The theoretical fundaments and milk testing results are showed in the following sections.

## 6.2 Device design and fabrication protocol

### 6.2.1 Somatic cell counter operation

Our mastitis detection device provides a real-time and quantitative method for milk quality monitoring. The detection is based on capacitive sensing. The main structure of the cow-side somatic cell counter is shown in figure 6-1. The SCC sensor uses a side

channel off the main milking tube to sample the milk. Two mesh electrodes intersect the detection channel with a spacing of 40 μm between them. The two mesh electrodes are made from stainless mesh filters with opening of 100 μm (top electrode) and 30 μm (bottom electrode), which will allow milk and its constitutes to pass through for in-line SCC monitoring. By measuring the capacitance between the two mesh electrodes, capacitance of the milk sample between them can be found that will quantitatively indicate the milk SCC level.

Once milking starts, milk will be led through the side detection channel. A valve below the SCC sensor will close and allow milk to fill the space between the electrodes and settle. The capacitance of the electrode flow cell will be continuously measured during milking, for approximately 5 minutes. The capacitance data will be recorded by a microcontroller. When the milking process is over, the valve will open for milk to flow out and the channel will be flushed, getting ready for next milking. The change rate of milk capacitance will be calculated at the end of sampling, which will be compared with a look-up table to yield the milk SSC.

A critical issue in the detection of somatic cells in milk is the separation of few somatic cells from a large number of lipid. The sizes of somatic cells and lipids are almost the same; therefore, separation by filtration in terms of size is difficult and cannot be used for in-line monitoring. Centrifugation is another approach often adopted by laboratory testing. However, this alternative is not applicable for cow side detection. To separate somatic cells from lipids, the differences in specific gravity between the two types of particles are utilized here. Lipids will levitate and eventually leave the sampling space through the openings in the mesh electrode, while somatic cells will enter

the sampling space due to sedimentation.

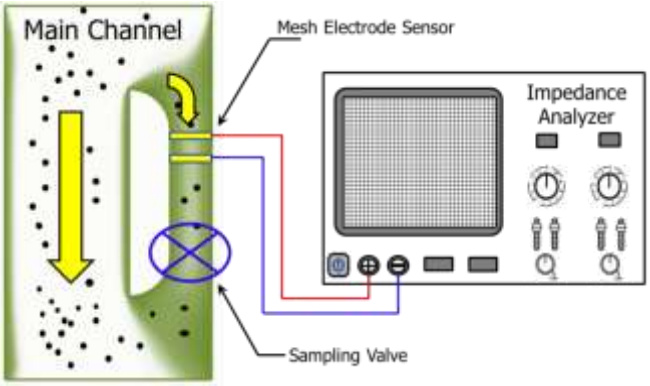


Figure 6- 1 Conceptual illustration of microfluidic SCC sensor being incorporated into a milking tube

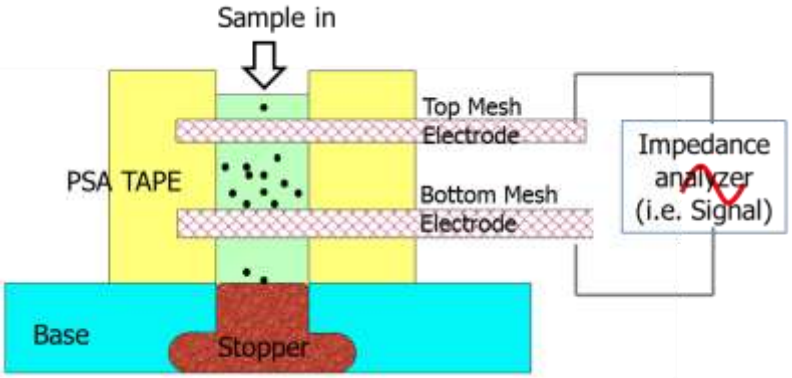


Figure 6- 2 Structure of our prototyped in-line somatic cell counter

### 6.2.2 Rapid prototyping of in-line somatic cell counter

Fabrication procedure of the prototype SSC is as described in figure 6-3. Figure 6-2 shows the cross-sectional view of a prototyped SCC sensor, which is built out of stainless steel mesh filter and pressure sensitive adhesive (PSA) tape on a glass slide. Space is allowed below and above the electrodes to simulate the in-line detection scenario. In actual application, the glass slide should be replaced by the valve in figure 6-1.

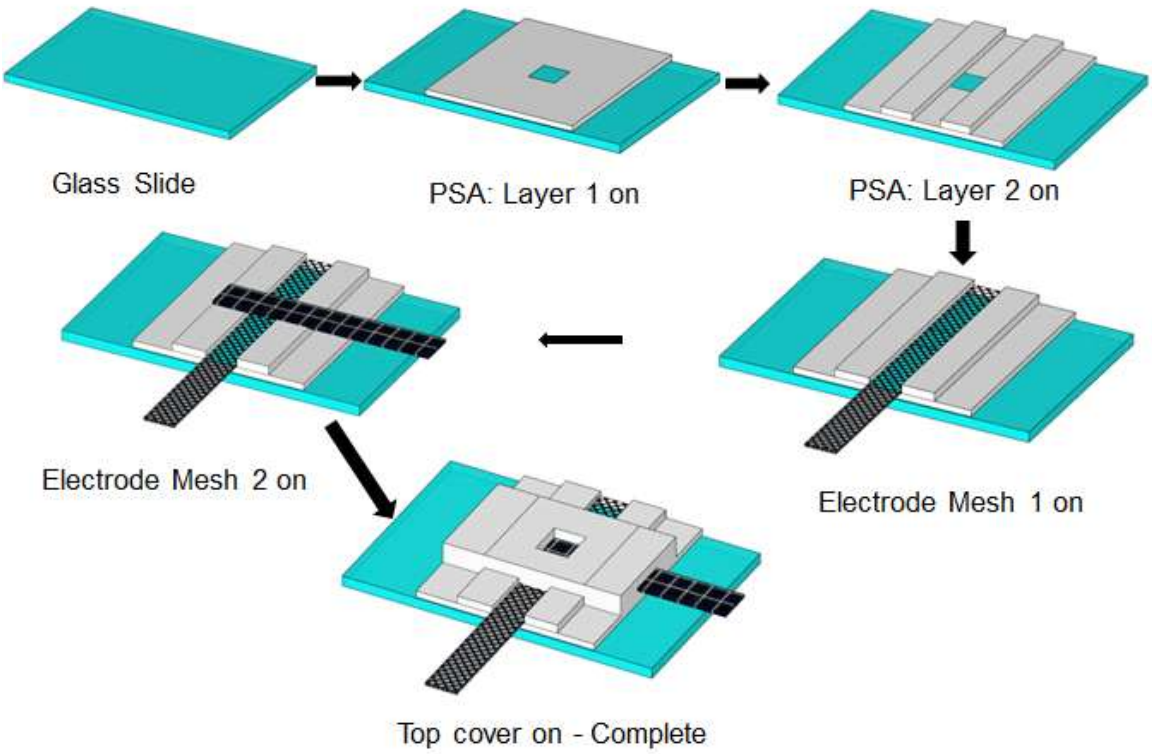


Figure 6- 3 Step by step fabrication of the microfluidic SCC sensor

A pre-cleaned glass slide was used as the base support of the whole device. The slide was sequentially cleaned with acetone, isopropyl alcohol (IPA) and Deionized water (DIwater) for 5 minutes each in an ultrasonic bath, and then dried by an air gun. The microfluidic chamber was fabricated with double-side pressure sensitive adhesive (PSA) tape (Scotch, 3M, USA). The thickness of a single layer PSA tape is approximately 40 μm measured by micrometer, and a microchamber or a spacer of various thickness can be easily achieved with stacking layers of PSA tapes. A digital crafter cutter (Quick Silhouette SD) was employed to cut the PSA tapes into desired shapes. Designs of various PSA layers were created using AutoCAD and converted to the format recognizable by the crafter cutter. A tweezers was used to remove the air bubble between layers to get a complete attachment. The material shows very good chemical resistance

and temperatures stability (~200C) [3M datasheet].

The microfluidic SCC sensor has two mesh electrodes intersecting the detection channel. The two mesh electrodes are made from grade 304 stainless mesh filters with 100 μm (top electrode) and 30 μm (bottom electrode) openings, which will allow milk and its constitutes to pass through for in-line SCC monitoring. The thickness of the top mesh electrode and bottom electrode are around 50 μm and 20 μm. The spacing between the two mesh electrodes is around 50 μm. Lastly, we use epoxy glue to seal all possible leaking parts of the device.

Afterwards, the finished device was cleaned by rinsing with de-ionized (DI) water, acetone and isopropyl alcohol multiple times. The details for the device cleaning follow the procedure of washing with DI-water 5 times, each time last 2 minutes, acetone and IPA cleaning 3 times, each time last 3 minutes. Rewashing with DI-water 2 times. Finally, the device was dried with a pressurized air gun and plasma treated for 30 seconds at 100 watt by PE-50 Plasma Cleaner (Plasma Etch Inc. NV, USA).

## 6.3 Sample preparation and impedance measurement procedure

### 6.3.1 Preparation of artificial and real raw milk samples

We evaluated the microdevice by using artificial mastitic milk prepared by adding white blood cells and real mastitis whole milk samples. Milk samples were collected directly from Holstein lactating cows at the University of Tennessee dairy farm.

In order to preserved the sample during storage, we use 1xPBS mixed with broponol (final 0.05%) of the sample preparation for the initial proof of concept experiment. Total white blood cell was extracted from whole milk using centrifuge

device. First, 10 ml whole milk was directly centrifuged (Eppendorf 5810R) with 2000 rpm for 10 minutes ,and after that, the milk sample have been separated in three layers which are supernatant layer (mostly lipid), medium layer (pure milk without any particles) and bottom cell layers (mostly white cells). The supernatant layer has been removed by a swab and the medium layer was taken out of tube by pipette. Then, 10 ml PBS solution were added in to the tube and centrifuged again with 4000 rpm for 10 minutes. Next, the supernatant once again decanted out and the pellet at the bottom layer was suspended in 1ml of PBS. The mixture sample were centrifuged with 3000 rpm for 5 minutes again (Eppendorf 5417R). Pellet in the tube after the centrifuge were taken out and mixed with 500 µl 1xPBS. Finally, the particle concentration were counted by hemocytometer.

After counting , the particle concentration of original 500 µl sample was around $7.7x10^6$ cells/ml, and it has been diluted into 5 different concentrations of 106 cells/mL, $10^5$ cells/mL, $10^4$ cells/mL, $10^3$ cells/mL and control sample. 1xPBS with broponol (0.05%) was used as the control sample for each experiment, respectively.

Also, we did the follow up optimization experiments directly on whole milk and the somatic cell count was verified by flow cytometry (BIO-RAD). 17 samples have been test in our microchip and the result will be shown in section 3.

### 6.3.2 Testing procedure and impedance measurement method

Impedance data were acquired using a high precision impedance analyzer (Agilent® 4294A), and the data were transferred to a laptop through its LAN port with its software Data Transfer V3.0. Two types of impedance data were obtained. One is the impedance spectrum from 40Hz to 10MHz at 5mVrms of excitation voltage. The

voltage is too low to induce appreciable ACEK effect, so that the fluid/electrode system is not disturbed by the measurement. The other type of measurement is to continuously record the impedance at a fixed excitation frequency and a selective voltage level of 1Vrms, which will induce ACEK effect at that frequency and provide us with information on the impedance change as a result of cell concentration.

## 6.4 Detection mechanisms

### 6.4.1 Detection of cell concentration via capacitance

#### 6.4.1.1 Mixture permittivity related with cell concentration

Our detection consists of two parallel metal plates separated by a certain distance and with a dielectric in between. The capacitance can be expressed as $C = \tilde{\varepsilon}_r \varepsilon_0 A / d$, where $\tilde{\varepsilon}_r$ is the relative permittivity of the medium between the electrodes, and $\tilde{\varepsilon}_0$ is the permittivity of free space, $\varepsilon_0 = 8.854 pF/m$, $A$ the area of the metal electrodes, and $d$ the distance between them. When there is a change in the dielectric properties in the material between the plates, a change in the capacitance will occur. Thus, to determine cell concentration suspended in a medium, capacitive sensing achieves this objective by extracting any change in the permittivity of the medium solution. For spherical particles with $\tilde{\varepsilon}_p$ dispersed in a suspending medium of $\tilde{\varepsilon}_m$ a volume fraction $\varphi$, the mixture permittivity can be described as [17]

$$\tilde{\varepsilon}_{mix} = \tilde{\varepsilon}_m \frac{1 + 2\varphi\left(\frac{\tilde{\varepsilon}_p - \tilde{\varepsilon}_m}{\tilde{\varepsilon}_p + 2\tilde{\varepsilon}_m}\right)}{1 - \varphi\left(\frac{\tilde{\varepsilon}_p - \tilde{\varepsilon}_m}{\tilde{\varepsilon}_p + 2\tilde{\varepsilon}_m}\right)} \qquad (6\text{-}1)$$

where $\tilde{\varepsilon}_m$ and $\tilde{\varepsilon}_p$ are the relative complex permittivity of the medium and particle,

respectively. In our case, particle is the cell and medium is pure milk. The relative permittivity of cell is around 7.2-12.8 [18], while that for water based sample (milk) is around 80, $\tilde{\varepsilon}_p << \tilde{\varepsilon}_m$. Therefore, equation (1) can be simplified as

$$\tilde{\varepsilon}_{mix} = \tilde{\varepsilon}_m \frac{1-\varphi}{1+\frac{1}{2}\varphi} \qquad (6\text{-}2)$$

where is $\tilde{\varepsilon}_{mix}$ the relative permittivity of the mixture. From the equation (6-2), we can clearly see that the total mixture permittivity decreases with increasing volume fraction $\varphi$. The cell concentration directly influenced the volume fraction, and the volume fraction $\varphi$ affects the mixture permittivity. The change of the mixture permittivity will directly lead to a change in the total capacitance of the device. Therefore, the cell concentration can be represented through the change of total capacitance of the device. This indicates more cell in the detection area, the smaller capacitance of the device will be.

#### 6.4.1.2 Capacitive sensing

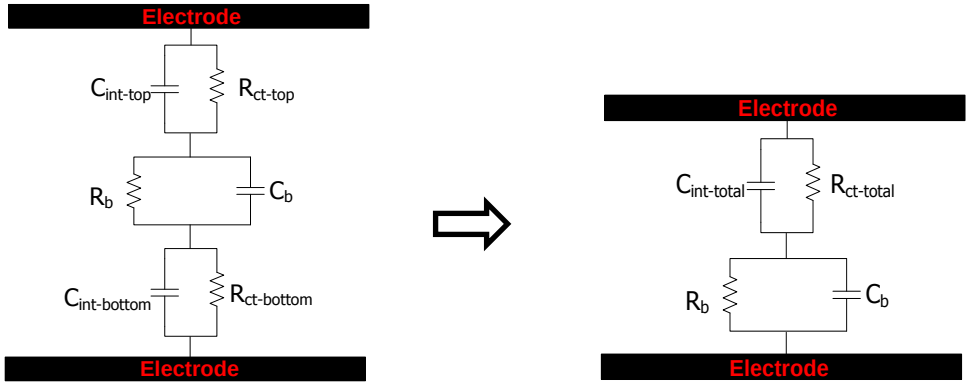


(a) (b)

Figure 6- 4 (a) Equivalent circuit of the whole sensing device, (b) Simplified circuit

Impedance between a pair of parallel electrodes immersed in liquid can be approximated as a network of capacitor and resistive components as shown in figure 6-4 (a).The interfacial capacitor $C_{int}$ mostly consists of equivalent capacitance caused by electric double layer, a resistive component $R_{ct}$ is parallelly connected with $C_{int}$. The $R_b$ and $C_b$ are the resistance and capacitance of bulk solution. Figure 6-4 (b) is the simplified equivalent circuit of figure 6-4 (a), the $R_{ct}$ and $C_{int}$ for the top and bottom mesh electrode are combined together for the simplification of calculation. The cell concentration will influence the permittivity of the mixture suspension as discussed earlier, and is expected to be manifested through changes in $C_b$. In the real experiment, $R_{ct}$ is a very large value which can be neglected in our situation. Then, the overall impedance of the device can be calculated as:

$$Z = \frac{R_b}{1+R_b^{\,2}\omega^2 C_b^{\,2}} - j\left(\frac{1}{\omega\left(C_b + \frac{1}{\omega^2 R_b^{\,2} C_b}\right)} + \frac{1}{\omega C_{\text{int}-total}}\right) \tag{6-3}$$

from the imaginary part, it can be considered as two capacitor series connection $C_{\text{int}-total} + C_b(1+1/(\omega R_b C_b)^2)$, in the series connection, the smaller capacitor dominate the total capacitance. Since milk is a very conductive liquid (0.5 S/m), the ELD thickness on the electrode surface is very thin and the $C_{int}$ is a rather large value compared with $C_b$, therefore $C_b$ is the main factor for change of the whole device capacitance.

In reality, when measuring the capacitance of an electrode/electrolyte cell, there always exist inconsistences from sensor to sensor, mostly due to the variations in electric properties of real life samples and the nature of electrode surface functionalization. Therefore, normalized capacitance change rate (i.e. $\Delta C/Cori$ over a fixed test period) is

employed to indicate the surface binding events. Because ΔC/Cori, can be directly correlated with the amount of cells in the sensor area, this is a potentially quantitative detection method. Also, using capacitance change rate, i.e. ΔC/Cori, helps to improve the test repeatability. As a result, the baseline and initial capacitances will have a range instead of a well-defined value. Using the capacitance change rate, the uncertainty in test results can be reduced, since the aforementioned test variations will be factored out.

### 6.4.2 Sensor operation

The demonstration of lipid and cell movement in the sensor site has been shown in figure 6-5. The figure describes the cross-section view of the sensor area. The movement of cell and lipid are influenced both by gravity, DEP and ACET. In the area closed to electrode edge, DEP and ACEK start to dominate the movement of the cells. Cells will be pushed away from the electrode due to N-DEP force, and go along with the vortices flow generated by ACET. However, once the cells reach the area far enough from electrode (>3μm), the gravity will dominate the cells moving, and finally make the cells pass down through the sensor area.

Since the velocity of lipid rising is relatively faster than the cell, nearly all the lipids will levitate out of the sensor area in 1 minutes. That is the reason why the results with a longer scanning time is better than the first 1 minute results. As shown in figure 6-5, there are two types of electrode meshes in the device, the electrode width for the top mesh is 50 μm with a 100 μm opening, and the electrode width for the bottom mesh is 20 μm with a 30 μm opening. The different opening size of these two meshes directly influence the electrical field strength in the sensor. Due to the different opening size of the electrode mesh, the magnitude of DEP and ACET at the top electrode mesh is less

than the forces at the bottom electrode. In our case, the negative DEP (N-DEP)phenomenon has been observed, which the cells will be repelled away from the electrodes. The N-DEP will try to slow the process of cell entering the sensor area at top electrode, and hinder the cell passing out of sensor area at bottom electrode. The total time of the cell passing through the sensor area will be extend due to the DEP and ACET effect. This will greatly increase the sensitivity and stability of our device. The influence of DEP and ACET for lipid is less than the cell, since the lipid rising velocity is much faster than cells. The time for DEP and ACET act on the lipid particles is very limited.

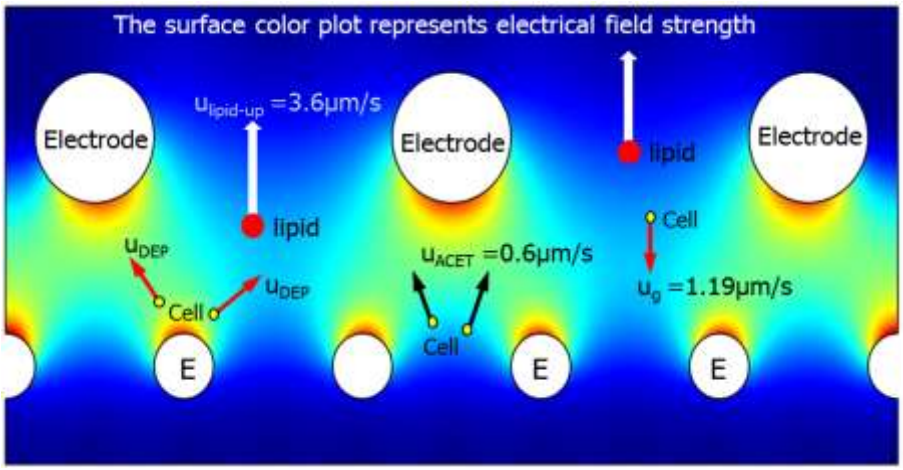


Figure 6- 5 Cross-section view of particles (cell and lipid) movement in the device sensor area

### 6.4.3 Cell movement in microfluidic environment

Cell in our detection device actually encountered two types of mechanism. One is sedimentation caused by gravity and the other is ACEK caused by applying electrical field. The ACEK mechanism has already introduced in chapter two, we are going to talk about the sedimentation in this section.

The sedimentation phenomena due to gravity is one major mechanism to be considered for our device. Sedimentation is the tendency for particles in suspension to settle out of the fluid in which they are entrained, the forces are due to gravity. The movement velocity of particle in the medium is governed by the equation:

$$u = \frac{2(\rho_m - \rho_p)}{9\eta} g a^2 \tag{6-4}$$

where $\rho_m$ and $\rho_p$ are the medium and particle mass density, respectively. $u$ is the particle velocity, $\eta$ is viscosity and $g$ is gravitational acceleration. $a$ is the radius of particle.

The general procedure of the detection is that, once the sample has been injected in the sensor, all the cells will fall down to the bottom chamber of the device. The density of cell is larger than the medium. Once the cell entered the sensor area, the capacitance of the whole device will change immediately. Since the permittivity of cells is less than the medium, the capacitance is decreasing with cells continually into the sensor space. The sample with high concentration indicates larger capacitance change. However, the cell finally will pass through the sensor area under gravity effect and after the cell totally dropped out of detection area, the capacitance of device will increase. Therefore, the capacitance change is the competition result of the numbers of cell into and out of the sensor area. Gravity is the main force which makes all cells settle down and pass through the sensor area, without the gravity the cell will only be suspended in the solution and there will be no capacitance change.

Also lipid is another particle in the milk solution, which can also influence the capacitance changes. Due to the difference of density of lipid, cell and milk, lipid and

cell can be separated by the sedimentation. From the reference[19], the mass densities of particles in the milk are $\rho_{cell} = 1077 kg/m^3$ for white blood cells and $\rho_{lipid} = 900 kg/m^3$ for lipid, $\rho_{milk} = 1033 kg/m^3$ for whole milk. The viscosity milk is $\eta_{milk} = 2.127 \times 10^{-3} Pa \cdot S$

The movement velocity for white blood cell and lipid can be calculated by equation (6-4). The velocity of lipid rising is 3.6 μm/s and the velocity of cell sediment is 1.19 μm/s. The distance from bottom of channel to upper side of electrode is around 150 μm, that means after 1 minute, all the lipid will totally leave the sensor area and will not affect the final detection.

## 6.5 Proof of concept of the impedimetric sensor

### 6.5.1 Impedimetric characterization of sensor

In the experiment, we found negative DEP and ACET flow happened below 100 kHz. The maximum negative DEP has been observed with frequency around 1 kHz. The chemical reaction happened with frequency lower than 500 Hz and will ruin the sensing result. In order to protect the mesh electrode and obtain precise result, the applied frequency is limited above 500 Hz.

Impedance spectra of the electrode/electrolyte system were examined to establish its electric equivalent circuit, and to determine which elements would predominately account for the changing of impedance for different cell concentration level. Impedance spectra of our detective were recorded at 5 mVrms from 40 Hz to 6MHz, a range of the most interest to our detection method. The impedance spectra together with fitted

curves are shown in figure 6-6 with extracted circuit parameters given in Table 6-1.

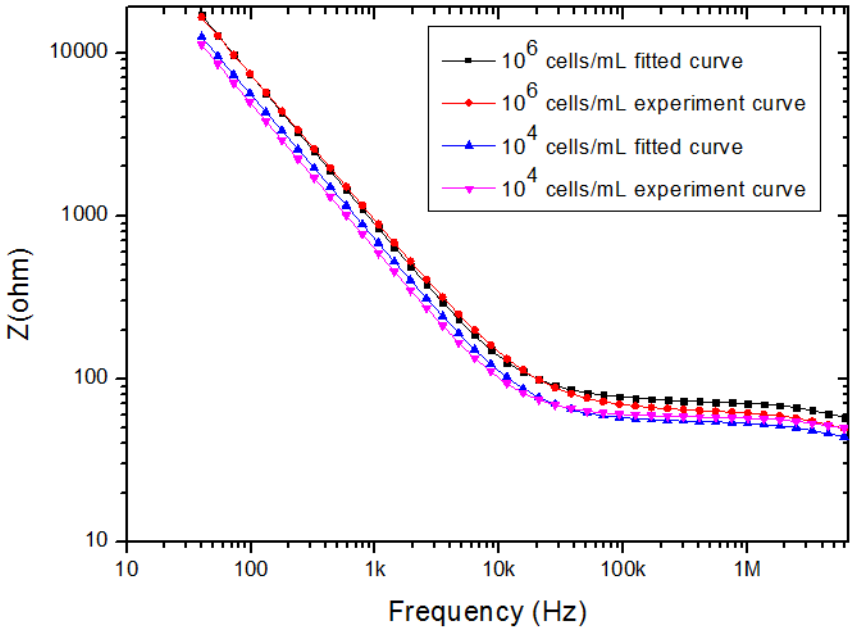


Figure 6- 6 The comparison results for measured impedance spectra and curve fitting

Table 6-1 Equivalent circuit parameters obtained by curve-fitting the experimental results with the equivalent circuit in figure 6-4 (b)

| **Steps** | **$R_b$(Ω)** | **$C_b$ (nF)** | **$R_{ct\text{-}total}$(Ω)** | **$C_{int\text{-}total}$ (nF)** |
|---|---|---|---|---|
| $10^4$ cells/mL | 75 | 30 | 800k | 180 |
| $10^6$ cells/mL | 80 | 20 | 800k | 180 |

The circuit elements listed in Table 6-1 demonstrates the electrical property for the detection device with applied frequency 1 kHz. $R_{ct}$ and $C_{int}$ describe the electrical properties at the electrode/electrolyte interface, while $R_b$ and $C_b$ describe the properties of the electrolyte bulk. From the curve fitting result, we know that the Cb is the main elements which dominate the change of the impedance.

For example, at 1 kHz, the reactance for $C_{int\text{-}total}$ and $C_b$ of sample $10^4$ cells/mL are

calculated to be 53 Ω (<<$R_{ct\text{-}total}$) and 5.5 Ω, respectively. Since the Rct is very large, it can be seen that Cint, Rb and Cb dominate the impedance response for the frequency of interest to this work (1 kHz). Cint-total and Cb is kind of series connection, and for the series capacitance connection calculation the smaller one dominates the change of the whole capacitance. Therefore, the change of the Cb will finally demonstrates on the capacitance measurement with different cell concentration level. since the resistance can be influenced by various factors. Also above 1 MHz, the reactance for $C_{int\text{-}total}$ and $C_b$ increased to around 500k nF and 5k nF, in that case the $R_{ct}$ can not neglected. Therefore, the differential result at high frequency should not be considered.

Compared with resistance, the capacitance is an effective parameter for representing the cell concentration level. The capacitance for each solution is rather stable and sensitive enough for the detecting.

### 6.5.2 Correlation of sensor capacitance with white blood cell concentration

The representative impedance spectra of the detection device with different cell concentrations were presented in figure 6-7. This artificial milk samples were prepared by extracting the cells from real milk and dilute in 1xPBS for different concentrations, as we discussed previously. The main content for control buffer is 1xPBS. The sample were tested under ultra- low voltage 5 mV with scanning frequency range 40 Hz – 6 MHz.

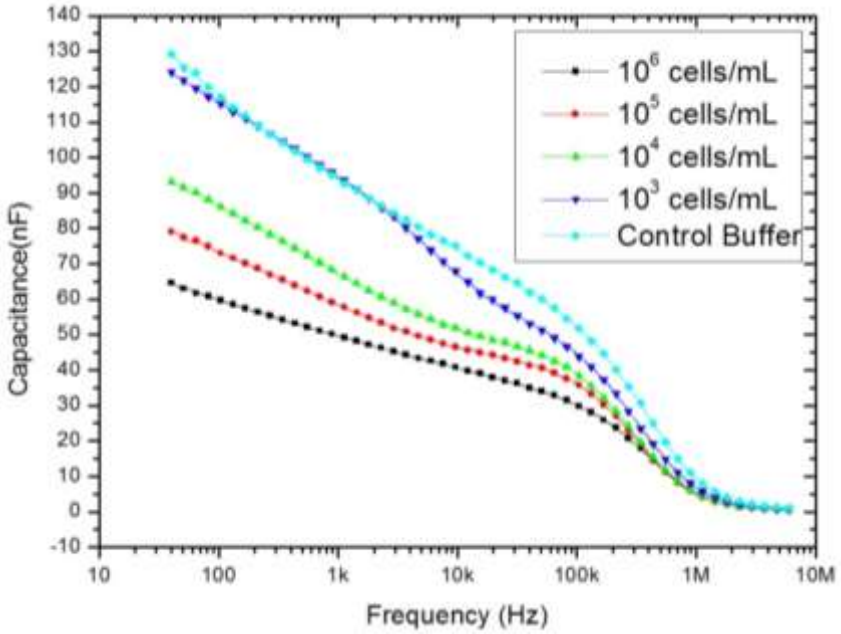


Figure 6- 7 The capacitance spectrum of the detection device with PBS based spiked sample

It is obviously to see that, the higher concentration of cell demonstrates a lower capacitance value, which is due to the difference of permittivity between cell and medium. However, the milk from different cow have different base capacitance value. It will not work for the sample with different cow supplier. The capacitance spectra detection is only workable for distinguishing artificial milk by diluting the sample from same cow at same time. But it successfully prove the correlation between capacitance and cell concentration. In order to solve the absolute value of capacitance from different cow, the normalized capacitance changes rate has been introduced and explained in next section.

### 6.5.3 Cell concentration detection by capacitance changing

The proof of concept experiment has been presented to demonstrate that our capacitance detection device is capable of distinguishing white blood cell concentration. The opening of top mesh electrode and bottom electrode are 100 μm and 50 μm,

respectively. The applied signal on the device is 1 kHz at 500 mVrms. The samples are diluted to five different concentration in a PBS based medium.

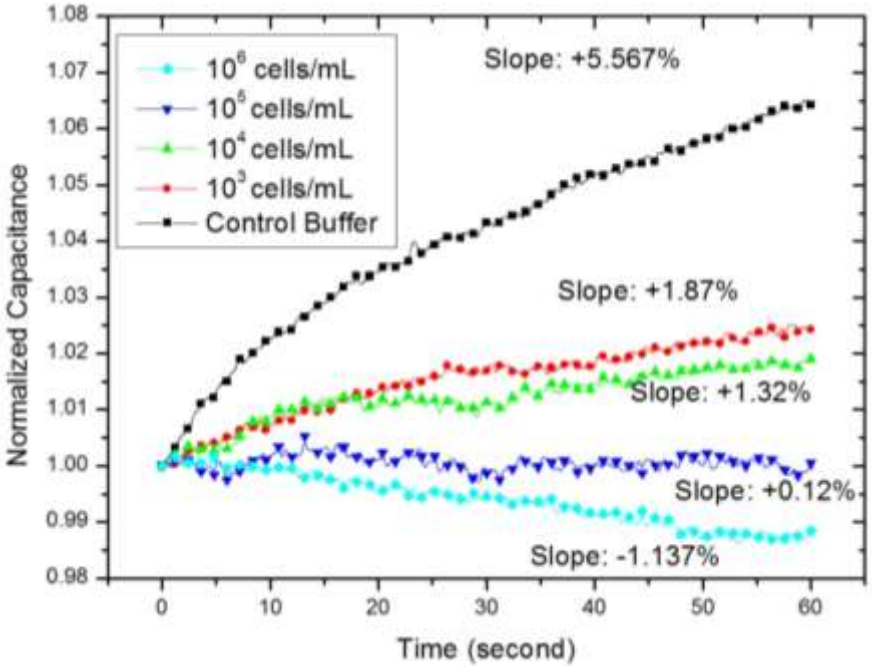


Figure 6- 8 Normalized dC/dt value as function of time with larger electrode mesh at top and smaller mesh electrode at bottom

In order to minimize the capacitance fluctuation from one electrode mesh to another, normalized capacitance were used and calculated as Norm(C)=C/Cori, and the change rates were plotted as a function of time in figure 6-8 for samples with five concentrations. From the figure 6-8, it clearly shows that, the capacitance of the control sample and the sample with a rather low cell concentration keep increasing, and the capacitance change rate reaches almost 55.67 ‰ per minute for the control sample. However, with a higher concentration of cell the capacitance change rates tends to be decreased and reached to -11.37‰ at the level of $10^6$cells/mL The comparison result of

control and sample with high concentration indicates that the test protocol can clearly distinguish and detect the cell concentration level.

Also in order to verify the DEP and ACET effect to the sensing result, the top and bottom mesh electrode have been switched, with smaller mesh electrode (30 μm opening) at top layer and larger mesh electrode ( 100 μm opening) at bottom. The results have been shown in figure 6-9.

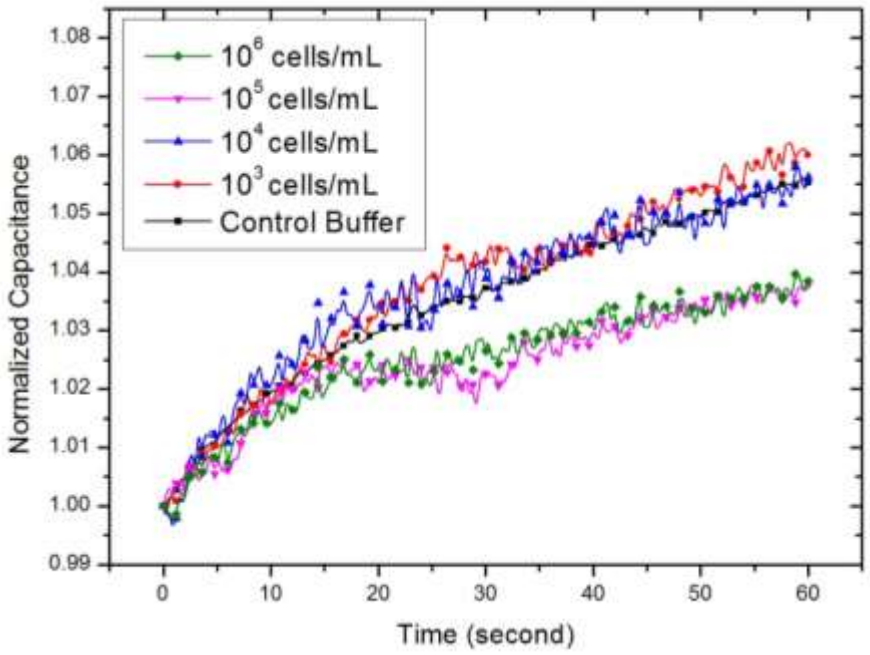


Figure 6- 9 Normalized dC/dt value as function of time with smaller electrode mesh at top and larger mesh electrode at bottom

It is clearly to see that the differentiae effect is not very obvious, the capacitance changing rate for sample with different concentration are almost same as the control

sample. It is difficult to see the capacitance change caused by cells. This can be explained that the DEP effect and ACET are getting less, since the opening of the mesh electrode is larger at the bottom. The deferring ability to cell from DEP and ACET decreased. The sensitivity of device reduced.

## 6.6 Optimization of impedimetric biosensor

In this section, the whole milk samples directly from dairy farm have been tested for verifying the optimized condition of the impedimetric biosensor. The somatic cell concentration level has been verified by flow cytometry (BIO-RAD).

### 6.6.1 Sensing frequency

Since ACEK is frequency dependent, the sensing frequency optimizations for whole milk sample have been designed and executed. The results are showing in figure 6-10, three frequencies (1 kHz, 50 kHz, 500 kHz) have been tested in the experiment. The sample with 1 kHz demonstrates the best detection results both on the aspect of standard deviation and Pearson correlation $R^2$. However, with increasing the frequency, the detection effect for different cell concentration is getting worse. The data with applied frequency 500 kHz shows a rather larger standard deviation and the distinguish of sample between low concentration and higher concentration are not very obvious.

There are three possible reasons for this phenomena. First, according to the DEP verified experiment, the N-DEP of white blood cell can only be observed with the applied frequency below 100 kHz. With a lower frequency, the N-DEP is getting stronger. At the

frequency 500 kHz, there is no obvious DEP effect, no matter N-DEP or PDEP. N-DEP is the main force which repels the cell adhesion on the electrode, without N-DEP the cell statistically can attach on the electrode which changed the capacitance and made the capacitance change more fluctuation and unstable. More important, if there is no N-DEP the cells will directly pass through the mesh opening and the dropping rate for top and bottom mesh will be same. The capacitance changing rate for different cell concentration will be similar to the control sample. Therefore with a high NDEP the result will be more precise and stable. This is proved by the standard deviation value on figure 6-10.

Second, all the dC/dt value at the frequency 500 kHz are less than the experiment data with applied 1 kHz and 50 kHz, even other experiment condition are exactly same. This can be explained by checking the impedance spectrum of the electrode. From the impedance spectrum, at 1 kHz or 50 kHz, the capacitance dominates the impedance value of the whole device. However, at 500 kHz, the impedance of the whole device are dominated by the resistance, the capacitance effect become relatively small. Therefore, the dC/dt value of capacitance with applied frequency 500 kHz decrease and the ability of distinguishing different cell concentration of the device is getting weaker.

Third, the permittivity of cell is a frequency dependent variable. With a higher frequency, the complex permittivity of cell is getting larger which will increase the capacitance value of the device. Therefore, the capacitance absolute value increase and finally influence the dC/dt value.

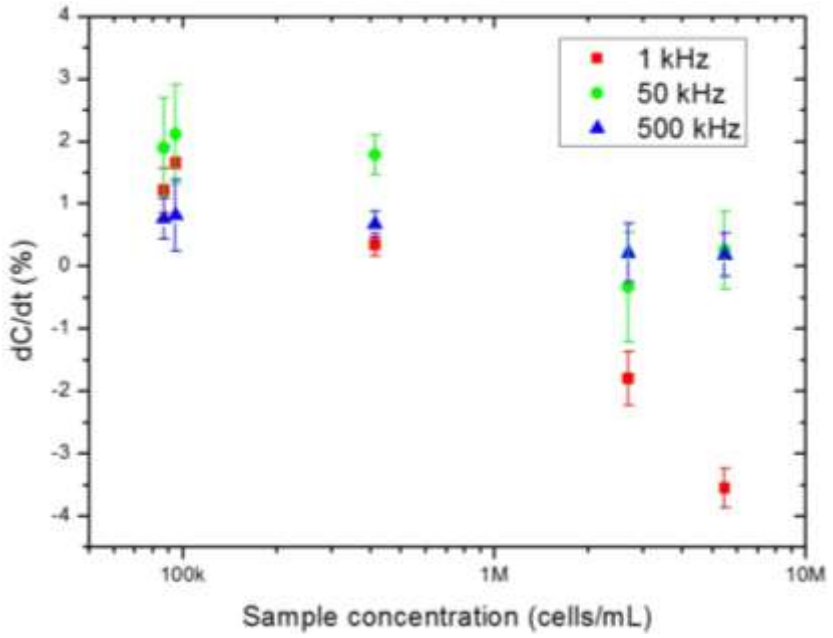


Figure 6- 10 Normalized capacitance changes rate for 6 cell concentration levels with three different frequency.

### 6.6.2 Voltage dependence of the cell detection

ACET effect is another factor which can influence the detection effect because the suspended cells encounter the drag force from flow motion. The cell mixing and acceleration from ACET can affect the internal flow field and detection ability for the sensor. Consider the result of frequency optimization, in the voltage dependence verification experiment, we use 1 kHz as the applied frequency for all the tests. The optimized results of dC/dt value have been shown in figure 6-11. From the plot, the sample with different concentrations almost can be all distinguished and detected. On the standard deviation aspect, the higher applied voltage 1 Vrms shows the better result. It indicates that ACET is one reason to enhance the detection effect of the device. However, the sensitivity improvement from increasing voltage is not very obvious since ACET is

still not the main force in this condition. However, the larger voltage (>1.5 Vrms) will cause the chemical reaction and electrolysis which total ruined and disturbed the sensor. Therefore, the 1 Vrms is the optimized voltage for our device.

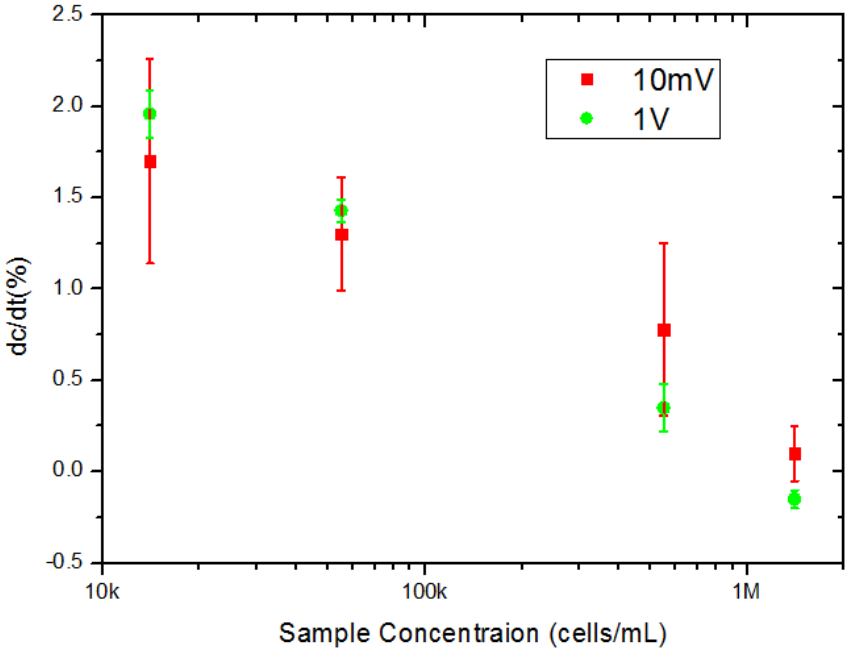


Figure 6- 11 Normalized capacitance changes rate for 4 cell concentration levels with three voltages

### 6.6.3 Optimization of scanning time

As we discussed above, the rising velocity of lipid is around 3.6 μm/s, and the thickness of the bottom chamber and the distance between mesh electrodes are 120 μm and 40 μm, respectively. Obviously, the total time for lipids completely rising out of the sensor area is more than 50 seconds. Also considered the N-DEP affect the lipid as well, the time actually will last longer. The electrical properties of lipid are different from cells, the sensing result will be affected with lipid in the sensing area. In order to reduce the lipid effect and increase the sensor sensitivity, the optimization of scanning time have been designed and executed. In this experiments, 17 raw milk samples with different

concentration have been scanned with different start time point. The total scanning time for each test still last 1 minute, but the data are recoded with different start time, 0, 1 minute, 2 minute, 3 minute, 4 minute, 5 minute. The results have been shown in figure 6-12.

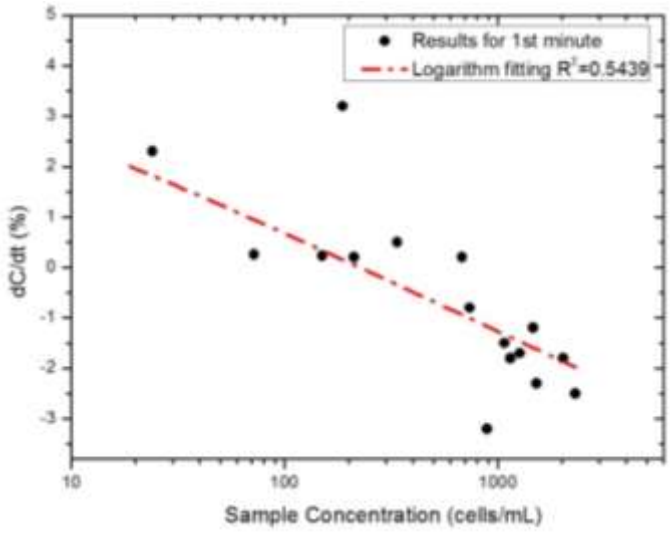


(a)

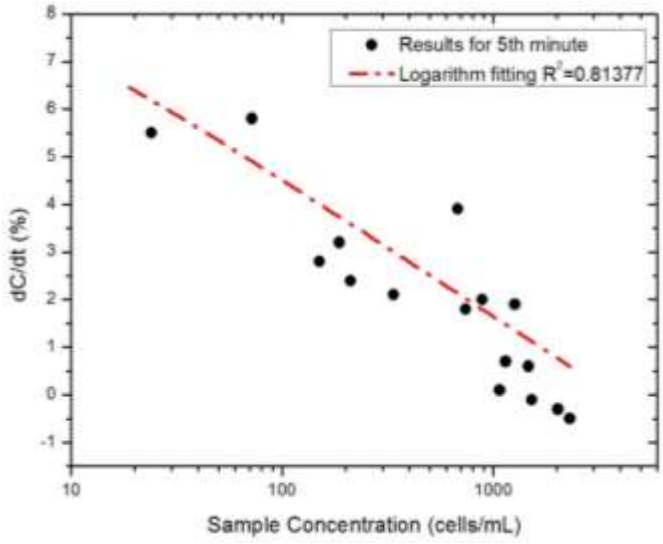


(b)

Figure 6- 12 Normalized capacitance changes of 1st and 5th minute for 17 milk samples

From the plot, the result of 5th minute is much better than the 1st minute on the aspect of R2. That proves that the lipid influence at 5th minute is almost over, and the capacitance change are mainly caused by the cells during that time. Also, with more cell passing through the bottom mesh electrode, the dC/dt value will be increased because the number of cells out of sensor area are getting larger. With longer testing time, when there is no more fresh cells coming into the sensor area, the capacitance will turn to positive value. The detection result during that time will become less accurate and sensitive.

## 6.7 Conclusion

In this chapter, we have demonstrated a robust sensitive biosensor device using sedimentation and ACEK mechanism for the real time monitor and diagnosis of the mastitis in milk. The milk sample with mastitis disease has been successfully differentiated by our device, which is considerably faster and more precise than the traditional method. In addition, our device testing procedure is very simple and the cost is really low. In the experiment, the optimization of frequency ,voltage and measuring time have been done. In summary, the impedance method by measuring the capacitance change has a shorter measuring time, reduced the device cost, simpler the testing procedure. With further research, highly integrate and automatic diagnosis bio-chip with this technology will be developed and prototyped.

# CHAPTER SEVEN: CONCLUSIONS AND FUTURE WORK

## 7.1 Conclusions

This dissertation focuses on the ACEK and acoustic based bio-particle enrichment and impedimetric particle detection and quantification. Due to the ultra- low density of our targets particle in nature, the real time detection by suing biology method becomes a very difficult issue no matter in medical diagnostics, drug screening or environment protection. In order to solve this problem, we develop a 3D multi-level electrode platform to initially trap chlorella via ACEO and N-DEP. The multi-level microfluidic channel makes our device reusable which can be implanted in the in-line sample test microsystem. Optimization on the aspect of applied frequency, external flow rate and mesh opening size have been done and verified for searching best trapping efficiencies. Also, ACEO is not suitable for the sample cells which live in an environment with high electrical conductivity. The acoustic trapping method has been implanted to develop the cell concentration devices. Rapid and high trapping effect has been achieved by employing the acoustic trapping. Although the acoustic trapping owns the defect of low external flow rate, compared with ACEO mechanism, the particle trapping efficiency can reach 80%, which is an incredible results for accelerating the target particle enrichment. More important, it is very feasible to achieve particle separation and sorting by using acoustic mechanism due to the different ultrasonic properties of target particles.

The purpose of particle enrichment is detection and quantification, the detection method for the ACEO and Acoustic is based on photosensitive instrument (CCD, microscopy, photodiode) based fluorometer. The experiment instrument is bulky and

expensive, and this will be a vital defect for the portable and low cost LOC detection technology. An ACEK enhanced impedance immunosensor for Somatic cell counter have been developed and optimized. The fabricated LOC impedimetric biosensor successfully diagnosed the cow with mastitis disease by detecting the concentration level of somatic cells in the milk.

## 7.2 Future work

### 7.2.1 Highly integrated and automated particle detection device

The LOC and microfluidic device consists of multiple functions, such as micropumping, target sample concentration, separation, sorting, detection and sensing. This dissertation have already studied and successfully developed the concentration, detection and sensing part. However, the system for each function is isolated each other. The next step is to develop the highly integrated and automated particle detection device. This universal detection device will use ACEK for the sample with low electric conductivity and acoustic for the sample with high conductivity for the preconcentration functions, and afterwards embedded with impedimetric sensor for the detection and quantification, as shown in figure 7-1. A microcontroller will be implanted to control all the necessary operation with the impedance analyzer, signal generator, I/O device (eg.LCD) and wireless emitter for data transmission.

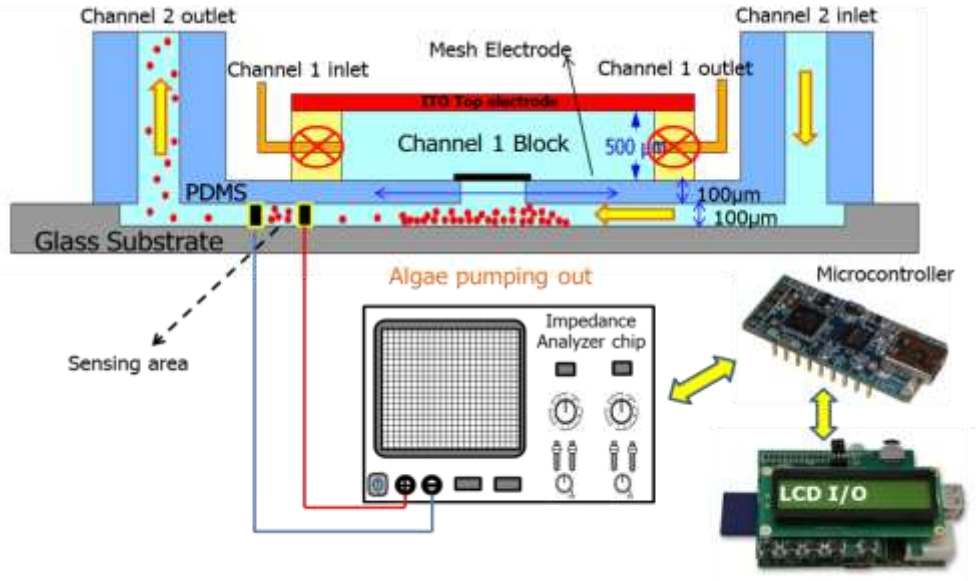


Figure 7- 1 Conceived fully automated lab on a chip multi-function micro particle detection and monitor device

### 7.2.2 ACEK flow through embedded impedimetric sensor

The micropumping device used in this dissertation are mainly depend on external pumping device, such as syringe pump. The traditional pumping device is bulky and low power efficiency, especially in the micro/nano scale. ACEK also is an notable candidate for supplying the micropumping for LOC chip. We plan to develop an automated particle detection device with functions of self-pumping, bio-signal amplify (particle concentration), particle quantification (impedimetric sensing) and data analysis. The main electro pattern has been shown in figure 7-2. The electrode inside the blue area is responsible for sensing only , and the rest area are designed to supply micro pumping. In order to avoid the electrical signal disturb each other, the operation procedure have been

divided into three steps. First, the ac signal for ACEK pumping is on, and the sample follow the trail of the electrode and coming to the central part of the sensor. Then, ACEK pumping signal off, the sensor power on and start to detect and measure the sample accumulated in the central area. Finally, after the detection, the sample can be released out of the sensor area which makes the device reusable.

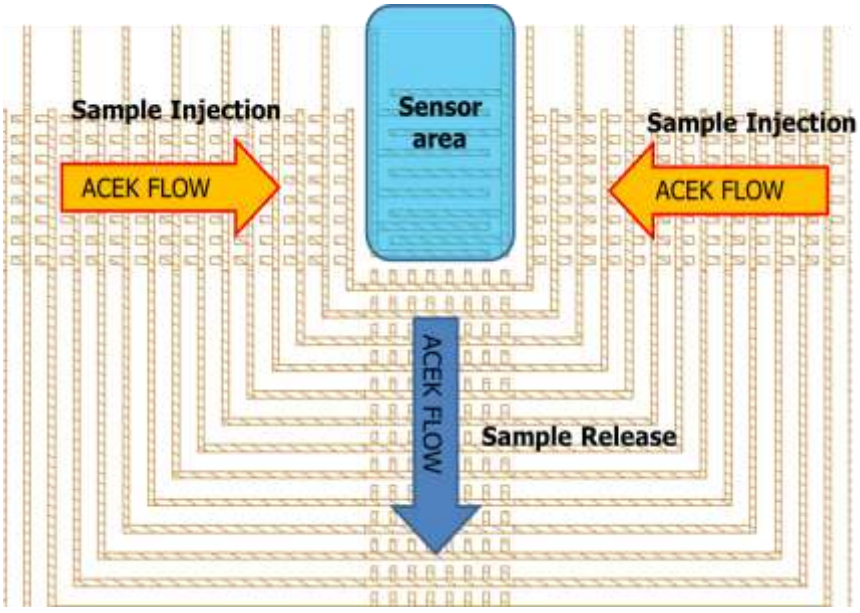


Figure 7- 2 Automated particle detection LOC device.

# LIST OF REFERENCES

Chapter 1

[1] Satcher D.S. Emerging infections: Getting ahead of the curve. Emerging infectious Diseases, 1995. 1:1-6

[2] Simon, JD.Biological terrorism: preparing to meet the threat. Journal of American Medical Association, 1997. 278: 428-430

Chapter 2

[1] W. H. Tan and S. Takeuchi, Proc. Natl. Acad. Sci. U. S. A., 2007, 104, 1146–1151.

[2] J. S. Lee, R. Dylla-Spears, N. P. Teclemariam and S. J. Muller, Appl.Phys. Lett., 2007, 90, 074103.

[3] B. R. Lutz, J. Chen and D. T. Schwartz, Anal. Chem., 2006, 78, 5429–5435.

[4] C. M. Lin, Y. S. Lai, H. P. Liu, C. Y. Chen and A. M. Wo, Anal. Chem., 2008, 80, 8937–8945

[5] D. Di Carlo and L. P. Lee, Anal. Chem., 2006, 78, 7918–7925

[6] A. M. Skelley, O. Kirak, H. Suh, R. Jaenisch and J. Voldman, Nat. Methods, 2009, 6, 147–152

[7] J. Sinclair and A. K. Salem, Biomaterials, 2006, 27, 2090–2094

[8] D. Di Carlo, N. Aghdam, L.P. Lee, Anal. Chem. 78 (2006) 4925.

[9] C. M. Schroeder, H. P. Babcock, E. S. G. Shaqfeh and S. Chu,Science, 2003, 301, 1515–1519

[10] T. T. Perkins, D. E. Smith and S. Chu, Science, 1997, 276, 2016–2021.

[11] W.H. Tan, S. Takeuchi, Proc. Natl. Acad. Sci. U.S.A. 104 (2007) 1146.

[12] Garces-Chave, V.et al., “Simulations micromanipulation in multiple planes using a self-reconstructing light beam.” Nature 419 (6903),pp. 145-147 (2002)

[13] Munce, N., J. Li, P. Herman, and L. Lilge, “Single cell analysis on a microchip platform using optical tweezers and optical scissors.” Proceeding s of SPIE 4982, pp.28-36 (2003)

[14] Flynn, R.A. et al., “Parallel transport of biological cells using individually addressable VCSEL arrays as optical tweezers.” Sensors and Actuators, B: Chemical 87(2), pp. 239-243(2002)

[15] Grover, S.C., A.G. Skirtach, R.C. Gauthier, and C.P. Grover, “Automated single-cell sorting system based on optical trapping system.” Optics Express 7(13),pp.533-539 (2000)

[16] M.A.M. Gijs, Microfluidics Nanofluidics 1 (2004) 22.

[17] K. Smistrup, T. Lund-Olesen, M.F. Hansen, P.T. Tang, J. Appl. Phys. 99 (2006) 3.

[18] H. Lee, A.M. Purdon, R.M.Westervelt, Appl. Phys. Lett. 85 (2004) 1063.

[19] Q. Ramadan, V. Samper, D.P. Poenar, C. Yu, Biosens. Bioelectron. 21 (2006) 1693.

[20] J. Wu, J. Acoust. Soc. Am., 1991, 89, 2140–2143.

[21] H. M. Hertz, J. Appl. Phys., 1995, 78, 4845–4849.

[22] M. Wiklund, S. Nilsson and H. M. Hertz, J. Appl. Phys., 2001, 90, 421

[23] J. F. Spengler, M. Jekel, K. T. Christensen, R. J. Adrian, J. J. Hawkes and W. T. Coakley, Bioseparation, 2000, 9, 329–341.

[24] W. T. Coakley, D. Bazou, J. Morgan, G. A. Foster, C. W. Archer, K. Powell, K. A. Borthwick, C. Twomey and J. Bishop, Colloids Surf., B, 2004, 34, 221–230.

[25] S. P. Martin, R. J. Townsend, L. A. Kuznetsova, K. A. J. Borthwick, M. Hill, M. B. McDonnell and W. T. Coakley, Biosens. Bioelectron, 2005, 21, 758–767

[26] R. Barnkob, P. Augustsson, T. Laurell and H. Bruus, Lab Chip, 2010, 10, 563–570.

[27] J. J. Shi, X. L. Mao, D. Ahmed, A. Colletti and T. J. Huang, Lab Chip, 2008, 8, 221–223. 22 J. J.

[28] PK. Wong, CY. Chen, TH. Wang and CM. Ho, Electrokinetic bioprocessor for concentrating cells and molecules, Analytical Chemistry 2004; 76 (23): 6908-6914

[29] K. H. Bhatt, S. Grego, and O. D. Velev, An AC electrokinetic technique for collection and concentration of particles and cells on patterned electrodes, Langmuir 2005; 21 (14): 6603-6612

[30] PK. Wong, CY. Chen, TH. Wang and CM. Ho, Electrokinetic bioprocessor for concentrating cells and molecules, Analytical Chemistry 2004; 76 (23): 6908-6914

[31] Jie Wu, Yuxing Ben, David Battigelli, and Hsueh-Chia Chang, Long-Range AC Electroosmotic Trapping and Detection of Bioparticles, Ind. Eng. Chem. Res. 2005, 44, 2815-2822

[32] Jie Wu, Senior Member, IEEE Biased AC Electro-Osmosis for On-Chip Bioparticle Processing, IEEE TRANSACTIONS ON NANOTECHNOLOGY, VOL. 5, NO. 2, MARCH 2006

[33] N.Islam, M.Lian and J.Wu, Enhancing microcantilever capability with integrated AC electroosmotic trapping, Microfluidics and Nanofluidics, 10404-006-0138-z,2006

[34] M. Lian, N. Islam and J. Wu, AC electrothermal manipulation of conductive fluids and particles for lab-chip applications, IET Nanobiotechnology 2007; 1(3): 36-43

[35] Khandurina, J.; McKnight, T.E.; Jacobson, S.C.; Waters,L.C.; Foote, R.S.; Ramsey, J.M. Integrated system for rapid PCR-based DNA analysis in microfluidic devices. Anal. Chem, 2000, 72, 2995-3000.

[36] Humble, P.H.;Kelly,R.T.;Woolley, A.T.; Tolley, H.D.; Lee, M.L. Electric field gradient focusing of proteins based on shaped ionically conductive acrylic polymer. Anal. Chem. 2004, 76, 5641-5648

[37] Jung,B.; Bharadwaj, R.; Santiago, J.G. Thousandfold signal increase using field-amplified sample stacking for on-chip electrophoresis. Electrophoresis 2003, 24, 3476.

[38] Yang, H.; Chien, R.L. Sample stacking in laboratory-on-a-chip devices. J.Chromatogr. A 2001, 924, 155-163

[39] Jung, B.; Zhu,Y.; Santiago, J.G. Detection of 100 aM fluorophores using a high sensitivity on-chip CE system and transient isotachophoresis. Anal. Chem. 2007, 79(1), 345-349

[40] Medoro, G. et al. "A lab-on-a-chip for cell detection and manipulation", IEE sensors Journal 3(3), pp. 317-325 (2003)

[41] N. G. Green, A. Ramos, and H. Morgan, Ac electrokinetics: a survey of sub131 micrometre particle dynamics, J. Phys. D: Appl. Phys. 33 632 (2000)

[42] Li, H and R. Bashir, "Dielectrophoretic orientation, manipulation and separation of live and heat-treated cells of listeria on microfabricated devices with interdigitated electrodes." Proceedings of MRS 729, pp. 167-172 (2002)

[43] Nicolo Manaresi, Aldo Romani, Gianni Medoro, Luigi Altomare, Andrea Leonardi, Marco Tartagni, Roberto Guerrieri, A CMOS Chip for Individual Cell Manipulation and Detection, IEEE Journal of Solid-state circuits, Vol 38, No. 12, 2003

[44] Kentsch, J.et al. “Microdevices forseparation, accumulation, and analysis of biological micro-and nanopraticles.” Proceedings of IEEE Nanobiotechnology 150 (2), pp. 82-89 (2003)

Chapter 3

[1] Glenn Whitworth and W.T. Coakely, Particle column formation in a stationary ultrasonic field, J.Acoust. Soc. Am, 91 (1), January 1992

[2] H.M.Hertz, Standing-wave acoustic trap for nonintrusive positioning of microparticles, J.Appl.Phys. 78(8), 15 October 1995

[3] Thomas Laurell, Filip Petersson and Andreas Nilsson, Chip integrated strategies for acoustic separation and manipulation of cells and particles, Chem.Soc.Rev.,2007, 36, 492-506

[4] M. Evander, Cell and Particle Trapping in Microfluidic Systems using Ultrasonic StandingWaves, Department of Electrical Measurements and Industrial Engineering and Automation, Lund University, Lund, 2008.

[5] Takashi Masudo and Tetsuo OKADA, Ultrasonic Radiation – Novel Principle for Microparticle Separation, ANALYTICAL SCIENCES 2001, VOL. 17 SUPPLEMENT, 2001

[6] Louis V.King, On the Acoustic Radiation Pressure on Circular Discs: Inertia and Diffraction Corrections, Proc. R. Soc. Lond. A 1935 153, doi: 10.1098/rspa.1935.0218

[7] Yoshioka K and Kawashima Y, Acoustic radiation pressure on a compressible sphere, 1955 Acoustica 5-167

[8] Martin Groschl, Ultrasonic Separation of Suspended Particles – Part I: Fundamentals, ACUSTICA,acta acustica, Vol, 84 (1998) 432-447

[9] Nyborg, W.L. (1978) Physical principles of ultrasound. In Ultrasound : Its Applications in Medicine and Biology, Part 1 ed. Fry, F.J. pp. 1–76. New York : Elsevier.

[10] Coakley, W.T., Bardsley, D.W., Grundy, M.A., Zamani, F. and Clarke, D.J. (1989) Cell manipulation in ultrasonic standing wave fields. Journal of Chemical Technology and Biotechnology 44, 43–62.

[11] H. A. Pohl, "The Motion and Precipitation of Suspensoids in Divergent Electric Fields", J. Appl. Phys. 22(7), 869–871 (1951).

[12] Pohl, H. A., 1958, "Some effects of nonuniform fields on dielectrics", J. Appl. Phys., 29(8), 1182 – 1188

[13] Ramos, A., Morgan, H., Green, N. G., & Castellanos, A. (1999) AC electric-field induced fluid flow in microelectrodes, Journal of Colloid and Interface Science 217:420-422.

[14] Ajdari, A (2000) Pumping liquids using asymmetric electrode arrays. Physical Review E 61: R45-R48

[15] V. Studer, A. Pépin, Y. Chen, and A. Ajdari, Analyst (Lond.) 129, 944(2004).

[16] Martin Z.Bazant, “AC Electro-osmotic Flow”

Chapter 4

[1] Miguel Rodriguez, J. and Elias Greenbaum, Detection Limits for Real-Time Source Water Monitoring Using Indigenous Freshwater Microalgae, Water Environment Research, Volume 81

[2] P. Mazzinghi A laser diode fluorometer for field measurements of the F685/F730 chlorophyll fluorescence ratio, Rev. Sci. Instrum. 67 (10), October 1996

[3] Jeffrey Cosgrove Michael Borowitzka, ‘Applying Pulse Amplitude Modulation (PAM) fluorometry to microalgae suspensions: stirring potentially impacts fluorescence’, Photosynth Res (2006) 88:343–350

[4] Ulrich Schreiber, Christian Neubauer & Ulrich Schliwa, PAM fluorometer based on medium-frequency pulsed Xe-flash measuring light: A highly sensitive new tool in basic and applied photosynthesis research, Photosynthesis Research 36: 65-72, 1993

[5] P.Mazzinghi, A laser diode fluorometer for field measurements of the F685/F730 chlorophyll fluorescence ratio, Rev.Sci.Instrum. 67(10). October 1996

[6]U.SCHREIBER, U.SCHLIWA and W.BILGER, Continuous recoding of photochemical and non-photochemical chlorophyll fluorescence quenching with a new type of modulation fluorometer, Photosynthesis Research 10:51-62

[7] Sachiko Ogata, Tomoyuki Yasukawa, Tomokazu Matsue, Dielectrophoretic manipulation of a single chlorella cell with dual-microdisk electrode, Bioelectrochemistry 54 (2001) 33-37

Chapter 5

[1] Pulak Nath, Derek Fung, Yuliya A.Kunde, Ahmet Zeytun, Brittany Branch and Greg Goddard, Rapid prototyping of robust and versatile microfluidic components using adhesive transfer tapes, Lab on a Chip, 2010, 10, 2286-2291

[2] S.S.Guo, L.B.Zhao, K.Zhang, K.H.Lam, S.T.Lau, X.Z.Zhao, Y.Wang, H.L.W.Chan, Y.Chen, and D.Baigl, Ultrasonic particle trapping in microfluidic devices using soft lithography, APPLIED PHYSICS LETTERS 92, 213901 (2008)

[3] Mikael Evander, Linda Johansson, Tobias Lilliehorn, Jure Piskur, Magnus Lindvall, Stefan Johansson, Monica Almqvist, Thomas Laurell, and Johan Nilsson, Noninvasive Acoustic Cell Trapping in a Microfluidic Perfusion System for Online Bioassays, Anal. Chem. 2007, 79, 2984-2991

Chapter 6

[1] L.M.Sordillo, K.Shafer-Weaver and D.DeRosa, J.Dairy Sci.,1997,80,1851-1865

[2] B.M. Jayarao, S.R.Pillai, A.A.Sawant, D.R.Wolfgang, and N.V.Hegde, J.Dairy Sci. 2004,87:3561-3573

[3] Eberhart, R.J., H.C. Gilmore, L.J. Hutchinson, and S.B. Spencer. 1979. Somatic cell counts in DHI samples. Proc. Ann. Mtg. Natl. Mastitis Counc., p. 32.

[4] Harmon, R.J. 1994. Physiology of mastitis and factors affecting somatic cell counts. J. Dairy Sci. 77:2103.

[5] Shohei Kimura, Junji Fukuda, Atsushi Tajima and Hiroaki Suzuki, On-chip diagnosis of subclinical mastitis in cows by electrochemical measurement of neutrophil activity in milk, Lab chip, 2012,12,1309

[6] M.Janzekovic, M.Brus, B.Mursec, P.Vinis, D.Stajnko, F.Cus, Mastitis detection based on electric conductivity of milk, Volume 34, Issue 1, May, 2009

[7] K.R.Petrovski, M.Trajcev and G.Buneski, A review of the factors affecting the costs of bovine masttis, Tydskr.S.Afr.vet.Ver, (2006) 77(2):52-60

[8] Crist, W.L. and R.J. Harmon. 1991. Controlling mastitis - The problem, its impact and future perspectives. In: T.P. Lyons (Ed.) Biotechnology in the Feed Industry. Alltech Technical Publications, Nicholasville, KY. pp 265-276

[9] Eberhart, R.J., R.J. Harmon, D.E. Jasper, R.P. Natzke, S.C. Nickerson, J.K. Reneau, E.H. Row, K.L. Smith, and S.B. Spencer. 1987. Current Concepts of Bovine Mastitis. 3rd ed. Natl. Mastitis Counc., Inc., Arlington, VA.

[10] Laevens, H., H. Deluyker, Y.H. Schukken, L. de Meulemeester, R. Vandermeersch, E. de Muelenaere, and A. de Kruif. 1997. Influence of parity and stage of lactation on somatic cell count in bacteriologically negative dairy cows. J. Dairy Sci. 80:3219.

[11]M.Morgante, S.Ranucci, M.Pauselli, D.Beghelli and G.Mencaroni, Total and Differential Cell Count by Direct Microscopic Method and Ewe Milk, J.Vet.Med. A 43. 451-458 (1996)

[12] Gonzalo, C., J. R. Martı´nez, J. A. Carriedo and F. San Primitivo, Fossomatic cell-counting on ewe milk: comparison with direct microscopy and study of variation factors. J. Dairy Sci. 2003, 86:138-145.

[13] Alan W.Hill, Kenneth G.Hibbitt and Jonathon Davies, Particles in bulk milk capable of causing falsely high electronic cell counts, Volume 49, Issue 02, Journal of Dairy Research, pp 171-177

[14] P.Schmidt Madsen, Fluoro-opto-electronic cell-counting on milk, Journal of Dairy Research, Volume 42, Issue 02, pp 227-239

[15] Sargeant, JM, Leslie KE, Shirley JE, et al: Sensitivity and Specificity of Somatic Cell Count and California Mastitis Test for Identifying Intramammary Infection in Early Lactation. J Dairy Sci 84:2018-2024, 2001

[16] Richard Pursley and Joao Paulo Martins, Michigan Dairy Review, Volume 16, No.2,2011

[17]Hywel Morgan, Nicolas G.Green, AC Electrokinetic: Colloids and Nanoparticles (Microtechnologies and Microsystems)

[18]Yulia Polevaya, Irina Ermolina, Michael Schlesinger, Ben-Zion Ginzburg, Yuri Feldman, Time domain dielectric spectroscopy study of human cells II. Normal and malignant white blood cells, Biochimica et Biophysica Acta 1419(1999) 257-271

[19]Sherbon JW, Physical Properties of Milk, Chapter 8 in Wong et al, 1988

# VITA

Quan Yuan was born in Kaifeng (Henan Province, PRC), a famous city as the ancient capital of seven dynasties in China. He received the B.S degree in Electrical Engineering from Changsha University of Science & Technology (CSUST), China in June 2006. From 2006 to 2007, he worked at Zhengzhou Xinli Electric Company, Henan, China. He came to the US in 2007 to pursue graduate degree at the University of Tennessee-Knoxville and received Master of Science degree in August, 2010, and Doctor of Philosophy degree in August, 2014, both in Electrical Engineering. His research interests concentrate on the development of bioMEMS microfluidic device, bio-particle manipulation (human serum sample, algae, somatic cell, etc), microfabrication and biosensor assays. He has a good academic background and received "Extraordinary Professional Promise" award of the University of Tennessee, 2013. Also as a key member of "Lab Chip-Based Chlorophyll Fluorometer" team, he has joined and received the semi-final award of the Global Venture Challenge 2010, Oak Ridge National Lab.